A metabolic support system for engineered (micro)tissues using glycogen-releasing micromaterials

A novel approach to bridge the prevascular phase of tissue engineered constructs

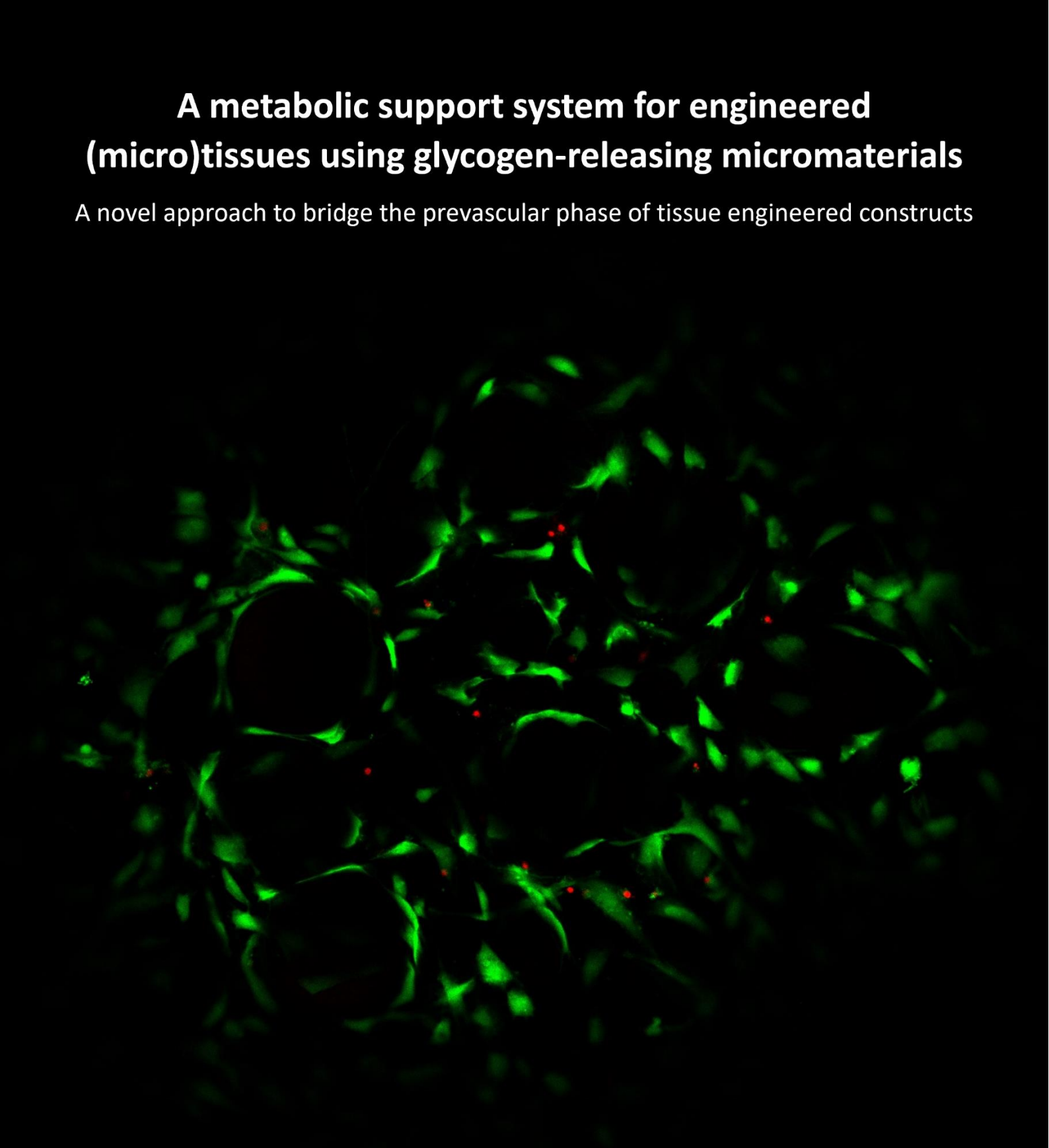

Master Thesis Biomedical Engineering
Isa Robin Porsul
June 2023

UNIVERSITY OF TWENTE. | TECHMED CENTRE

A metabolic support system for engineered(micro)tissues using glycogen-releasing cell-adhesive micromaterials

A novel approach to bridge the prevascular phase of tissue engineered constructs

Isa Robin Porsul
Master Thesis Biomedical Engineering
Bioengineering Technologies

Graduation Committee

Supervisor and Chairman of the Committee Prof. Jeroen Leijten
Professor, Developmental Bioengineering
Daily Supervisors MSc N.G.A. Willemen, MSc M. Gurian
PhD Candidates, Developmental Bioengineering
External Member Dr. ir. Tom Kamperman
Enterpreneur and founder, IamFluidics

Developmental BioEngineering

UNIVERSITY OF TWENTE. | TECHMED CENTRE

Developmental BioEngineering (DBE)
Faculty of Science and Technology (TNW)
Enschede, Netherlands
June 2023

Summary

Tissue engineering aims at the creation of living implants to replace, repair, or regenerate damaged, diseased, or aged tissues. However, the current methods to create engineered tissues are limited to either small or thin tissues and creating clinically relevant sized tissues remains one of the major challenges in the field of tissue engineering. These larger tissues are characterized by limited oxygen and nutrient diffusion during the prevascular phase, leading to the formation of a necrotic core within days. This prevascular phase can be bridged by continuously supplying the incorporated cells with nutrients. Glycogen is a molecule that is present in the human body, and functions as a storage and release system of glucose molecules. It was already known that glycogen is present inside cells, but we show that cells can survive with the supply of solely exogenous glycogen. To use glycogen as a controlled release system of glucose molecules, we incorporated it into liquid core shell microgels. We showed that upon culture of human mesenchymal stem cells (hMSCs) with glycogen loaded core shell microgels, a high cell viability and metabolic activity can be maintained not only in 2D culture but also in 3D utilizing collagen hydrogels. The data obtained thus far have demonstrated promising and further research will be performed to investigate the potential of glycogen-loaded core shell microgels to fully bridge the prevascular phase of tissue engineered constructs.

Samenvatting

Weefseltechnologie streeft naar de creatie van levende implantaten om beschadigd, ziek of verouderd weefsel te vervangen, repareren of regenereren. De huidige methoden om weefsel te creëren zijn echter beperkt tot kleine of dunne weefsels, en het creëren van klinisch relevante weefsels van grotere omvang blijft een van de belangrijkste uitdagingen op het gebied van weefseltechnologie. Deze grotere weefsels kenmerken zich door beperkte zuurstof- en voedings-diffusie tijdens de pre-vasculaire fase, wat binnen enkele dagen leidt tot de vorming van een necrotische kern. Deze pre-vasculaire fase kan overbrugd worden door de cellen continue te voorzien van voedingsstoffen. Glycogeen is een molecuul dat aanwezig is in het menselijk lichaam en fungeert als een opslag- en vrijgavesysteem van glucosemoleculen. Het was al bekend dat glycogeen aanwezig is in cellen, maar wij tonen aan dat cellen kunnen overleven met uitsluitend exogeen glycogeen als bron van voedingsstoffen. Om glycogeen te gebruiken als een gecontroleerd afgiftesysteem van glucosemoleculen, hebben we het geïntroduceerd in core shell microgels. We hebben aangetoond dat bij het kweken van humane mesenchymale stamcellen met glycogeen-beladen core shell microgels, niet alleen een hoge cel levensvatbaarheid en metabole activiteit behouden blijven in een 2D-kweek, maar ook in 3D in een collageen hydrogel. De tot nu toe verkregen resultaten lijken veelbelovend en verder onderzoek zal uitwijzen of glycogeen-beladen core shell microgels potentieel hebben om de pre-vasculaire fase van gekweekte weefsels volledig te overbruggen.

List of abbreviations

TE	tissue engineering
3D	three-dimensional
ATP	adenosine triphosphate
ROS	reactive oxygen species
hMSCs	human mesenchymal stem cells
HBOC	hemoglobin-based oxygen carrier
PFC	perfluorocarbon
O2	oxygen
CO2	carbon dioxide
H2O	water
G6P	glucose 6-phosphate
G1P	glucose-1-phosphate
UDP	uridine 5’-diphosphate
UDPG	UDP glucose
GLUT-1	glucose transporter 1
Pi	phosphor
NSG	naturally derived glycogen
ESG	enzymatically synthesized glycogen
GP	α-glucan phosphorylase
BE	Branching enzyme
SP	sucrose phosphorylase
AM	amylomaltase
IAM	isoamylase
OCN	osteocalcin
OPN	osteopontin
ALP	alkaline phosphatase
PYGB	glycogen phosphorylase
ab	antibody
BMP-2	bone morphogenetic protein 2
GSD	glycogen storage disease
BMD	bone mineral density
ECM	extracellular matrix
DexTA	dextran tyramine
PNC	p-nitrophenyl chloroformate
HRP	horseradish peroxidase
H2O2	hydrogen peroxide
PDMS	polydimethylsiloxane
PMMA	poly(methyl methacrylate)
α-MEM	minimal essential medium alpha
ITS	insulin transferrin selenium
PBS	phosphate buffered saline
DMEM	Dulbecco’s modified eagle’s medium
AsAP	ascorbic acid

FBS	fetal bovine serum
DPBS	Dulbecco's phosphate buffered saline
GelMA	gelatin methacrylate
Df	degree of functionalization
VEGF-A	vascular endothelial cell growth factor A
Ru	ruthenium
SPS	sodium persulfate
M	molar
PI	phosphorylase inhibitor
DoS	degree of substitution
FITC	fluorescein isothiocyanate
PP	parallel plate
FGF	fibroblast growth factor
OG	oyster glycogen
BG	bovine glycogen
HA	hyaluronic acid
CV	coefficient of variation
SD	standard deviation
d	diameter
st	shell thickness
TEM	transmission electron microscopy
PD	Parkinson's disease
AD	Alzheimer's disease
ALS	amyotrophic lateral sclerosis
PVA	Polyvinyl alcohol
PVA-VEA	vinyl ether acrylate-functionalized PVA
PVA-VEA-SH	thiolated PVA-VEA
PEG	polyethylene glycol
PEG-PLA	PEG polylactic acid
PEG-PLA-DA	PEG-PLA diacrylate
MPI	phosphomannose isomerase
AA	amino acid
NEAA	non essential amino acid
EtOH	ethanol

Contents

1. Introduction to Tissue Engineering

Tissue engineering (TE) is an interdisciplinary field that merges principles from engineering and life sciences with the objective of developing biological tissues capable to restore, replace, improve or regenerate damaged, aged, or diseased tissues [1, 2]. The main goal of TE is to utilize patient-specific cells to overcome current challenges associated with organ transplantation, such as organ scarcity and immune responses triggered by tissues and organs from other species or human beings. Additionally, TE focusses on the development of personalized pathological models for drug screening and development. TE is a promising alternative for new therapy development, as animal models often fail to mimic conditions in the human body due to physical differences in for example size and function, as well as differences on signaling mechanisms associated with disease onset and progression [3]. In addition to the benefits offered by TE in terms of tissue regeneration and drug development and testing, the implementation of TE constructs holds the potential to overcome ethical and economic concerns [1, 3].

The paradigm of TE describes the integration of engineering principles with living tissues to fabricate three-dimensional (3D) tissue constructs that closely mimic the structural, functional, and mechanical characteristics of native tissue (Figure 1) [1].

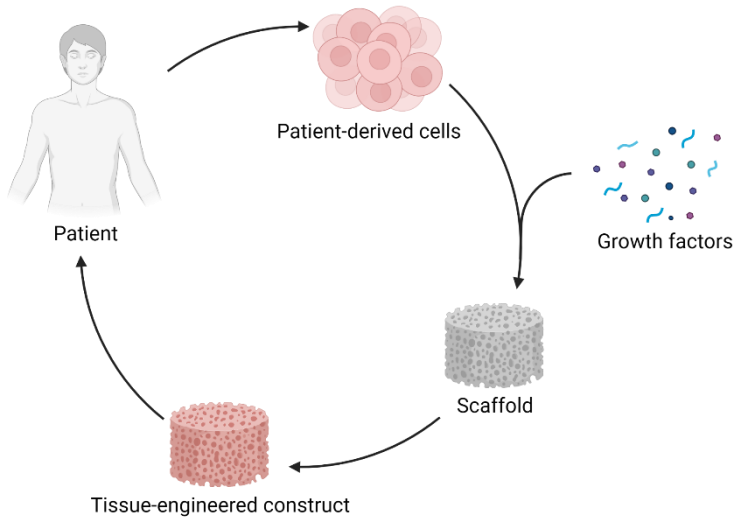

Figure 1: The paradigm of tissue engineering. Patient-specific cells are incorporated in a scaffold together with the desired growth factors to create a tissue engineered construct which can be implanted in the patient. Created with BioRender.com

1.1 The current challenge in TE

In the human body, the complex vascular network plays a vital role in facilitating the delivery of nutrients and oxygen to tissues exceeding a thickness of 2 mm [2,4]. Despite the promising results in tissue regeneration and replacement though TE, the application of TE models in the clinic is currently limited to constructs with a thickness less than 2 mm. This limitation is caused by the fact that most TE constructs do not have a vascular network [3, 4]. While it is possible for a vascular network to develop within such a construct, the process typically requires up to 21 days for complete vascularization [o3, t6]. After implantation, the host's vascular network typically infiltrates the construct in response to the signals released by cells due to hypoxic conditions [4]. However, prior to achieving full vascularization, which is crucial for long-term cell viability and functionality, the tissue relies completely on the diffusion of nutrients and oxygen [2-4, 6]. Small TE constructs are able to rely on diffusion, and thus remain viable upon transplantation [6]. For larger constructs of clinically relevant size, the diffusion limitation results to anoxic conditions in the construct, subsequently leading to cell death and

eventually implant failure (Figure 2) [1, 4, 6, 7]. As for this moment, the development of TE constructs larger than 2 mm that maintain viable remains a significant challenge [2].

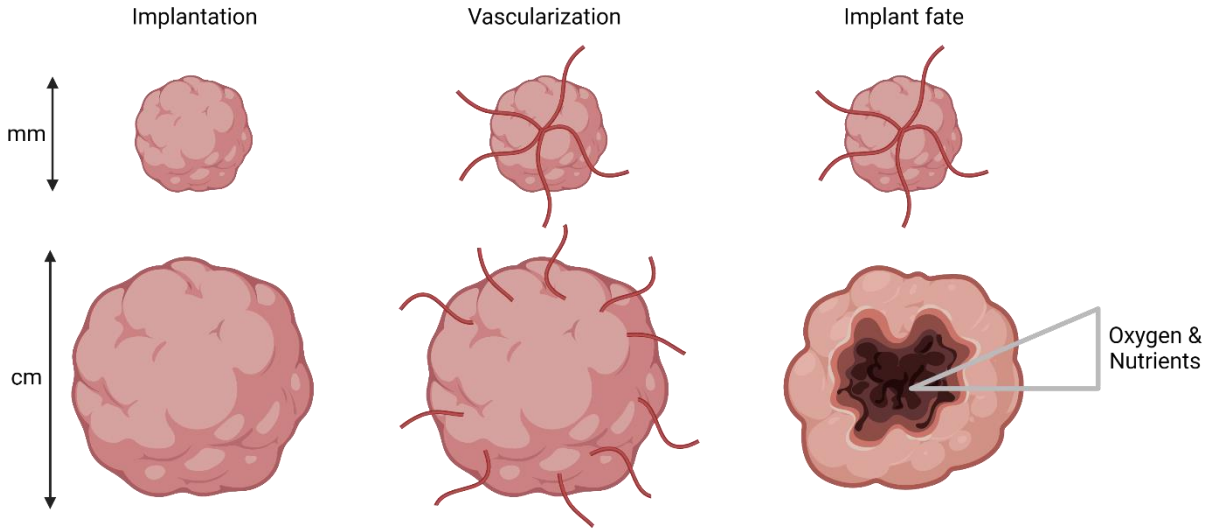

Figure 2: Small constructs are able to survive because of nutrient and oxygen diffusion. Larger constructs cannot rely on diffusion and eventually develop a necrotic core which in the end leads to implant failure. Created with BioRender.com

1.2 Research aim and objectives

Currently, a lot of research focusses on oxygen-releasing materials with the aim of enhancing the cell viability of TE constructs (refer to section 2 for more information). However, these materials still have their drawbacks in terms of safety and oxygen release kinetics. An alternative approach to ensure cell viability in TE constructs might be the long-term release of essential nutrients, such as glucose. The human body already possesses a glucose release mechanism through the glycogen particles [8-10] (section 3.1). Glycogen is a branched polymer, that can be regarded as a natural nanoparticle, and serves as a way of storing excess glucose and releasing it in a controlled manner in times of need. Therefore glycogen itself represents a controlled nutrient release system and can thus be a promising candidate to ensure cell viability in TE constructs. Through the encapsulation of glycogen within micromaterials, these micromaterials can hold potential for application in tissue engineering, enabling the delivery of adequate nutrients to an otherwise nutrient-deprived construct.

For this study, several objectives were formulated:

- Assessment of glycogen's potential for long-term cell viability.
    - Comparative analysis of glycogen in relation to other metabolites in its ability to maintain long term cell viability in anoxic conditions.
    - Evaluation of potential toxicity of glycogen on human mesenchymal stem cells (hMSCs) by examining different glycogen concentrations.
- Identification of the most suitable material for long-term encapsulation of glycogen.
    - Characterization of glycogen based on size, charge, and osmolarity.
    - Determination of release profiles of oyster and bovine glycogen, as well as glucose, from various hydrogels over a two-week period.
- Encapsulation of glycogen within micromaterials (e.g. microgels) applicable within tissue engineered constructs.
    - Determination of optimal parameters for microgel formation, including flow rate ratios and crosslinking density.
    - Characterization of acquired micromaterials based on size, crosslinking density and mechanical properties.

  - Evaluation of the glycogen release profile from these micromaterials.
- Assessment of glycogen-loaded micromaterials' potential to sustain cell viability and metabolic activity of hMSCs cultured in a 2D monolayer.
  - Analysis of cell viability, metabolic activity, and release of vascular endothelial growth factor (VEGF).
- Examination of glycogen-loaded micromaterials' potential to support hMSC viability within a 3D construct:
  - Implementation of hMSC-laden bulk hydrogels with incorporated glycogen-loaded micromaterials.
  - Evaluation of cell viability, metabolic activity, and release of VEGF.

2. State of the art

A variety of approaches have been investigated to enhance the viability of larger TE constructs. Some of these approaches focus on speeding up the process of vascular network formation. This can be achieved by the utilization of angiogenic factors, the incorporation of endothelial cells and angiogenic factors into scaffolds, or the pre-vascularization of constructs using advanced 3D printing techniques (Figure 3) [2, 6]. While these methods have demonstrated to be promising in small constructs, they still require invasion of the host vascular network, thereby the challenge of cell death in the central area of the constructs remains. Besides that, the incorporation of angiogenic factors within a construct increases the cellular stress experienced within an already metabolically deprived environment [6].

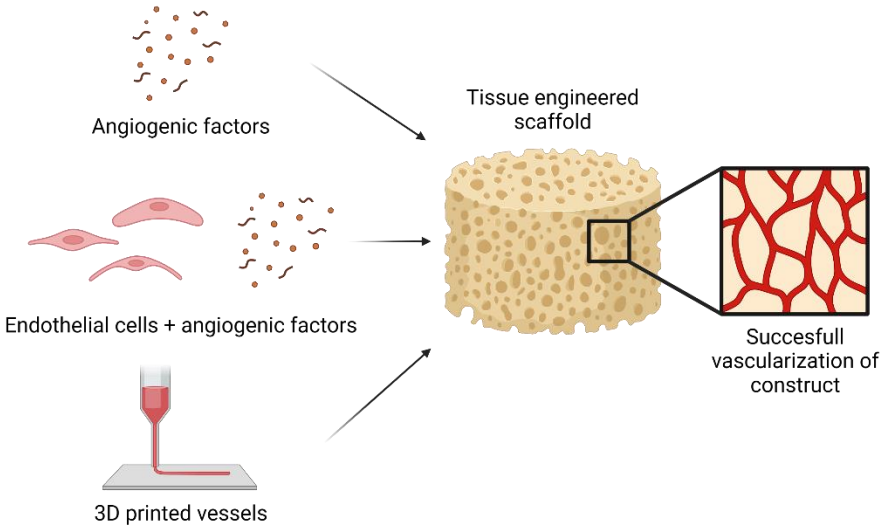

Figure 3: Common vascularization methods for tissue engineered constructs. Created with BioRender.com.

Incorporating a controlled system for oxygen release shows potential to solve the diffusion limitation encountered in TE constructs [6]. By implementing controlled oxygen release systems, it becomes feasible to bridge the prevascular phase of the constructs, thereby creating a pro-angiogenic and hypoxic environment that supports vascular growth and development.

Over the past years, a variety of oxygen release systems have been developed, like hemoglobin and myoglobin alternatives, liquid and solid peroxides, perfluorocarbons and oxygen carriers made of polymers, as well as more novel approaches such as lipid-based oxygen microbubbles, metallic nanoparticles and oxygen-loaded nano-sponges (Figure 4) [6, 11]. However, main disadvantage of these methods is the rapid oxygen release already within minutes to hours, thereby limiting the ability of oxygen release over longer time periods necessary for sufficient vascularization. Additional drawbacks associated with these systems include the short half-life of molecules, rapid clearance from the bloodstream, oxidative stress resulting from the formation of radicals, the need for external stimuli such as catalysts to trigger oxygen release, and the generation of by-products formed during the process [11].

To achieve oxygen release over a prolonged period of one week, one could encapsulate a solid peroxide like calcium peroxide within a hydrophobic material [6, 11]. For solid peroxides to release oxygen they require interaction with water molecules. Therefore, the use of a hydrophobic material is necessary to limit the exposure of the solid peroxides to water, thereby extending and regulating the duration of oxygen release within the construct. However, the utilization of peroxides for oxygen release is associated with severe cytotoxicity due to the high levels of H_2O_2, which forms as an intermediate product during their hydrolysis [11]. In order to mitigate the toxicity associated with

these high levels of H_2O_2, catalysts such as catalase and magnesium dioxide can be employed to decrease the H_2O_2 levels [11, 12]. However, it is important to acknowledge that the introduction of an additional compound can be regarded as a potential drawback in itself.

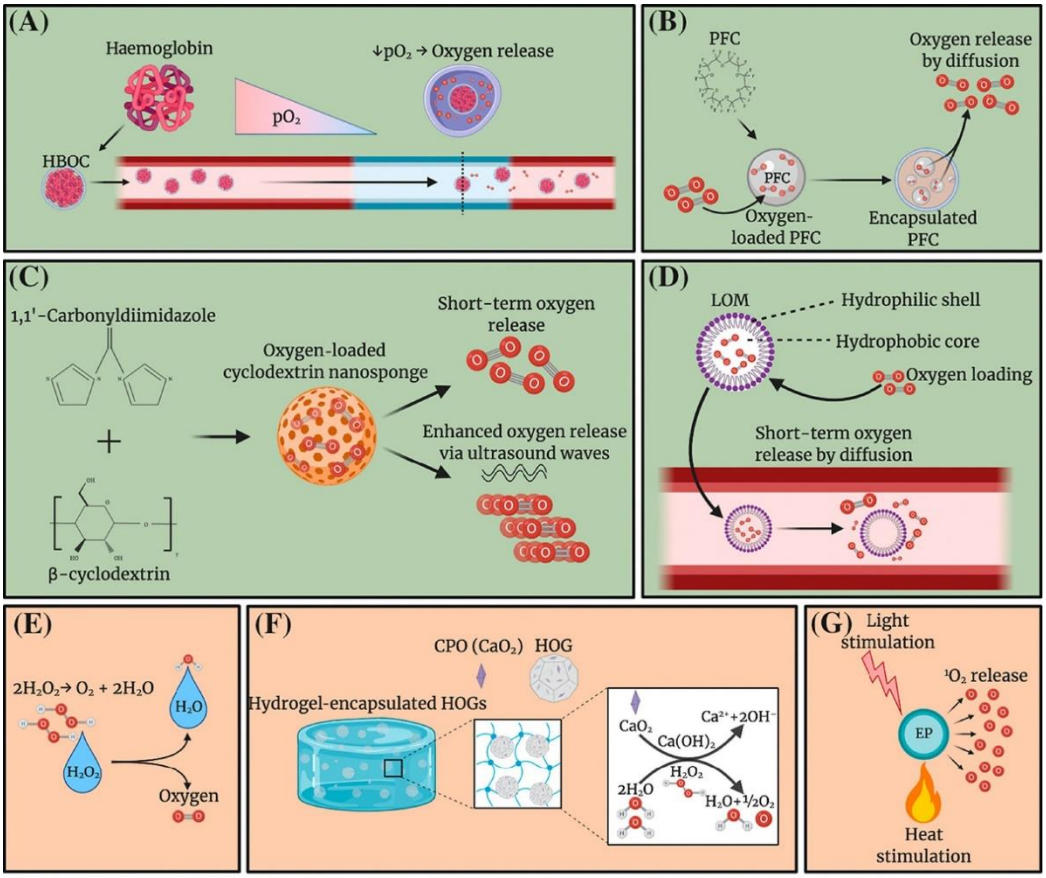

Figure 4: Oxygen-releasing (green) and oxygen-generating (orange) materials. A) Hemoglobin-based oxygen carrier (HBOC), B) Perfluorocarbon (PFC), C) Oxygen-loaded nano-sponges, D) Lipid-based microbubbles, E) Liquid peroxide, F) Solid peroxide, G) Endoperoxide [11].

A lot of research has been devoted to the generation and advancement of materials capable of releasing or producing oxygen [11]. However, the majority of these materials exhibit limited control over the release of oxygen, often following a burst release profile thus restricting controlled oxygen release over time. Moreover, the use of such materials is associated with the production of various (potentially toxic) by-products. Oxygen-releasing materials thus can be promising for future *in vivo* applications, but a lot of improvements are still required to enhance their performance and safety.

2.1 The absence of oxygen is not the detrimental factor for cell death in TE constructs

Oxygen is essential for the survival and optimal functioning of aerobic organisms [11], which is probably why much of the research in the field is focused on the development of oxygen-releasing materials for TE construct survival. Oxygen plays a crucial role in the human body, particularly in the oxidation of nutrients such as glucose. When glucose is metabolized in the presence of oxygen, a process known as aerobic respiration, it yields approximately 30-36 adenosine triphosphate (ATP) molecules as illustrated in Figure 5. ATP molecules are the main biomolecules for energy transfer in animals. In contrast, during anaerobic respiration, which occurs in the absence of oxygen, glucose metabolism produces only 2 ATP molecules. Thus, a limited availability of oxygen leads to a restricted production of ATP, which can cause metabolic stress, autophagy and the generation of reactive oxygen species (ROS). These events can in turn lead to cell death though mechanisms like apoptosis and

necrosis [11, 13]. To avoid these detrimental effects arising from insufficient oxygen levels, the human body continues to break down nutrients to supply energy and maintain tissue and cellular viability. However, this process comes at the cost of consuming tremendous amounts of glucose and internal glycogen, leading to fast depletion of both [14].

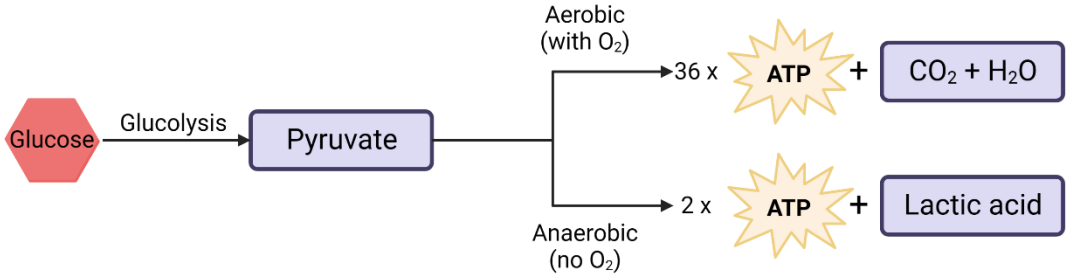

Figure 5: In the presence of oxygen, one glucose molecule is converted to 36 ATP molecules, while in the absence of oxygen it is converted to only 2 ATP molecules. ATP: adenosine triphosphate, O_2: oxygen, CO_2: carbon dioxide. Created with BioRender.com.

Several studies have demonstrated that the absence of glucose, rather than oxygen, is eventually fatal for transplanted cells [5, 15-17]. Deschepper *et al.* (2011) revealed that the survival of hMSCs relied more on glucose availability than on oxygen [15]. In the absence of oxygen, but with a sufficient supply of glucose, hMSCs were able to survive for over two weeks [15, 16]. It is important to note that this study did not investigate the impact of varying oxygen tensions on cell viability, suggesting that glucose availability might be of less importance under normoxic conditions [5]. Following up on this, Rizzo *et al.* cultured MSCs in normoxic and near-anoxic conditions using oxygen producing microspheres, with varying glucose concentrations [5]. Although the oxygen-release had a positive effect on cell survival, the results indicated that even under normoxic conditions MSC viability was dependent on glucose availability. In the absence of glucose, MSC viability decreased to 60% in normoxia within just four days of culture, while in the presence of glucose, cell viability remained as high as 80% both in the presence and absence of oxygen.

Moya *et al*. were the first to demonstrate that hMSCs located in the core of hydrogels experienced a near-anoxic microenvironment, where 0.1% O_2 best reflects the *in vivo* situation experienced by hMSCs at the core of tissue engineered scaffolds post transplantation [17]. The study showed that in such scenario, cells produce ATP through anaerobic respiration, as hMSCs did survive with a sufficient supply of glucose once they adapted to a near-anoxic environment.

3. Background

3.1 Glycogen

3.1.1 Glycogen as glucose storage in the human body

Glycogen is a branched polymer composed of glucose molecules acting as the human body's energy storage system, predominantly located in the liver and skeletal muscles, with smaller amounts present in the brain (Figure 6) [8-10]. Approximately 60% of the total amount of glucose in the human body is consumed daily by the brain [18]. Any remaining glucose that is not utilized by other organs is absorbed by the liver from the bloodstream where it is converted into glycogen. In times of metabolic need, glycogen from the liver is broken down to glucose molecules to supply the brain and the rest of the human body [9, 18]. As glycogen is produced in the liver, the liver possesses the highest glycogen content among all organs, accounting for up to 10% of its total weight. The glycogen found in skeletal muscles on the other hand, represents a smaller fraction with a maximum of 2% of its muscle weight. Glycogen found in muscles serves a different function as glycogen in the liver and is used to cover the energy requirements during intense exercise and muscle contraction.

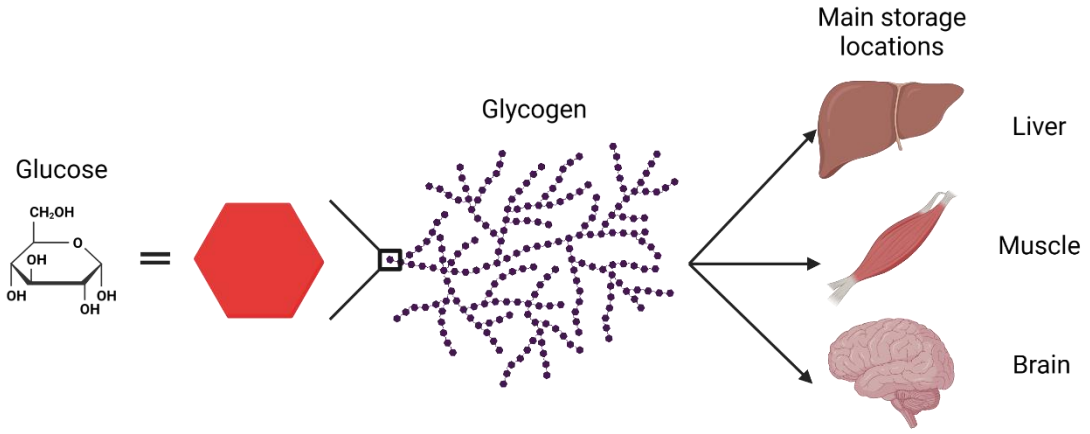

Figure 6: Glycogen is a nanoparticle consisting of multiple glucose molecules and in the human body it is mostly found in the liver, muscle and brain. Created with BioRender.com

3.1.2 Glycogen synthesis and degradation mechanism

Glycogen and glucose can convert into one another by synthesis and degradation pathways (Figure 7). Glucose molecules enter the cell via specific glucose transporters [8]. Once in the cytoplasm, glucose is phosphorylated to glucose 6-phosphate (G6P) by hexokinase isoenzymes, which is then isomerized to glucose 1-phosphate (G1P) by phosphoglucomutase-1. The enzyme UDP-glucose phosphorylase converts G1P to uridine 5'-diphosphate (UDP)-glucose, the specific form of glucose required for glycogen synthesis. The initiation of glycogen synthesis is done by glycogenin.

Glycogenin attaches glucose residues from UDP glucose, forming a chain of approximately 10-20 glucose residues [8, 9, 19-22]. In most mammalian species, including humans, two isoforms of glycogenin are present; glycogenin 1, which is predominantly expressed, and glycogenin 2, which is the primary isoform found in the liver [22]. Notably, only one single gene encoding for glycogenin is expressed in all tissues. Glycogenin together with the short glucose chains forms the core of the glycogen molecule [8, 9, 19-22]. Subsequently, glycogen synthase adds glucose residues to the glycogen core via α-1,4 linkages. The glycogen debranching enzyme introduces α-1,6 branch points after every 12-13 glucose residues. Glycogen synthase and glycogen debranching enzyme continue the addition of glucose residues, resulting in a large glycogen molecule consisting of up to 50,000 glucose residues, with glycogenin covalently bound at its center [8-10, 19, 22]. Since glycogen is naturally present in the cytoplasm of cells, little is known about the uptake of exogenous glycogen, such as

glycogen derived from sources like oyster, bovine, rabbit etc. Ida-Yonemochi *et al.* investigated glycogen uptake and found that it was associated with increased expression of the glucose transporter 1 (GLUT-1) protein [23]. Inhibition of this protein led to the aggregation of exogenous glycogen on the cell surface, with only a few molecules being internalized.

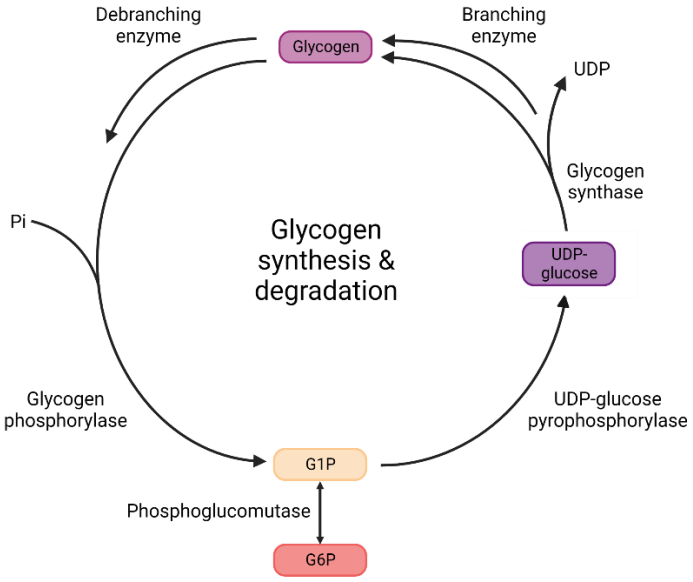

Figure 7: Glycogen synthesis and degradation pathway (simplified version). Abbreviations in figure: UDP: uridine 5'-diphosphate, Pi: phosphor, G1P: glucose-1-phosphate, G6P: glucose-6-phoshpate. Created with BioRender.com.

The degradation of glycogen occurs in both the cytosol and lysosomes [8]. In the cytosol glycogen phosphorylase and glycogen debranching enzyme work together to break down glycogen. Glycogen phosphorylase cleaves the α-1,4 linkages, while the glycogen debranching enzyme breaks down the branching points releasing glucose 1-phosphate. Subsequently, glucose 1-phosphate is isomerized to glucose 6-phosphate, which is converted to a free glucose molecule by glucose 6-phosphatase. Free glucose molecules are able to exit the cell via glucose transporters and enter the bloodstream. In the lysosomes, glycogen breakdown is facilitated by acid α-glucosidase (also known as α-glucan hydrolase or acid maltase), which hydrolyzes glycogen to glucose. However, the precise mechanism by which this enzyme breaks the glycogen branching points within the glycogen particles remains unknown.

3.1.3 Glycogen consists in various forms

The size of glycogen varies depending on the tissue type [18]. Glycogen found in the liver can be up to 10 times larger than glycogen found in skeletal muscle cells [18, 21]. This difference in size is attributed to the presence of α-particles in the liver [8, 21]. The glycogen molecule, formed by the linkage of glucose molecules through α-1,4 linkages and α-1,6 bonds, gives rise to a so called β-particle [8, 19, 21, 22] (Figure 8). B-particles have molecular weights of approximately 10^6 Da and a diameter of 10-30 nm. On the other hand, α-particles are assemblies of multiple β-particles, a process that is not yet fully understood due to the complex nature of glycogen metabolism [22]. As a result, α-particles have molecular weights exceeding 10^8 Da and sizes up to 200 nm. This makes α-particles promising candidates for controlled glucose release, as they degrade more slowly compared to β-particles. The liver primarily contains α-particles, while skeletal muscle cells show the presence of β-particles only. This suggests that α-particles serve as an energy reserve (which makes sense as those are found in the liver), while β-particles act as a source of readily available carbohydrates [22].

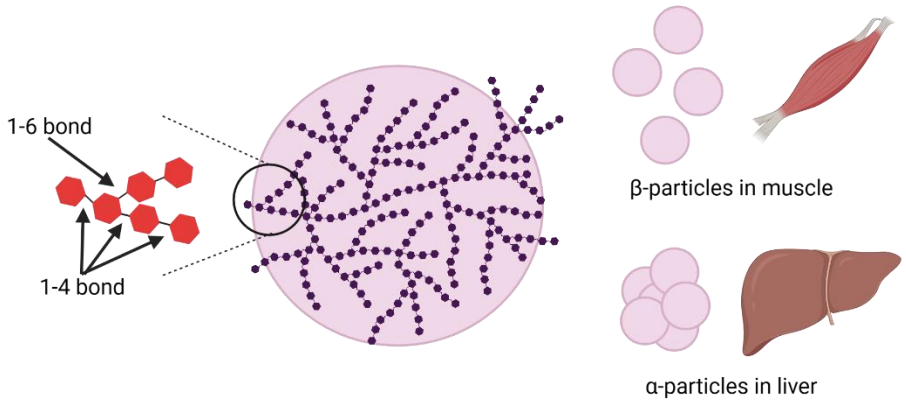

Figure 8: Glycogen in skeletal muscle is arranged in β-particles while glycogen in the liver is arranged in larger α-particles, which is the assembly of multiple β-particles. Figure based on [19]. Created with BioRender.com

Glycogen shows great biocompatibility and biodegradability. It is widely available, highly soluble in water, and can be easily modified with various molecules [23-25]. Additionally, glycogen can be administered into the bloodstream without the risk of rapid renal clearance, as its molecular weight exceeds the renal threshold [24]. The unique dendrimer-like structure of glycogen sets it apart from other polysaccharides, making it an attractive molecule for biomedical applications [23].

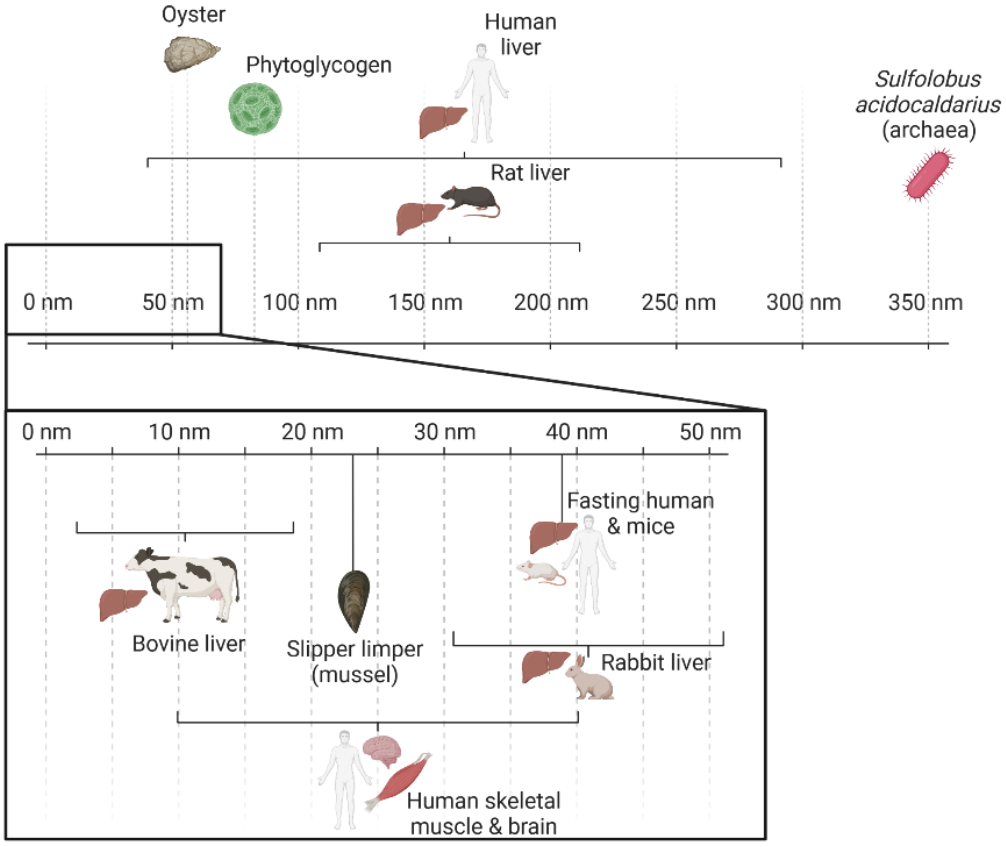

Figure 9: Glycogen size depends on its source but is also organ specific. Created with BioRender.com.

Glycogen varies not only per tissue of origin, but can be quite divergent in size depending on the glycogen source as well (Figure 9). For instance, glycogen derived from human liver can range in size from 110 to 290 nm [26, 27], similar to rat glycogen where α-particles have an average diameter of 158 nm (ranging from 110 to 290 nm), and β-particles measure around 20-25 nm [28]. Another study

reported the size of human liver glycogen to be approximately 40 nm, comparable to the size of liver glycogen in mice [29]. Fasting humans and mice also exhibit similar glycogen sizes, approximately 37 nm and 38 nm, respectively. In rabbit liver, glycogen sizes range from ~32 nm [28] to ~52 nm [30] and ~80 nm [23].

Glycogen isolated from slipper limpet, a mollusc species, shows the presence of β-particles with a size of approximately 23 nm [28]. Oyster glycogen displays sizes ranging from 35 to 75 nm, while phytoglycogen measures around 82 nm [23]. Bovine glycogen, on the other hand, appears to consist solely of β-particles with sizes ranging from 5 to 19 nm [23, 28, 30].

Back to glycogen within the human body, glycogen in skeletal muscle ranges from 10 to 44 nm, [26-28], whereas glycogen found in the brain ranges from 10 to 30 nm and sometimes to 44 nm, with a mean value of 25 nm [26, 31]. The thermophilic archaeon *Sulfolobus acidocaldarius* has the largest glycogen size reported in literature, reaching up to 350 nm [32].

3.1.5 Enzymatic extracellular synthesized glycogen

The two main ways to obtain glycogen are its extraction from natural sources (NSG), such as bovine, rabbit, and oyster, and the *in vitro* synthesis of glycogen, also known as enzymatically synthesized glycogen (ESG) [33, 34]. *In vitro* synthesis of glycogen was first achieved by Cori & Cori in 1943, combining the activities of two enzymes; α-glucan phosphorylase (GP) and branching enzyme (BE), along with glucose-1-phosphate (G1P) as a substrate [33, 34]. This approach mimics the *in vivo* glycogen synthesis process, starting from an α-(1→4)-glucan which is elongated by GP, followed by the introduction of branch points into the elongated chains by BE. Kajiura *et al.* made improvements to this method by utilizing glucose-1-phosphate derived from sucrose via the action of sucrose phosphorylase (SP). Another synthesis method involves the use of short-chain amylose in combination with branching enzyme and amylomaltase (AM). In this method, isoamylase (IAM) is used to generate short-chain amylose from starch or dextrin. BE and AM are then able to act on the short-chain amylose, synthesizing glycogen. The molecular weight of the resulting glycogen can be tuned by adjusting certain reaction parameters in the synthesis.

Treatment with α-amylase showed that NSG and ESG had comparable physicochemical and structural characteristics regarding the branch frequency, molecular shape and weight [33-35]. Both NSG and ESG demonstrated slow digestion upon addition of α-amylase [33, 34]. However, ESG showed greater resistance to breakdown compared to NSG [35]. Furthermore, ESG readily dissolves in water, forming an opaque solution comparable to NSG in water [34]. Besides that, ESG has been shown to possess biological functions, including the stimulation of macrophages and immunomodulating activity [34, 35].

Long-term oral administration of ESG in rats for a duration of 13 weeks demonstrated its safety, as no toxic effects were observed [35]. Additionally, a bacterial mutagenic assay indicated the absence of mutagenic properties in ESG.

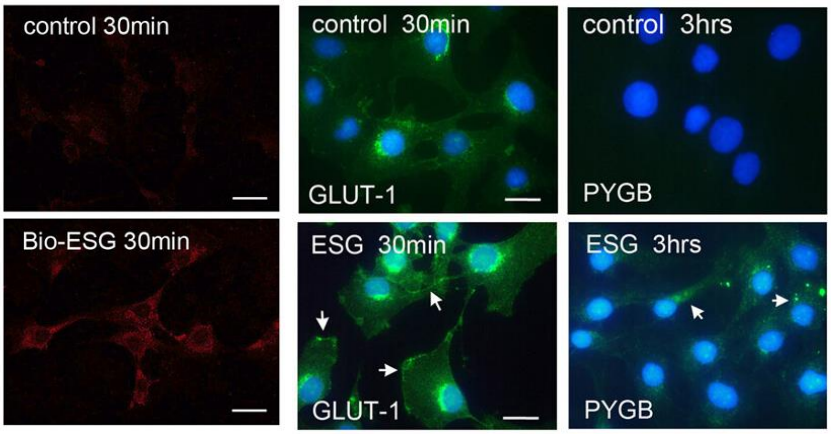

Figure 10: Staining of cells treated with enzymatically synthesized glycogen (ESG). Left: ESG conjugated to Texas Red-Streptavidin. Middle: glucose transporter 1 (GLUT-1) signal (FITC, in green) was enhanced for cells treated with ESG at 30 min compared to cells without ESG. Right: glycogen phosphorylase (PYGB) was detected in abundance in cells treated with ESG after 3h. Nuclei were stained with DAPI (blue). Scale bar: 33 µm [35].

It is noteworthy that ESG can be taken up by cells [35]. Ida-Yonemochi *et al.* conducted a study demonstrating that MC3T3-E1 cells were capable of internalizing ESG already within 30 min (Figure 10, left). Interestingly, when glucose-free media was used, MC3T3-E1 cells responded faster to the presence of ESG compared to cells cultured in glucose-containing media. Glycogen phosphorylase (PYGB) was detected in abundance in cells after 3h of exposure to ESG (Figure 10, right). It was observed that GLUT-1, a glucose transporter protein, translocated to the cell membrane within 30 min upon exposure to ESG (Figure 10, middle), while GLUT-3 was expressed in the cytoplasm but not detected on the cell membrane, suggesting that GLUT-1 may be responsible for the uptake of ESG.

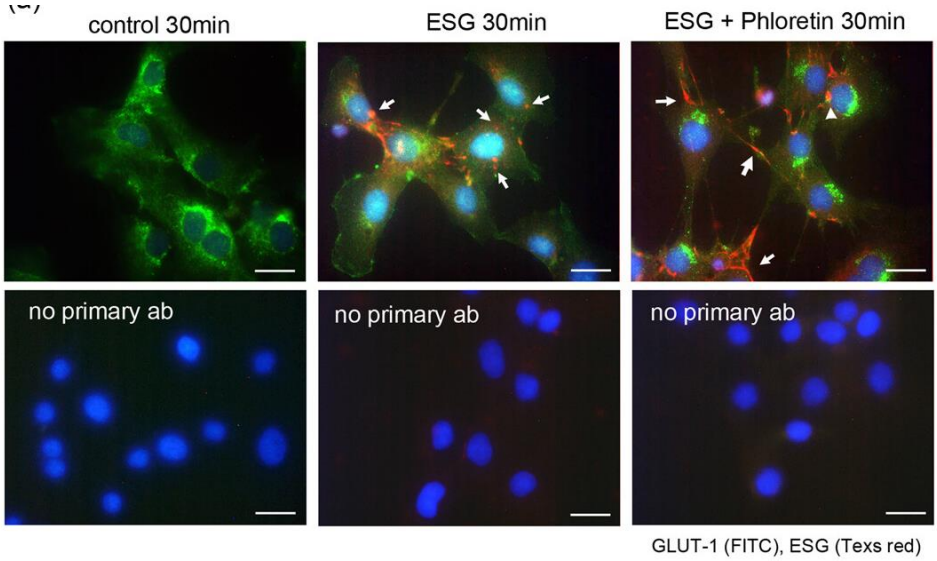

Figure 11: Uptake of enzymatically synthesized glycogen (ESG) by MC3T3-E1 cells is associated with glucose transporter 1 (GLUT-1). ESG can be taken up by the cells (middle), but when phloretin (a GLUT-1 inhibitor) is used (right), ESG accumulates on the cell membrane (indicated by the arrows). Scale bar: 33 µm. [35]

To evaluate the role of Glut-1 in the uptake of ESG, the GLUT-1 inhibitor phloretin was used [35]. In the absence of phloretin, ESG particles were observed in the cytoplasm of MC3T3-E1 cells within 30 min. however, in the presence of the inhibitor, ESG particles were predominantly observed on the cell surface, with only a limited number of ESG particles detected in the cytoplasm (Figure 11).

3.1.5.1 The role of ESG in osteogenesis

Based on the advantages of ESG, Ida-Yonemochi *et al.* evaluated the impact of ESG on osteogenesis [35]. The study showed that ESG exhibited the ability to promote MC3T3-E1 cell proliferation, and upon differentiation, it enhanced the mRNA expression of osteocalcin (OCN) and osteopontin (OPN) on day 7. Differentiation was achieved in osteogenic medium consisting of α-MEM supplemented with 10 mM β-glycerophosphate, 50 µg/ml ascorbic acid, and 100 nM dexamethasone. Immunocytochemistry confirmed the increased expression of OPN. Furthermore, ESG induced calcium deposition (Figure 12) and both alkaline phosphatase (ALP) and OPN staining intensities were enhanced (Figure 13).

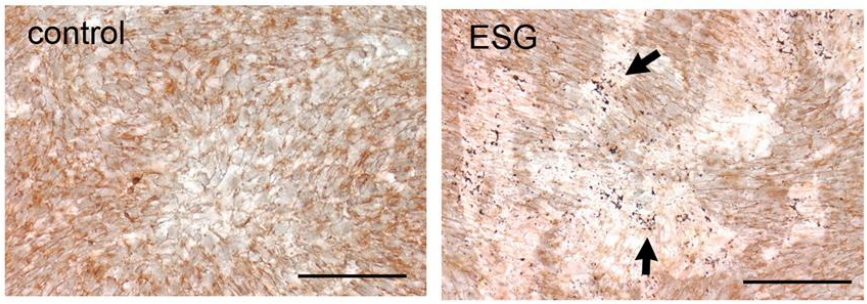

Figure 12: A von Kossa staining was performed to show increased calcium deposition (black spots) for cells treated with ESG. Scale bar: 250 µm [35].

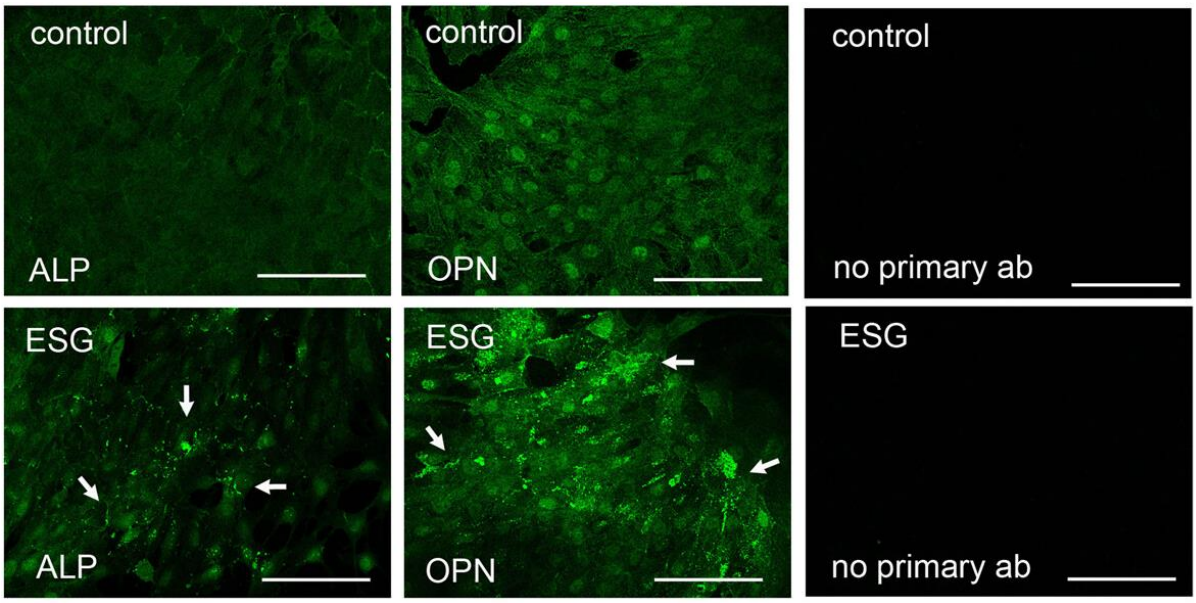

Figure 13: Alkaline phosphatase (ALP) and osteopontin (OPN) expression was enhanced upon treatment with ESG [35]. Scale bar: 250 µm.

However, in the absence of osteogenic medium, ESG alone did not induce differentiation of MC3T3-E1 into osteoblasts, indicating that ESG alone cannot entirely stir cell fate [35].

To further explore the role of ESG in osteogenesis, collagen gel scaffolds were used with and without ESG, but in both cases, no obvious bone formation was observed [35]. For the next study, collagen scaffolds were used with one group containing only BMP-2 and the other group containing BMP-2 along with ESG. These scaffolds were placed in bone defects and evaluated two weeks post-operation. The scaffolds with both BMP-2 and ESG showed new bone formation, while the scaffold with BMP-2 alone demonstrated limited bone formation only at the periphery (Figure 14).

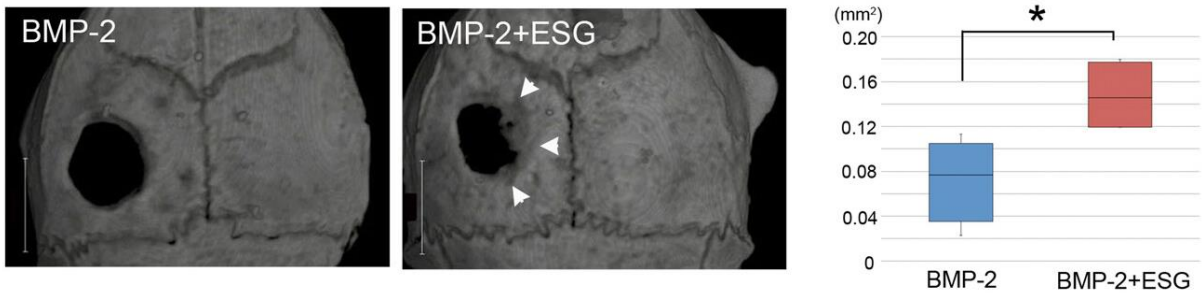

Figure 14: Scaffolds containing both bone morphogenetic protein (BMP-2) and enzymatically synthesized (ESG) showed more new bone formation than scaffold with BMP-2 only. Scale bar: 5 mm [35].

The areas of the bone defects were predominantly filled with fibrous connective tissue in both scaffold types [35]. Within the BMP-2 and ESG scaffold, OPN-positive bone fragments were observed. Also, in the BMP-2 and ESG scaffold, hMSCs showed an increased proliferation rate in the central region of the connective tissues.

3.1.6 Possible applications and roles of glycogen

Glycogen plays an important role not only in energy storage and supply during times of need but also in the maintenance of healthy tissues and organs [18]. In the liver and skeletal muscles, for instance, glycogen plays a critical role in cell signaling, differentiation and the regulation of redox reactions [35]. An intermediate molecule in glycogen synthesis, UDPG, can together with mast cells, guide the differentiation of MSCs towards adipose or bone tissue [18]. UDPG also holds potential as a therapeutic agent for the treatment of allergies.

While certain sources suggest that glycogen may possess some anti-tumor effect, this remains debatable [34] (see also section 3.1.7). The oral administration of ESG has demonstrated to prevent the development of metabolic disorders [35]. Besides that, glycogen metabolism can significantly impact the regulation of T cell memory and the polarization of M1 macrophages [18].

Besides the advantageous effects of glycogen in organisms, glycogen finds application in the cosmetic industry as well and can be used for DNA precipitation [34].

3.1.7 Diseases associated with glycogen

It is already known that glucose and glycogen can convert into one another by following multiple enzymatic steps. Defects in these enzymes associated with degradation and synthesis can give rise to various diseases accompanied by diverse symptoms [9]. Defects in enzymes, depending on the site of the defect, can result in hypoglycemia, hepatomegaly, liver disorders, or skeletal and cardiac myopathies. Conditions caused by the mutations in genes encoding for enzymes involved in glycogen metabolism are known as glycogen storage diseases (GSDs), and most of them are congenital. GSDs lead to a wide variety of symptoms, depending on the affected enzyme and its expression in organs like the liver, heart, kidney, and skeletal muscle.

GSDs associated with enzymes in the liver commonly lead to hypoglycemia and/or hepatomegaly. GSDs affecting skeletal muscle can result in exercise inability, rhabdomyolysis or muscle weakness. A comprehensive overview of GSDs, including the corresponding affected enzymes and their consequences, can be found in Table 2 in supplementary material 1.

In addition to GSDs, there are other diseases in which glycogen plays a role. For instance, in the absence of glycogenin, previously considered crucial for glycogen synthesis, glycogen accumulation occurs in muscles causing metabolic rearrangement and impaired muscle function [19].

Certain diseases, such as Lafora disease and Anderson's disease, are characterized by the abnormal elongation of glucose chains within the glycogen molecule. This leads to glycogen buildup, especially in the kidneys of diabetic patients, forming double helices that hinder glucose release when required [21].

In type 2 diabetes, the inability to maintain the blood glucose levels can be caused by the structure of the glycogen molecule [20]. In the liver, as discussed in section 3.1.3, glycogen predominantly exists as larger α-particles. These particles degrade and release glucose slower compared to the smaller β-particles, serving as a controlled glucose release system. However, studies have observed faster breakdown of glycogen α-particles into β-particles in diabetic mice, resulting in faster glucose release.

Glycogen metabolism also influences tumor development [18]. Hypoxic conditions often emerge in tumor tissues due to the disorganized vascular network. These hypoxic conditions are often associated with tumor metastasis. Hypoxia promotes increased glycogen degradation. Studies have been conducted on the inhibition of glycogen breakdown in tumors, leading to cell apoptosis inside the tumor.

Current treatment for GSDs affecting the liver primarily focus on dietary management, including carbohydrate restriction and periodic intake of uncooked cornstarch to maintain normal glucose levels and slow down symptom progression [36]. Restriction of carbohydrates varies depending on the specific GSD type. Also, high protein diets and glucose infusions at night are common, while liver transplantation remains the only option for severe cases with worsening symptoms.

3.1.8 Role of glycogen in osteoporosis

The precise effect of glycogen and GSDs on bone mineral density (BMD) remains unclear. The majority of GSD cases are GSD type I, III and IX [37]. Several studies have reported a correlation between GSD patients and reduced BMD, which consequently increases the risk of bone fractures. These patients often respond less to osteoporosis treatments. The diversity of the symptoms can vary depending on factors such as age, gender, vitamin D deficiency, and hyperactivity of parathyroid glands. Due to limited sample sizes in existing studies, conclusions regarding the association between BMD and GSDs can not be drawn [36, 37]. All studies though did show that patients with GSD showed higher incidence of osteoporosis [36-39].

3.2 Hydrogels and microgels

Hydrogels are three-dimensional (3D) networks formed through the crosslinking of specific polymers [40]. They can hold large amounts of water. However, when in their crosslinked state, they can not be dissolved in water. Because of their water-absorbing ability and soft, porous structure, hydrogels are capable to mimic the characteristics of the extracellular matrix (ECM). By manipulating factors such as pH, light exposure, temperature, or the incorporation of chemical reagents, the physical characteristics of hydrogels can be altered, as well as the hydrogel's permeability to certain molecules. However, it is important to note that variations in the environmental conditions may also lead to the disintegration of the hydrogel network.

Microgels, as implied by their name, are hydrogels characterized by dimensions in the micron range [40]. They can be produced by a variety of methods, including micromolding, ultrasonication, atomization, extrusion through nozzles or syringes, as well as via molecular self-association. Microgels can be either homogenous (Figure 15), or show a core-shell structure (Figure 16). Homogenous microgels can be easily produced using water-in-oil emulsions, while core-shell microgels feature a gel-like outer layer (shell) while maintaining an unaltered core. The field of microfluidics has demonstrated to be very promising for the precise fabrication of microgels [40].

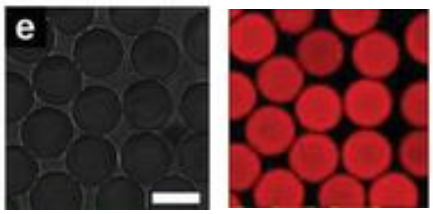

Figure 15: Ethidium staining of homogenous microgels (fully crosslinked). Scale bar: 20 µm [41].

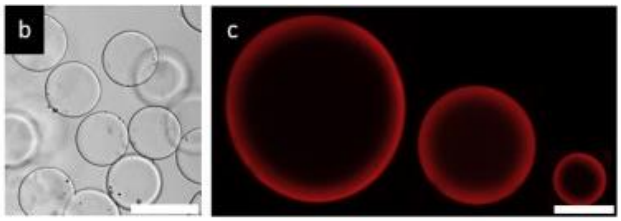

Figure 16: Ethidium staining of core shell microgels (crosslinked shell, non crosslinked core). Scale bar: 100 µm [42].

3.2.1 Microfluidics for the production of microgels

The field of microfluidics has grown tremendously over the past decades and is now of extreme importance in a variety of applications in fields like nanotechnology, biochemistry and engineering [43]. Microfluidics is defined as "the science and technology of systems that process or manipulate small (10^{-9} to 10^{-18}) amounts of fluids, using channels with dimension of tens to hundreds of micrometers." [44].

Recently, microfluidics has been widely used for the production of microparticles, offering numerous advantages over conventional bulk methods in terms of precise control over microgel size distribution, morphology and crosslinking density [40, 43]. Especially droplet-based microfluidics has emerged as an effective method for the generation of monodisperse microgels (Figure 17).

The generation of spherical-like microgels typically involves two steps: the formation of droplets containing a polymer solution capable of gelation, followed by the crosslinking of the polymer chains within the droplet [40]. It is important that these two steps are separated, meaning that the droplets should be formed prior to crosslinking, to avoid blockage of the channels where the droplets are formed. The crosslinking process can be conducted either on the microfluidic chip at a later stage or off the chip in for example a crosslinking bath. Chemical microgels are typically formed by the formation of covalent bonds upon crosslinking or by polymerizing the monomers present within the droplets.

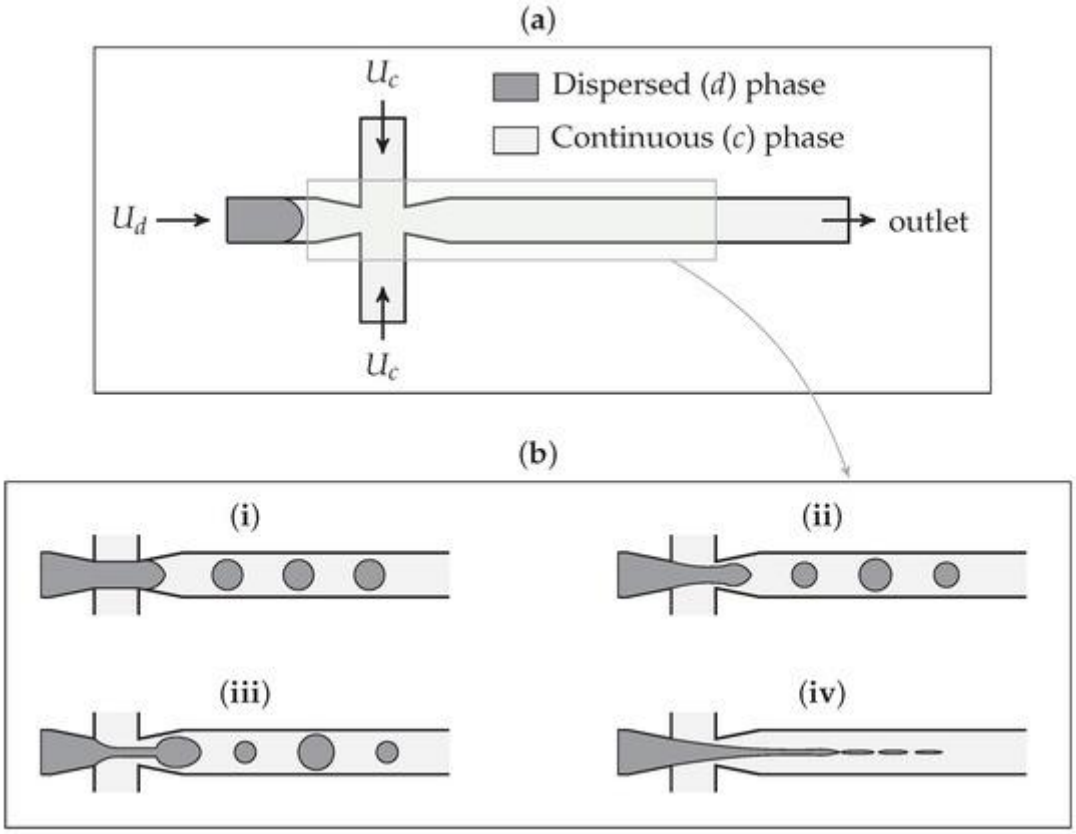

Figure 17: Schematic of microgel fabrication on chip with drop formation. A) Chip/channel design. B) The different regimes that can take place in droplet formation on chip: i) squeezing (desired for production of monodisperse microgels), ii) dripping, iii) jetting, iv) tip-streaming [45].

3.2.2 DexTA as material for microgels

Dextran-tyramine (DexTA) is one of the most researched materials for microgel fabrication on microfluidic chips [40]. Dextran offers several advantages, such as its bioinert nature, cytocompatibility, and ease of modification, while tyramines can enzymatically crosslink with one another [41, 46, 47].

Dextran can be conjugated to tyramine molecules by the activation of the hydroxyl groups present in dextran with p-nitrophenyl chloroformate (PNC) [40]. The Dex-PNC conjugate that is formed can react with tyramine to form Dex-TA conjugates.

3.2.3 Crosslinking DexTA into microgels

DexTA can be crosslinked into a microgel using horseradish peroxidase (HRP) as a catalyst for the bond formation between phenol groups in the presence of H_2O_2 (oxidizer) [40, 41]. It is possible to encapsulate cells in DexTA microgels, by mixing the polymer solution, cell suspension and crosslinker together prior to droplet formation [40, 42]. Covalent crosslinking can be achieved by controlling the supply of H_2O_2 via diffusion (Figure 18) [41, 48, 49]. This can be achieved by utilizing for example a polydimethylsiloxane (PDMS) wall or though silicone tubing in an H_2O_2 bath [40, 42].

Van Loo *et al.* introduced a system for producing monodisperse core-shell microgels by using tyramine-conjugated materials and crosslinking them through the addition of HRP and exposure to an H_2O_2 bath (Figure 19) [42]. Successful fabrication of core-shell microgels was demonstrated, and their size could be adjusted by modifying the flow rates of the oil and polymer solutions.

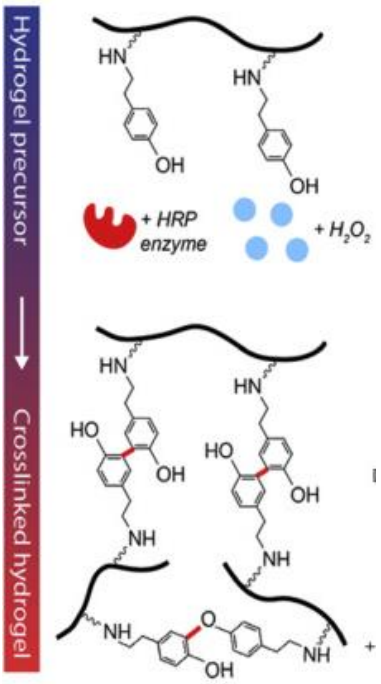

Figure 18: Dextran tyramine (DexTA) is crosslinked by horseradish peroxidase (HRP) in the presence of hydrogen peroxide (H_2O_2) [42].

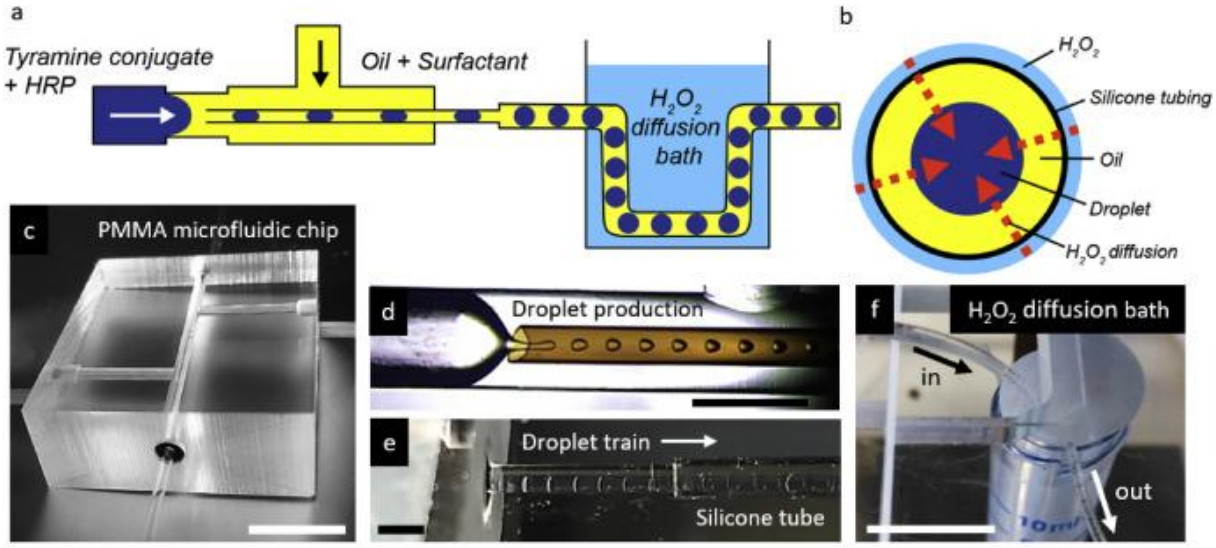

Figure 19: Set up for the formation of core shell microgels. a) Schematic overview of core shell fabrication principle, b) Slow diffusion of H_2O_2 is achieved using silicone tubing, c) Chip design used for droplet formation, d) Droplet formation is achieved using a nozzle e) After formation the droplets enter the silicone tubing f) silicone tubing is placed in an H_2O_2 bath to achieve slow H_2O_2 diffusion towards the microgels. [paper bas] Abbreviations: HRP: horseradish peroxidase, PMMA: poly(methyl methacrylate). White scale bar: 1 cm. Black scale bar: 1 mm. [42]

Additionally, the concentration of H_2O_2 was found to be critical in microgel formation [42]. A too low H_2O_2 concentration resulted in incomplete crosslinking (Figure 20, left) leading to the formation of "broken" microgels, whereas excessive H_2O_2 concentration led to the crosslinking of not only the shell but also partially within the core of the core shell microgels (Figure 20, right).

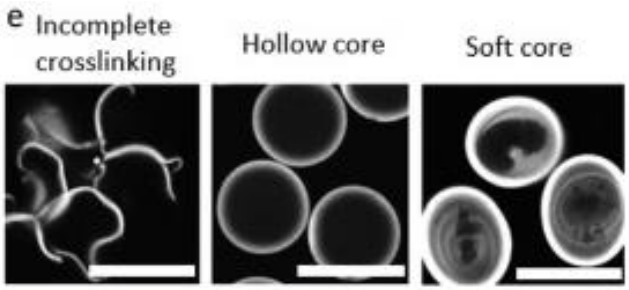

Figure 20: H_2O_2 concentration is of outmost importance for proper core shell microgel formation. Left: Low H_2O_2 concentration leads to incomplete crosslinking of the shell, Middle: The appropriate amount of H_2O_2 leads to the formation of microgels with a crosslinked shell and a liquid core, Right: High H_2O_2 concentration leads to the partial crosslinking of the core of the microgels. Scale bar: 100 µm [42].

4. Materials & Methods

4.1 Materials

Minimal essential medium α with nucleosides, penicillin, streptomycin, trypsin-EDTA, GlutaMAX, D-glucose (dextrose) and Insulin-Transferrin-Selenium (ITS) 100X were purchased from Gibco. Basic fibroblast growth factor (ISOKine bFGF) was purchased from Neuromics. Phosphate Buffered Saline (PBS) was purchased from Lonza. Dulbecco's Modified Eagle's Medium powder (DMEM powder without glucose, L-glutamine, phenol red, sodium pyruvate and sodium bicarbonate), Glycogen from bovine liver, Glycogen from oyster, D-(-)-Fructose, D-(+)-Mannose, Fluorescein Isothiocyanate-Dextran (average mol wt 2,000,000), Sodium Acetate, Sodium Butyrate, L-ascorbic acid 2-phosphate sesquimagnesium salt hydrate, Palmitic acid, Creatine monohydrate, L-aspartic acid, Sodium Pyruvate, α-Ketoglutaric acid, Linolenic acid, Linoleic acid, Oleic acid, Amyloglucosidase from Aspergillus niger, Dopamine Hydrochloride, Sodium Bicarbonate, Glyceraldehyde, n-hexadecane, Span80, hydrogel peroxide (H2O2), horseradish peroxidase (HRP), ascorbic acid (AsAP), calcein AM, ethidium homodimer-1 (EthD-1), Fetal Bovine Serum (FBS), CP-316819, Dulbecco's Phosphate Buffered Saline (DPBS) and Dextran were purchased from Sigma-Aldrich/Merck. Dextran was conjugated with tyramine moieties as described by T. Kamperman *et al.* [50]. Gelatin-Methacrylate (GelMA, 60% degree of functionalization, Df) was provided by the DBE research group and was synthesized following standardized protocol. Human phosphorylase glycogen liver form (PYGL) ELISA kit was purchased from Novus Biological. Human VEGF-A (Vascular Endothelial Cell Growth Factor A) ELISA kit was purchased from Elabscience. Sucrose was purchased from Albert Heijn. EVE™ Cell Counting Slides, EVE™ PLUS Automated Cell Counter and Trypan blue stain (0.4%) were purchased from NanoEntek. PrestoBlue™ cell viability reagent, Alexa Fluor™ 647 Tyramine Reagent, 2"-[4-ethoxyphenyl]-5-[4-methyl-1-piperazinyl]-2,5"-bi-1H-benzimidazole) (NucBlue, Hoechst) and Nalgene Filtration Products were purchased from Thermo Fischer Scientific. Collagen Type I (rat tail) was purchased from Corning. Fluorinated silane (Aquapel) was purchased from Vulcavite. Ruthenium (Ru) and sodium persulfate (SPS) were purchased from Advanced BioMatrix. Polydimethylsiloxane (PDMS, Sylgard 184) and Silicone Elastomer Curing Agent (Sylgard 184) were purchased from Dow Corning. UltraPure™ Agarose was purchased from Invitrogen/Life Technologies. MagnetOS (9x6mm) P21007B X100 was kindly provided by prof. dr. M.C. Kruijt from UMC Utrecht. Well plates and culture flasks for cell culture were purchased from Greiner Bio-One (Cellstar) and Avantor/VWR (VWR Tissue Culture plate). Millicell Cell Culture Inserts 24-well Hanging Inserts 3.0um PET were purchased from Sigma-Aldrich/Merck. Vivaspin 6 tubes were purchased from Sartorius. The Hypoxia Incubator and Glovebox Configuration of the Xvivo System, Model X3 was purchased from BioSpherix. Low pressure syringe pumps (neMESYS) were purchased from Cetoni. Gastight syringes (Hamilton) were purchased form IDEX Health & Science. Silicone tubing (inner diameter: 300µm, outer diameter: 640µm, thickness: 170µm) was purchased from Helix Medical.

4.2 Methods

4.2.1 Glycogen characterization

Dynamic Light Scattering (DLS) for glycogen particles size and charge distribution

Size and charge distribution measurements were conducted using the Zetasizer (Malvern Panalystical). A solution containing 0.025 mg/ml of glycogen in deionized water (DI H_2O) was pipetted into a DLS cuvette which was inserted into the zetasizer instrument. The experimental parameters used for both size and charge measurements were as follows: optical absorbance of 0.2, peak wavelength at 450 nm, and a refractive index of 1.687. to ensure robust data acquisition, each sample was measured five times, with 15 runs per measurement.

Osmolarity

The osmolarity of different glycogen and glucose solutions in PBS was measured with the K-7400S Semi-Micro Osmometer (Knauer).

Concentration measurements

Glycogen concentration in the supernatant was determined based on the principles of an H_2O_2 assay. The sample solution was mixed with Amyloglucosidase enzyme (15 U/ml) in MilliQ water at a 1:1 (v/v) ratio and incubated for 30 min at 37°C. Subsequently, the glycogen-enzyme mixture was combined with glucose oxidase (GOX) enzyme (400 U/ml) and incubated at room temperature for 20 min. To perform the assay, 10 µl of the resulting sample solution was mixed with 40 µl of 1X Reaction Buffer (5X reaction buffer: 0.25 M sodium phosphate, pH 7.4), and 50 µl Amplex Red-HRP solution, resulting in a final concentration of 0.2 U/ml HRP and $100x10^{-6}$ M Amplex Red. This mixture was further incubated for 30 min at room temperature, protected from light, after which fluorescence intensity was measured using a VarioskanLUX plate reader (Thermo Fischer Scientific) at excitation/emission wavelengths of 530/590 nm. Alternatively, but much more expensive option to measure glycogen concentration is by using the glycogen assay kit provided by Abcam. This assay kit was used before the development of the adjusted H_2O_2 assay.

Blocking phosphorylase activity

hMSCs were seeded with a density of 10,000 cells/cm^2 and allowed to adhere overnight. A stock solution of the blocker CP-316819, prepared at a concentration of 10 mM in 100% ethanol was used. The proliferation medium of the hMSCs was replaced with chemically defined medium containing oyster glycogen at a concentration of 1 g/L, supplemented with 30 µM blocker. hMSCs were subjected to anoxic conditions (0.1% O2). For three consecutive days, daily a ratio of 10 µl/ml of the blocker stock was added to the medium. Following this treatment, cell viability was assessed.

Conjugation with Alexa Fluor™ 647 Tyramine Reagent

Glycogen particles were conjugated to Alexa Fluor™ 647 Tyramine Reagent by mixing the Tyramine Reagent with a 1 g/L oyster glycogen solution with a 1:100 (v/v) ratio. The solution was transferred to a Vivaspin 6 tube, and placed on a roller bank at room temperature overnight. The solution remaining on the top of the filter was imaged using a confocal microscope (Zeiss LSM 880).

Mechanical characterization – Nanoindentation

Core shell microgels were mechanically characterized using nanoindentation (Optics11, Pavone) [41]. Indentation measurements were performed in PBS using a cantilever (spring constant 0.47 N m−1) with a glass colloidal probe (radius = 27 µm) attached to the tip. The probe was brought into close contact with the surface of the microgel and indentation was performed using the following indentation procedure: an indentation of 5000 nm (depending on the size of the gel) for 2 s followed by a 1 s holding and 2 s retraction time. The obtained indentation curves were fitted between 0 and 1500 nm indentation using the Hertzian model from which the effective elastic modulus was obtained, according to $P = 4/3\ E_{eff}R^{1/2}h^{2/3}$, where P is the applied load, E_{eff} is the effective Young's Modulus, R is the radius of the indentation tip, and h is the indentation depth. The elastic modulus (herein also referred to as stiffness) was calculated by $E = E_{eff}(1 - \nu^2)$, assuming a Poisson's ratio of $\nu = 0.5$.

4.2.2 Bulk hydrogel preparation

For the following, PBS was utilized for non-cell experiments such as glycogen release and compression tests, and media was used for cell-laden bulk hydrogels. In the case of cell-laden bulk hydrogels, the

media was replaced once after 30 min to remove any potential radicals formed during the crosslinking process.

GelMA hydrogel

GelMA bulk gels were prepared using a 10% GelMA solution with 2% Ru/SPS. GelMA and Ru/SPS were thoroughly mixed and pipetted into a wells plate. The plate containing the gels was then placed in a crosslinking chamber and exposed to visible light for 15 min at room temperature to initiate crosslinking. Afterwards, 500 µl PBS or media was added to the GelMA bulk gels.

DexTA hydrogel – Crosslinking with HRP and H_2O_2

DexTA bulk hydrogels were prepared using a 10% solution of DexTA with a 15% degree of substitution (DoS), 3 U/ml HRP and 0.03% H_2O_2 final concentrations. A solution of DexTA and HRP was prepared, supplemented with PBS or media to achieve the desired total volume. A small droplet of the H_2O_2 solution was pipetted into a well plate, followed by the addition of the DexTA-HRP solution. The mixture was quickly resuspended 4-5 times before gelation. After 5 minutes, 500 µl of PBS or media was added to the DexTA bulk hydrogels.

DexTA hydrogel – Crosslinking with Ru/SPS

DexTA hydrogels were prepared using a 10% solution of DexTA (15% DoS) and 2% of Ru/SPS. DexTA and Ru/SPS were mixed together and supplemented with PBS or media until the desired final volume was reached. Hydrogels of 40 µl were pipetted into a wells plate and allowed to crosslink in the crosslinking chamber under visible light for 15 min at room temperature. After crosslinking, 500 µl of PBS or media was added to the gel.

4.2.3 Chip production

The mold for the chip was printed with the Form 3B+ (Formlabs) using Clear V4 resin (Formlabs). After printing, the molds were post-treated. Microfluidic chips were made by pouring PDMS with a 10:1 (w/w) PDMS pre-polymer to curing agent ratio in the molds. Chips were degassed to remove possible air pockets, after which they were placed in a 60°C oven overnight. In-and outlets were made using an 1 mm puncher. Chips were oxygen plasma treated and bonded to a microscope glass slide, after which they were placed in the 60°C overnight.

4.2.4 Core shell microgel production

Before use, aquapel was introduced in the chips in order to make the channels hydrophobic. For core shell microgel formation a polymer solution was prepared from PBS with 10% DexTA (15% Degree of Substitution) and 80 U/ml HRP with and without glycogen/glucose. For glycogen/glucose encapsulation, the final concentrations varied (30 g/L, 50 g/L and 100 g/L). For the oil solution, N-hexadecane was used with 1% Span80. The flow rate ratios were varied to create microgels of different sizes. Final flow rates used were 80 µl/min for the oil solution and 10 µl/min for the polymer solution. Oil and polymer solutions were connected to the chips through flexible tubing at the designated inlets. On the other side of the chip, the tubing led the core shell microgels to an H_2O_2 diffusion bath for shell crosslinking, after which core shell microgels were collected in an Eppendorf tube. Core shell microgels were washed 4-5 times with N-hexadecane. N-hexadecane was removed, after which the emulsion was broken by adding PBS. On chip droplets and droplet formation were visualized with a stereomicroscope set-up (Nikon SMZ800 with Leica DFC300 FX camera). For post-crosslinking, core shell microgels were added to 500 µl PBS with 10 U/ml HRP and 3% H_2O_2 for 15 min. Afterwards, core shell microgels were washed thoroughly with PBS to remove any excess H_2O_2.

4.2.5 Core shell microgel characterization

Diameter and shell thickness

In order to determine the size distribution and the shell thickness of the core-shell microgels, they were stained with 15 µl/ml ethidium homodimer-1 in PBS. Microgels were incubated with the staining at 4°C overnight under constant rotation using a roller bank, covered from light. After incubation, core shell microgels were washed 3 times with PBS. For size measurements, microgels were imaged using the EVOS FL Imaging System, while for shell thickness measurements microgels were imaged using a confocal microscope (Zeiss LSM 880). Image analysis was done with ImageJ software. The shell thickness was determined by subtracting the lowest value from the highest value between the full width half maximum (FWHM) value of the intensity of the shell measured.

Glycogen release

Core shell microgels were prepared as described previously using various concentrations of glycogen from oyster or bovine, as well as glucose. To assess glycogen release, 10 µl of core shell microgels were mixed with 490 µl PBS. At specific time points, 250 µl of the supernatant was collected and replaced with fresh PBS. The glycogen concentration in the supernatant was determined using the procedure outlined in section 4.2.1.

Compression of glycogen-loaded core shell microgel-laden GelMA bulk gel

Compression testing of GelMA as well as glycogen-loaded core shell microgel-laden GelMA samples were performed with a rheometer (TA instruments HR20), equipped with a 8mm parallel plate (PP) setup. Disc shaped samples (1mm high, ϕ8mm), were prepared in Teflon molds and incubated over night in PBS to allow for full hydration. Samples were brought to 37°C prior to the measurements. All samples were compressed with a constant rate of 10 µm/s at 37°C to a depth of 10%, 20%, 30%, and 40% compressive strain, subsequently. Obtained stress/strain curves were fitted between 30-40% strain to obtain the elastic modulus.

4.2.6 Cell expansion

Human mesenchymal stem cells (hMSCs), D72, were cultured in standard proliferation medium consisting of α-MEM, supplemented with 10% (v/v) FBS, 100 U/ml penicillin, 100 mg/ml streptomycin, 2 mM L-glutamine, 0.2 mM ascorbic acid and 1 ng/ml fibroblast growth factor (FGF). Cell were cultured at 37°C and under 5% CO_2 in T300 flasks. Medium was replaced twice a week. When cells reached a confluency of ~80%, cells were detached with 0.25% (v/v) Trypsin-EDTA at 37°C and passaged or used for experiments. Cells were used from passage 3 to 7. For 2D culture experiments, cells were seeded at a density of 10,500 cells/cm^2 for a 24-wells plate and 31,250 cells/cm^2 for a 96-wells plate. For 3D culture experiments, $3x10^6$ cells/ml were used. For the experiments, hMSCs were placed in standard proliferation medium or chemically defined medium. Chemically defined medium was prepared by adding 8.3 g/L DMEM powder, 3.7 g/L sodium bicarbonate, 100 U/ml penicillin and 100 mg/ml streptomycin to distilled water. This medium was filtered with Nalgene Rapid-Flow sterile disposable filter units for sterilization prior to use.

4.2.7 Viability analysis

Cell viability was analyzed using calcein AM (live) and ethidium homodimer-1 (dead) staining, following protocol provided by the supplier. Imaging of stained cells was done with the EVOS FL Imaging System, a digital fluorescence microscope. Images were taken at a desired magnification and live/dead cells were counted for each condition to determine the % viability.

4.2.8 Metabolic activity analysis

Cell metabolic activity was analyzed using a PrestoBlue assay, whereby 10% PrestoBlue reagent (10% of total volume, after adding the reagent) was directly added to the medium surrounding the cells or cell-laden hydrogels. Incubation was carried out in an incubator, at 37°C and 5% CO_2. The duration of incubation varied depending on the experiment (90 min for 2D cultures and GelMA gels, and 4h for collagen-based gels). After incubation, the medium containing the reagent was removed and transferred to a 96-wells for fluorescence analysis (excitation/emission: 560/590nm) with the Victor$^3{}_{TM}$ 1420 Multilabel Counter. Fluorescence readings were normalized and plotted accordingly.

4.2.9 VEGF and glycogen phosphorylase enzyme release

VEGF and glycogen phosphorylase enzyme release were analyzed using a Human VEGF-A (Vascular Endothelial Cell Growth Factor A) and a Human Glycogen Phosphorylase liver form (PYGL) ELISA kit, respectively, following suppliers protocol.

4.2.10 Metabolite analysis

Metabolite analysis (metabolic library) was conducted by seeding hMSCs in a 96 well plate and allowing them to attach in standard proliferation medium for approximately 24h at 37°C and 5% CO_2. After complete attachment, the proliferation medium was replaced with chemically defined (metabolite-free) medium supplemented with a single metabolite for each experimental condition. Proliferation medium and chemically defined medium without any metabolites served as positive and negative controls, respectively. The metabolites were tested under both normoxic (21% O_2) and anoxic (0.1% O_2) conditions at three different concentrations (5.5, 0.55 and 0.055 mM). Cell viability was assessed on days 3, 5 and 7. Further details can be found in supplementary material 2.

4.2.11 Effect of glycogen-loaded core shell microgels on hMSC viability

hMSCs were seeded in a 24 wells plate and allowed to attach in standard proliferation medium for 24h. Following attachment, the proliferation media were removed, and fresh proliferation medium (as a positive control), chemically defined medium (metabolite free, as a negative control) or chemically defined medium with 1 g/L free oyster glycogen (as a positive control) were added. To investigate the impact of core shell microgels on hMSCs (without encapsulated glycogen, with 30 g/L and 100 g/L encapsulated glycogen, and post-crosslinked 30 g/L encapsulated glycogen), transwell (Millicell Cell Culture Inserts) were used. For these conditions, the proliferation medium was replaced with chemically defined medium and 20 µl of core shells were introduced into the transwell, which was then placed within the wells. Subsequently, the cells were subjected to anoxic conditions (0.1% O_2). Cell viability, cell metabolic activity and VEGF release were determined on day 7. On top of that, also glycogen phosphorylase enzyme release and remaining glycogen concentration in the medium were measured on the same day.

4.2.12 3D tissue formation (GelMA and collagen)

GelMA bulk hydrogel

GelMA bulk hydrogel was prepared with hMSCs and glycogen-loaded core shell microgels. The hydrogel was prepared by combining 10% GelMA, 2% Ru/SPS, $3x10^6$ cells/ml and 25% (v/v) glycogen-loaded core shell microgels (100g/L). The obtained solution was thoroughly mixed and 40 µl of the gel mixture was pipetted into a well plate. The plate was then placed in a crosslinking chamber and exposed to visible light for 15 min to initiate crosslinking. After crosslinking, media were added, which was replaced 30 min later to remove possible radicals generated during the crosslinking process. For the conditions involving chemically defined medium, the medium was supplemented with 10% ITS to

prevent hydrogel degradation by the cells caused by the absence of serum. The hydrogels were immediately placed in the XVivo system, and metabolic activity was analyzed on day 7.

Collagen bulk hydrogel

Collagen bulk hydrogels were prepared with hMSCs and glycogen-loaded core shell microgels. Collagen gel was prepared following the suppliers protocol. This involved combining 10% 10X PBS, 3 mg/ml collagen and 0.74% 1N NaOH in an Eppendorf tube, followed by the addition of $3x10^6$ cells/ml and 25% (v/v) glycogen-loaded core shells (100 g/L). The solution was thoroughly mixed, and 10µl of the gel mixture was pipetted into a well plate. The plate was placed in the incubator for 30 min for complete gelation, after which media were added. For the hydrogels placed in chemically defined medium, the medium was supplemented with either 10% FBS or 1% FBS and 9% ITS. The collagen gels were immediately transferred to the XVivo system (for anoxic conditions), and cell viability, metabolic activity, VEGF release and glycogen concentration in the medium were measured on day 7.

Collagen/GelMA bulk gel with hyaluronic acid blocks

Hydroxyapatite (HA) blocks (MagnetOS P21007B) were sterilized for 3h at 160°C prior to use. For incorporation of the blocks into GelMA or collagen cell-laden hydrogels, HA fragments were used to limit the amount of cells and materials required. HA fragments were placed in the center of a well, after which the either GelMA or collagen gel was pipetted on top of it. GelMA/collagen gel was prepared as described earlier.

4.2.13 Statistics

Statistics were performed with Origin Pro 2023 software. In the graphs, values are given as the mean value ± standard deviation. Normality was checked with the Shapiro-Wilk normality test. For normally distributed data, significance was checked with a Pair-Sample t-Test, while for non normal distributed data this was checked with a Mann-Whitney Test. Cell experiments had a sample size of n=3. For core shell microgel characterization, the mean value is given with the ± standard deviation, and for size measurements the coefficient of variation (CV) value was calculated as well. For core shell microgel characterization regarding size and shell thickness the sample size was 30 microgels. For the nanoindentation the sample size was 25 microgels.

4.2.14 Schematics & Graphs

All schematics were made with Biorender.com, and figures were made with Microsoft PowerPoint. All graphs were made using Origin Pro 2023 software (learning version).

5. Results & Discussion

5.1 Nutrients ensure cell survival under anoxic conditions

The viability of human mesenchymal stem cells (hMSCs) was examined under different culture conditions to determine the effects of oxygen tension and nutrient availability. hMSCs were cultured using either standard proliferation medium or chemically defined medium, and viability was assessed on days 3, 5, and 7. The results are presented in Figure 21.

When cultured in the presence of sufficient nutrients and serum (standard proliferation medium), hMSCs showed a consistently high level of viability over the course of one week regardless the oxygen tension. On day 7, the cell viability was found to be 97.83 ± 0.50% and 98.26 ± 0.40% for normoxic and anoxic conditions, respectively.

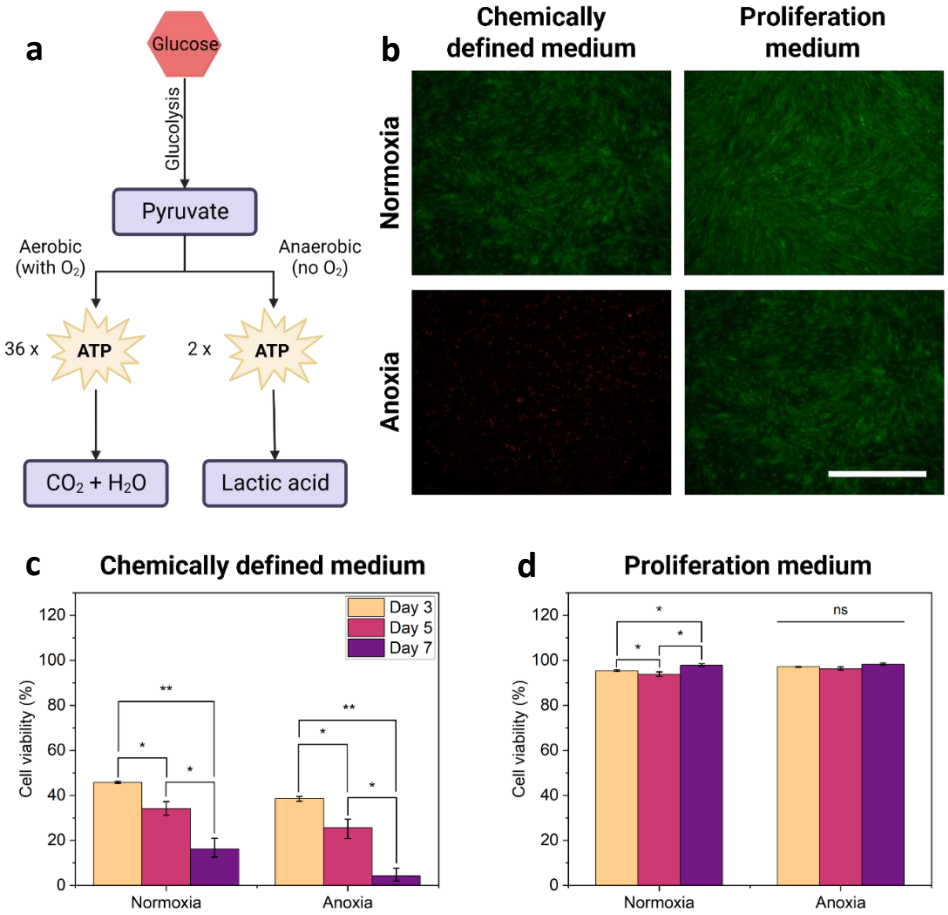

*Figure 21: Nutrients are essential for the maintenance of high human mesenchymal stem cell (hMSC) viability. A) Simple schematic of the metabolism of glucose in the presence and absence of oxygen. B) Live/Dead images on day 7 of hMSCs cultured in normoxia and anoxia with chemically defined medium and proliferation medium. Green: live (calcein AM), Red: dead (ethidium homodimer-1). Scale bar: 1000 µm. C) hMSC viability when cultured in chemically defined medium in normoxia and anoxia. D) hMSC viability when cultured with standard proliferation medium in normoxia and anoxia. ATP: adenosine triphosphate. Ns: non-significant p>0.05, *: p≤0.05, **: p≤0.01, n=3. Normally distributed data: Pair-Sample t-test. Non-normal data: Mann-Whitney test. Values presented in C) and D) are given as means ± SD.*

However, when cultured in the absence of nutrients and serum (chemically defined medium), the cell viability decreased significantly already on day 3 of culture, regardless of the oxygen tension. The cell viability continued to decrease until day 7, reaching a viability of 16.29 ± 3.49% and 4.39 ± 2.42% for normoxic and anoxic culture conditions, respectively. The difference in cell viability here between normoxic and anoxic conditions on day 5 and 7 can be explained by the adaptive metabolic changes

exhibited by hMSCs. Under low oxygen tensions, hMSCs show an increase in glycolysis [51]. However, since hMSCs in this condition do not receive any nutrients, the increased glycolysis is unable to sustain their viability. Consequently, hMSCs deplete their internal reservoirs even quicker leading to earlier cell death than when cultured under normoxia.

Overall, these results align with the theoretical principles of ATP production in aerobic and anaerobic respiration, as discussed previously in section 2.1 (Figure 5) and indicate the critical role of nutrient and serum availability in maintaining cell viability, irrespective of the oxygen tension.

5.2 Glycogen can function as long term metabolic substrate for cell survival

The survival of hMSCs is compromised in the absence of nutrients. When nutrients are present, like when cultured with standard proliferation medium, hMSCs are able to maintain a high cell viability irrespective of the oxygen tension. However, conventional media (e.g. DMEM, α-MEM), are often supplemented with fetal bovine serum (FBS). The components of FBS have not been fully identified, and conventional media contain a variety of components, hindering the identification of the specific nutrients responsible for maintaining long-term cell viability [52]. To address this, a metabolic library was established to investigate the impact of a diverse range of metabolites on hMSC viability. Supplementary material 2 provides an explanation for the selection of the tested metabolites. These metabolites were supplemented in chemically defined medium and administered to hMSCs, which were subsequently cultured under normoxic or anoxic conditions (Figure 22a).

At a concentration of 5.5 mM, only glycogen, mannose, and glucose showed to be promising for sustaining long-term hMSC survival under normoxic conditions. Similarly, under anoxic conditions, glycogen, mannose, and glucose, but also fructose, and pyruvate showed potential for promoting hMSC viability. It is not surprising that these molecules stand out. Glucose is the primary energy source in the human body, and pyruvate is the final product of the glycolysis pathway before ATP production (for further details refer to section 2.1 and 3.1.2). The other candidates, are sugars, just like glucose is (see supplementary material 2 for additional information). Interestingly, glutamine and α-ketoglutarate were able to sustain cell viability to a certain level. Glutamine is mostly taken up by highly proliferating cells (e.g. cells lining the gut) and used as an energy source [53]. The positive effect of α-ketoglutarate on cell viability is hard to explain, as it requires the presence of alanine for ATP production (supplementary material 2). As the hMSCs are solely supplied with one metabolite, there is no alanine present in the medium (the DMEM powder used for chemically defined medium does not contain alanine), and thus should be secreted by the cells. However, as alanine is a non-essential amino acid, this seems unlikely, and thus viability of hMSCs under culture of solely α-ketoglutarate cannot be completely explained [54].

Considering that 5.5 mM represents a healthy glucose concentration in humans, lower concentrations of the metabolites were also investigated to determine their ability to ensure cell viability when available in reduced amounts. Notably, glycogen emerged as the only candidate for hMSC survival, even at a concentration of 0.55 mM, both in the presence and absence of oxygen. Within the cell, glycogen can be broken down to glucose molecules, providing a continuous supply of glucose in times of need (see section 3.1.2). However, it is observed that hMSCs exhibit the ability to sustain viability in the presence of exogenous glycogen, thereby indicating their capacity to enzymatically breakdown extracellular glycogen through the secretion of enzymes. To assess the possibility of enzyme secretion by hMSCs for extracellular glycogen degradation, culture media were analyzed to detect the presence of glycogen phosphorylase (PYGL, glycogen phosphorylase liver form) using a PYGL ELISA kit. The

results can be found in supplementary material 5, Figure 38. Upon culturing hMSCs with freely available glycogen, secretion of glycogen phosphorylase was observed by hMSCs. Furthermore, the levels of glycogen phosphorylase in the culture media increased with increasing cell seeding density, thereby suggesting that all hMSCs possess the capacity to secrete the enzyme for extracellular glycogen degradation. Consequently, this enzymatic activity enables hMSCs to utilize exogenous glycogen as an energy source, thereby promoting their survival.

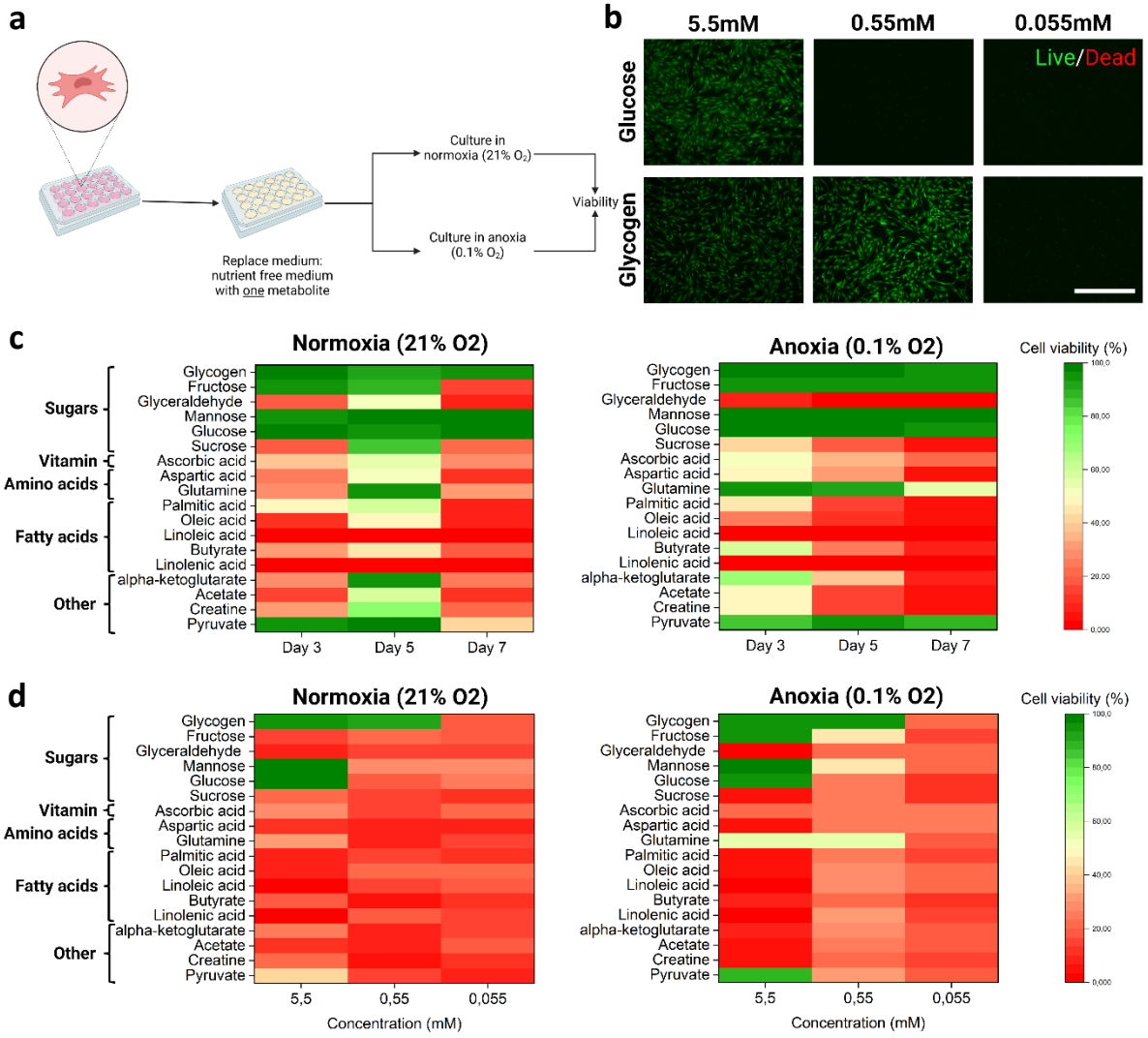

Figure 22: A metabolic library was established to screen a variety of nutrients. A) Schematic overview of the experimental setup. B) Live/Dead images of human mesenchymal stem cells (hMSCs) cultured under anoxic conditions (0.1% O2) in chemically defined medium supplemented with either glucose or glycogen. Green: Calcein AM, red: Ethidium Homodimer-1. C) Cell viability results on day 3, 5, and 7 for all metabolites tested at a concentration of 5.5 mM in normoxic and anoxic conditions. D) Cell viability measured on day 7 for 5.5, 0.55 and 0.055 mM for all metabolites in normoxic and anoxic conditions. Scale bar: 1000 µm.

5.3 Glycogen is non-toxic for hMSCs

As shown in section 5.2, glycogen emerges as the most promising candidate for ensuring long-term survival of hMSCs under anoxic culture conditions. To validate this, hMSCs were subjected to culture conditions involving varying seeding densities while maintaining a fixed glycogen concentration. A second set of culture conditions involved a fixed seeding density while employing different glycogen concentrations.

In the case where the glycogen concentration was held constant, it was observed that hMSC viability remained high (>80%) across all seeding densities until day 7 (Figure 23). However, on day 14, the cell viability decreased to 44.85 ± 18.03% and 73.57 ± 1.09% for the two lowest seeding densities (2,000 and 5,000 hMSCs, respectively). On the other hand, the viabilities for the seeding densities of 10,000 and 20,000 remained high, measuring 87.02 ± 2.87% and 81.72 ± 2.91% respectively on day 14. The lower cell viability observed for the lower two cell densities could be attributed to either an insufficient cell seeding density or an excessive glycogen concentration, which could potentially exhibit toxicity towards hMSCs.

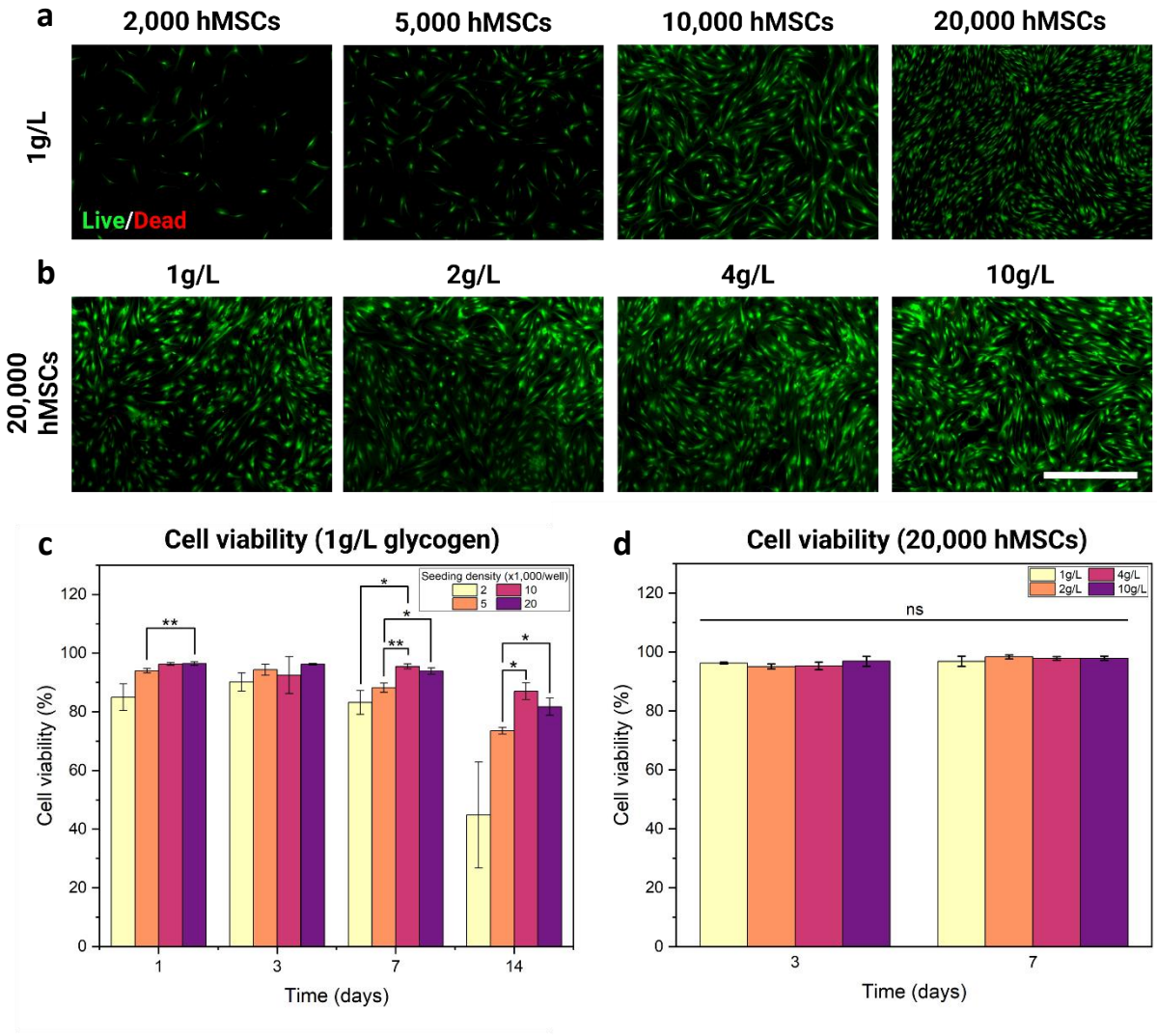

*Figure 23: Glycogen is not toxic for human mesenchymal stem cells (hMSCs) in anoxic conditions. A) Live/Dead images of hMSCs cultured at different seeding densities with 1 g/L free glycogen in chemically defined medium on day 7. B) Live/Dead images of hMSCs cultured with different glycogen concentrations (seeding density: 20,000 cells/well) on day 7. Green: Calcein AM, Red: Ethidium Homodimer-1. Scale bar: 1000 µm. C) Cell viability graph of hMSCs cultured at different seeding densities with 1g/L free glycogen. D) Cell viability graph of hMSCs cultured with different glycogen concentrations (seeding density: 20,000 cells/well). Ns: non-significant p>0.05, *: p≤0.05, **: p≤0.01, n=3, Pair-Sample t-test. Values presented in C) and D) are given as means ± SD. For C) All other conditions holds: non-significant.*

To explore the possibility of glycogen-induced toxicity at higher concentrations, different glycogen concentrations were assessed. When hMSCs were seeded at a density of 20,000 cells/well, their viability remained almost unaffected by increasing the glycogen concentration over a one week period. Interestingly, the glycogen concentration appeared to have no noticeable impact on cell viability, as all tested glycogen concentrations yielded comparable viability results on both day 3 and day 7 under anoxic conditions. This phenomenon can be attributed to the ability of hMSCs to utilize glucose

molecules during times of metabolic demand. This suggests that glucose is released in a controlled manner by the degradation of glycogen, likely regulated by cellular processes (for more information refer to section 3.1.1). The examination of glycogen toxicity was also conducted under normoxic conditions (for detailed refer to supplementary material 8).

5.4 Breakdown of glycogen is a cell-driven process

As previously described in section 3.1.2, the enzymatic degradation of glycogen to glucose follows multiple sequential steps. In theory, blocking one of these steps should hinder glycogen breakdown, resulting in the absence of glucose release (Figure 24 a). Since cells utilize glucose rather than glycogen, as an energy source (refer to section 2.1 for more information), the inability to break down glycogen should lead to significant cell death within a short time frame [55]. Indeed, when hMSCs are cultured in a chemically defined medium supplemented with 0.001 g/L glycogen, the cell viability remains nearly 100%. However, when a phosphorylase inhibitor (CP-316819) is introduced to the medium, cell viability decreases to approximately 20% within just three days of culture (Figure 24 b). The presence of viable cells following the introduction of the phosphorylase inhibitor suggests a phenomenon that can be simply explained by the continuous secretion of various enzymes, including glycogen phosphorylase, by the cells. Although the inhibitor effectively blocks the functionality of secreted

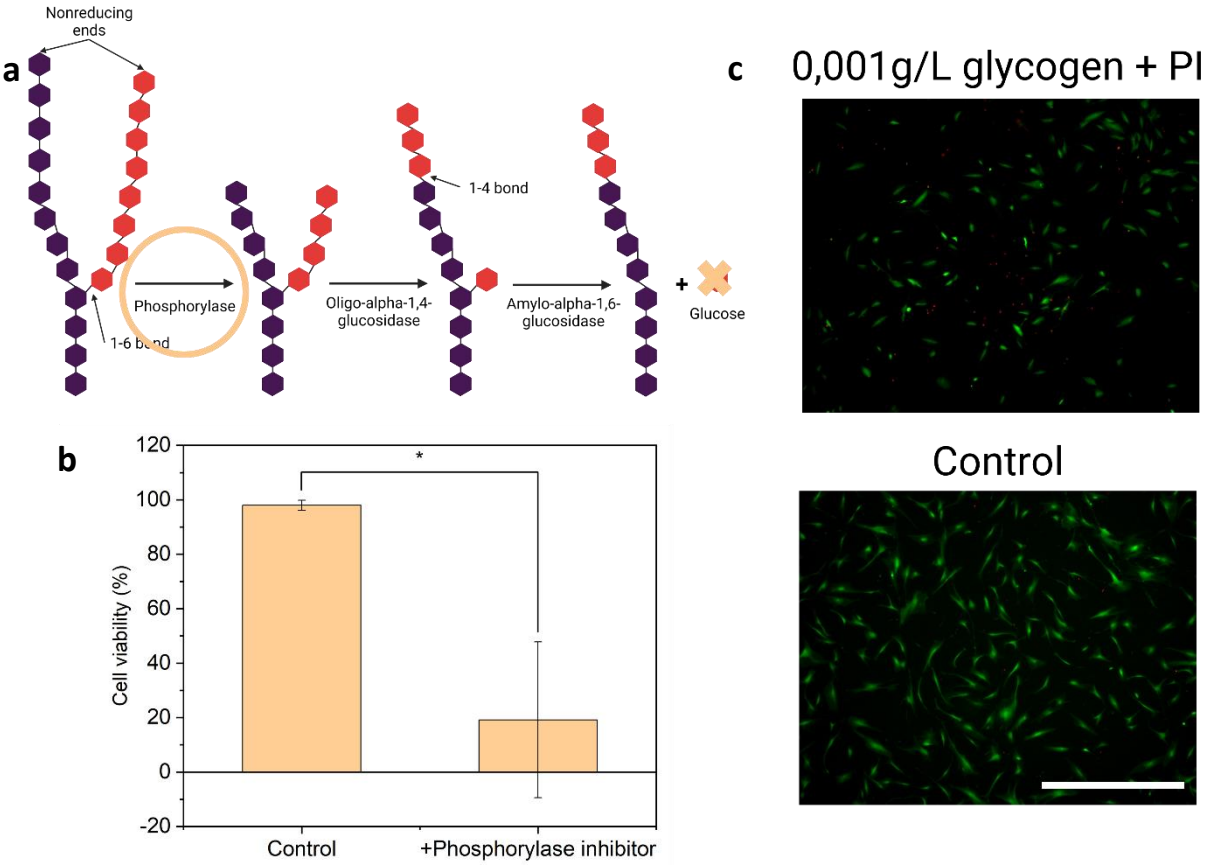

*Figure 24: The breakdown of glycogen to glucose is a cell mediated process. A) Schematic representation of the enzymes acting on a strand of glucose molecules in the glycogen nanoparticle for the release of glucose. When the activity of the phosphorylase enzyme is blocked, no glucose will be released. B) human mesenchymal stem cells (hMSCs) cultured with 0.001 g/L glycogen show a high cell viability on day 3, while when the phosphorylase activity is blocked, cell viability is decreased to less than 20%. C) Live/dead images of hMSCs cultured with 0,001 g/L glycogen and phosphorylase inhibitor (PI) and control condition (chemically defined medium with 0.001 g/L glycogen). Scale bar: 1000 µm. *: p≤0.05, Mann-Whitney test, n=3. Values presented in B) are given as means ± SD.*

phosphorylase, the surviving cells continue to secrete new enzymes, which, in turn, are inhibited. This pattern persists until a stage is reached where the inhibitor is depleted, while the remaining living cells continue with the secretion of glycogen phosphorylase. Therefore, fresh inhibitor is supplemented into the culture medium on a daily basis. Nonetheless, it is plausible that the provided quantity of inhibitor may be inadequate, and multiple supplementation moments throughout the day can be considered in further experiments.

5.5 Oyster and bovine glycogen can be encapsulated in DexTA hydrogel without being released

As explained in section 3.1.3, glycogen differs in size for different organisms and tissues of origin. To investigate potential variations in glycogen size among batches from the same origin, three different batches of oyster glycogen were analyzed. The size of glycogen particles exhibited slight variations, measuring 32.24 ± 1.88 nm, 30.81 ± 1.49 nm, and 32.45 ± 1.23 nm for the respective batches (Figure 25a). Additionally, the size comparison between oyster and bovine glycogen was also assessed, revealing a size of 16.65 ± 0.17 nm for bovine glycogen (Figure 25a). These findings align with relevant literature (see also Figure 9).

To be able to better characterize the glycogen molecules in terms of possible morphological differences, osmolarity measurements were conducted on glucose, oyster glycogen, and bovine glycogen at three different concentrations (1, 10, and 50 g/L) in PBS. Regarding oyster glycogen, osmolarity measurements were solely performed on the first batch. Glucose exhibited osmolarities of 4.33 ± 0.47, 60.67 ± 0.00, and 294.00 ± 2.49 mOsm for the three concentrations, respectively. For oyster glycogen, the osmolarity values were 0, 0.22 ± 0.31, and 23.67 ± 0.82 mOsm, while for bovine glycogen they were 0, 0.22 ± 0.31, 26.33 ± 2.05 mOsm for the three concentrations respectively (Figure 25b). The observed increase in osmolarity with increasing concentration aligns with the expectations. Notably, the solutions containing glucose exhibit the highest osmolarity, while bovine and oyster glycogen solutions display considerably lower and similar osmolarities. This difference in osmolarity can be attributed to the presence of a greater number of osmotically active molecules in the glucose solution [56, 57]. It is important to note that the same concentrations were employed for glucose and the two types of glycogen. Given that glycogen is composed of multiple glucose molecules, the overall quantity of molecules present in the glycogen solutions is lower relative to the glucose solution, elucidating the higher osmolarity observed in the glucose-containing solution. Interestingly, the glycogen solutions exhibit similar osmolarities, irrespective of the difference in size between oyster and bovine glycogen. This finding potentially provides insights into the molecular morphology of glycogen. The comparable osmolarities suggest a comparable number of glycogen molecules within the solutions, implying that the difference in size could be attributed to a denser packing arrangement of the bovine glycogen molecule in comparison to oyster glycogen molecules.

Additionally, the charge of glycogen molecules was assessed to check for potential interactions with materials like gelatin and dextran. The charge measurements for the three batches of oyster glycogen were -0.00523 ± 0.063476, -0.0899 ± 0.064186 and -0.00568 ± 0.089619 mV, respectively. For bovine glycogen, the charge was determined to be 0.007668 ± 0.030628 mV (Figure 25c).

Based on the previously described size measurements, it is hypothesized that glucose molecules are too small to be encapsulated over a long time period within a gel matrix, and the prolonged encapsulation of bovine and oyster glycogen will be determined by the pore size characteristics of the hydrogels employed. To explore this, two different types of hydrogels were investigated: a gelatin

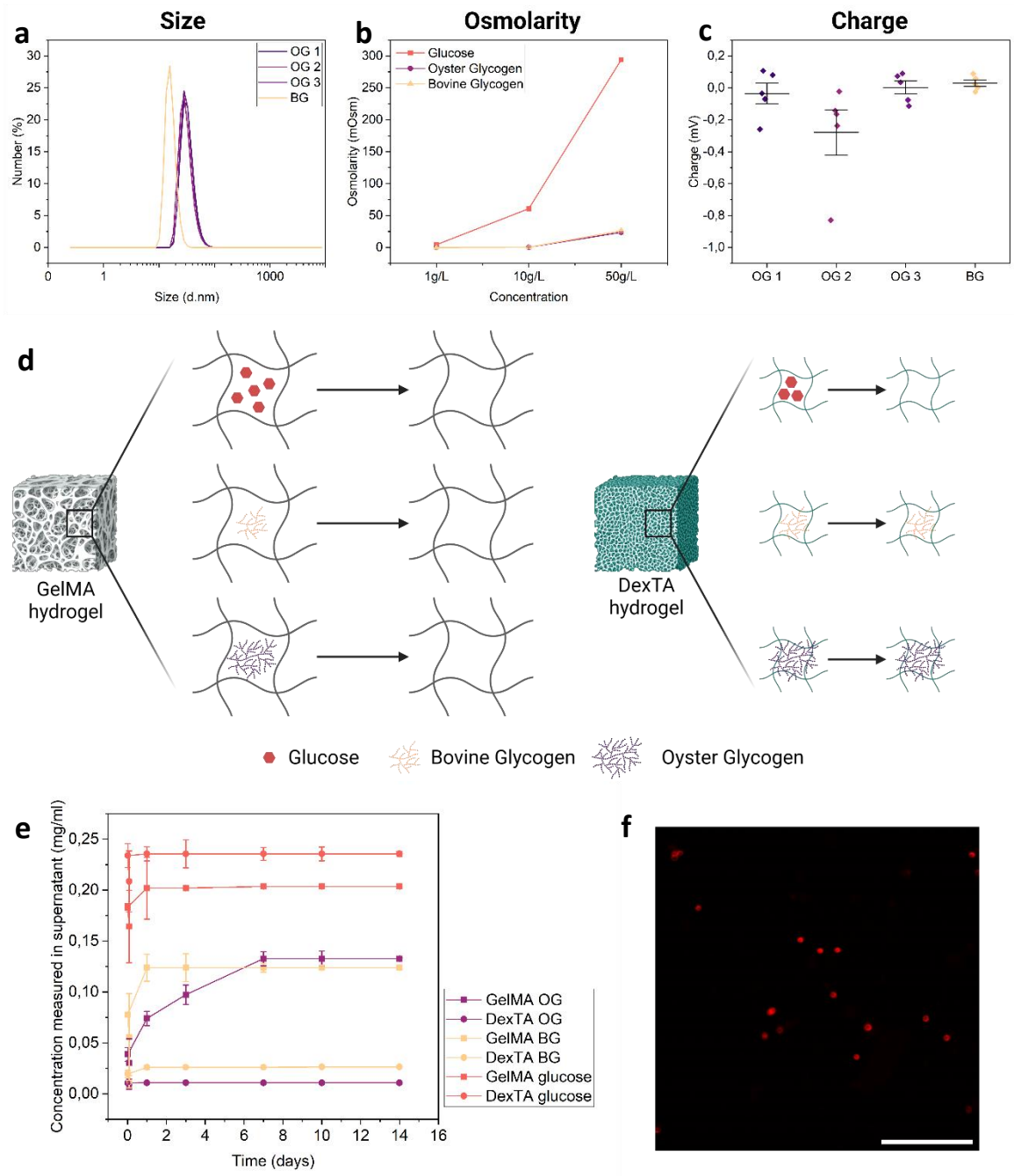

Figure 25: Glycogen characterization and encapsulation in bulk hydrogels. A) Size distribution of three different batches of oyster glycogen and one batch of bovine glycogen. B) Osmolarity of three concentrations of glucose, oyster glycogen (corresponding to OG1 of size and charge measurements) and bovine glycogen in PBS. C) Charge distribution of three batches of oyster glycogen and one batch of bovine glycogen. D) Schematic representation of the possibility of long-term encapsulation of bovine and oyster glycogen in DexTA bulk gel due to the molecules being bigger in size compared to glucose (~1.5 nm)[u12] and due to smaller pore size in DexTA hydrogel compared to GelMA hydrogel. E) Glucose, oyster glycogen and bovine glycogen release from GelMA and DexTA bulk hydrogels over time. F) Conjugation of oyster glycogen to Alexa Fluor™ 647 (red) Tyramine Reagent for glycogen visualization. Scale bar: 200 µm. Abbreviations in figure: GelMA: Gelatin methacrylate, DexTA: Dextran-tyramine, OG: Oyster glycogen, BG: Bovine glycogen. For A) and C) n=5, for B) and E) n=3. Values presented in B), C) and E) are given as means ± SD.

methacrylate (GelMA) hydrogel and a dextran-tyramine (DexTA) hydrogel. Gelatin-based hydrogels typically exhibit larger pore sizes (80-120 µm [58], 187.9 ± 4.7 µm for 10% GelMA [59]), whereas dextran-based hydrogels feature smaller pore sizes (6.25-7 µm for dextran-based [59], 0.065-10 µm dextran acrylate hydrogels [60]). Within each hydrogel, oyster glycogen, bovine glycogen, or glucose

was encapsulated, and their release profiles were monitored over time. The release patterns are shown in Figure 25e. Glucose is released almost immediately from both hydrogel matrices, which is not surprising considering its small size. When encapsulated in GelMA, approximately half of the encapsulated oyster and bovine glycogen was released over a two-week period. In contrast, when encapsulated in a DexTA hydrogel, oyster glycogen remained entirely confined within the gel, while only a small fraction of bovine glycogen was released. This can be explained by the size of the encapsulated molecules and the pore dimensions of the hydrogels used. The larger pore sizes in the GelMA hydrogel facilitate the faster release of the encapsulated molecules, compared to when encapsulated in DexTA hydrogel, exhibiting smaller pore sizes. Consequently, glucose, due to its very small size (~1.5 nm [61]) is still released quickly from the DexTA hydrogel, whereas bovine and oyster glycogen are effectively retained within the gel matrix. Notably, oyster glycogen displays limited release compared to bovine glycogen, likely owing to its larger size (Figure 25a). Thus the encapsulation of oyster glycogen within a DexTA hydrogel matrix proposes the most promising combination for achieving long-term glycogen encapsulation.

To examine the feasibility of glycogen visualization using a confocal microscope, glycogen was conjugated with Alexa Fluor™ 647 Tyramine Reagent. The visualization of glycogen could give insights in the distribution of glycogen molecules throughout the hydrogel matrix. The resulting confocal microscopy image in Figure 25f reveal the successful visualization of present oyster glycogen particles. Importantly, the Alexa Fluor™ 647 Tyramine Reagent did not induce any background staining on its own after proper washing (see supplementary material 10). Other methods for glycogen visualization were investigated as well. However, the majority of available staining methods for glycogen exhibit specificity towards sugars rather than glycogen itself. Consequently, these staining options pose challenges as they tend to stain the dextran present in the DexTA hydrogel, resulting in non-selective staining of both glycogen and the entire hydrogel structure.

5.6 To ensure cell survival, glycogen in solution is required

The DexTA hydrogel loaded with oyster glycogen has been identified previously as the best combination for long-term encapsulation. Consequently, hMSC- and glycogen-loaded DexTA hydrogels were prepared. Two key experimental conditions were examined: the encapsulation of oyster glycogen within the DexTA hydrogel, and the supplementation of oyster glycogen to chemically defined medium. On day 7, the number of live hMSCs was assessed, while cell viability could not be determined due to the confounding effect of DexTA staining with ethidium homodimer-1 as a marker for dead cells.

As depicted in Figure 26, the positive control (standard proliferation medium) and glycogen in chemically defined medium exhibited (also acting as a positive control) the highest count of viable cells, while the cell count drastically decreased for encapsulated glycogen and reached 0 in the negative control group (chemically defined medium with no supplementation). These findings may be attributed to the complex degradation process of glycogen (refer to section 3.1.2 for more information), wherein limited enzymatic space within the dense DexTA hydrogel matrix may hinder proper enzyme functionality. However, when glycogen is freely available in the surrounding medium, the enzymes have plenty of space to effectively break down the glycogen into glucose. However, these are only speculations and have not been scientifically proven yet. Also, it should be noted that as this experiment contained only one sample per condition, and as the viability could not be determined, the results should be questioned and no conclusions can be drawn.

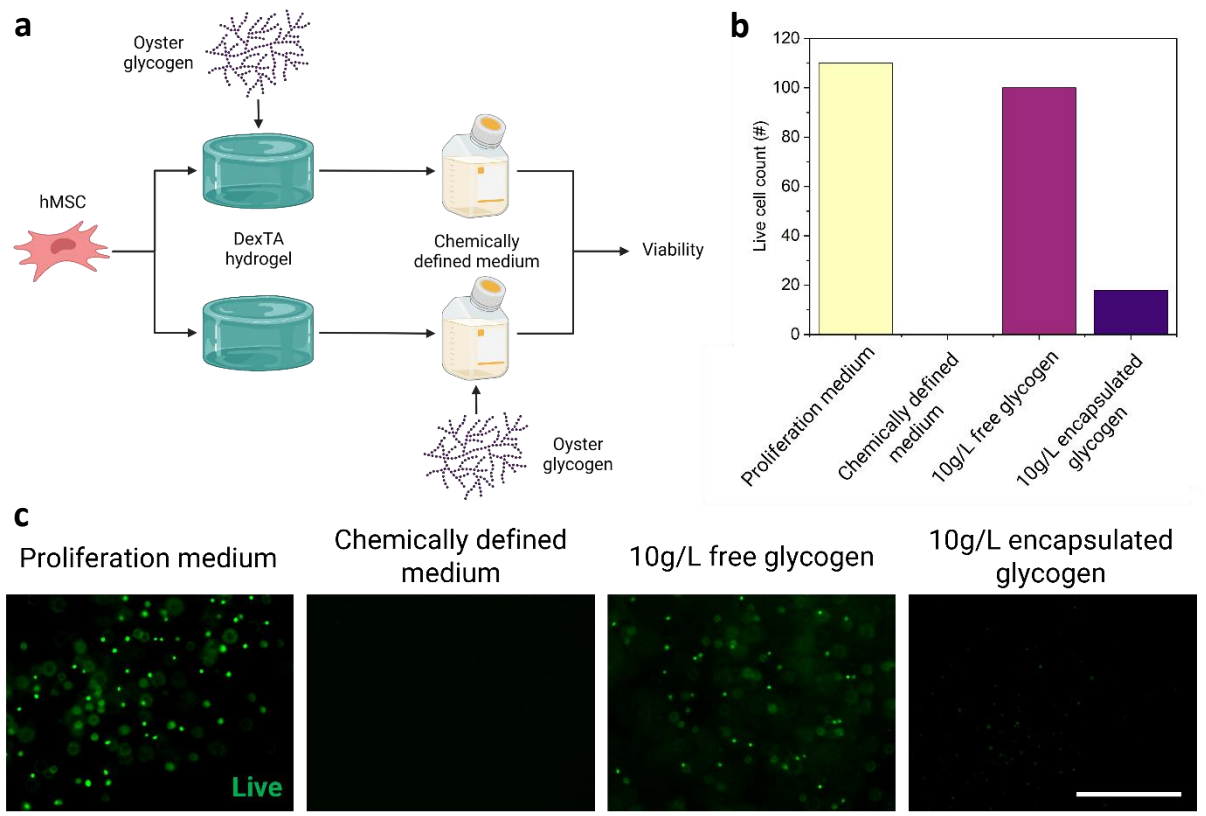

Figure 26: Glycogen should be free in solution for human mesenchymal stem cells (hMSCs) to survive. A) Schematic overview of experimental set up. B) Live cell count of the conditions tested. Only one sample was tested per condition. C) Live images of conditions tested. Live: green (calcein AM). Scale bar: 400 µm. Abbreviations in figure: hMSC: human mesenchymal stem cell, DexTA: Dextran Tyramine. No statistical analysis was performed as the experiment was conducted with n=1.

5.7 Production of hollow core glycogen-containing microgels to give the enzyme a space to function

Section 5.6 revealed that glycogen, when encapsulated within a dense hydrogel matrix, can not be utilized by hMSCs to sustain their survival. Glycogen in solution however, has been demonstrated promising in multiple experiments (Figure 22 and Figure 23). The challenge that arises therefore, lies in the encapsulation of glycogen within a suitable material (preferably DexTA as was concluded in section 5.5) wherein it can exist in a soluble form, providing sufficient space for enzymatic glycogen breakdown. A proposed solution entails the fabrication of core shell microgels, characterized by a liquid core within a crosslinked shell, effectively separating them from their environment [42]. The incorporation of glycogen within the liquid core of these microgels enables its encapsulation while still maintaining a soluble state, thereby providing the space for efficient enzymatic glycogen degradation.

Core shell microgels were fabricated on a microfluidic chip and subsequently crosslinked in an H_2O_2 solution. To achieve optimal core shell formation, different flow rate ratios of a polymer solution (DexTA with HRP) to oil (hexadecane with 1% Span80) were investigated. Supplementary material 12 contains information regarding the initial steps of core shell microgel fabrication. However, it is important to note that attempts to optimize the process by introducing glycogen into the polymer solution were unsuccessful. Additional information on this matter can be found in supplementary material 13.

The determination of the optimal oil flow rate was carried out through the initial production of core shell microgels in the absence of glycogen. These microgels were subsequently assessed in terms of their morphology, size distribution, and degree of crosslinking. Notably, the assessment of crosslinking focused solely on the shell component, as crosslinking of the core would eliminate the presence of a liquid core. Following the successful fabrication of core shell microgels, the exact same flow rate ratios were employed for the encapsulation of glycogen. The resulting microgels were evaluated. Interestingly, it was observed that the encapsulation of glycogen required higher flow rates to ensure successful production of microgels.

Following a series of trial and error experiments, an oil flow rate of 80 µl/min was determined to be optimal for both empty and glycogen-loaded core shell microgels. Figure 27c illustrates the bright field images of the core shell microgels produced at an oil flow rate of 80 µl/min and polymer solution flow rates of 6, 8, and 10 µl/min. Supplementary material 11 provides additional information regarding core shell microgels formed with alternative flow rates for the polymer solution.

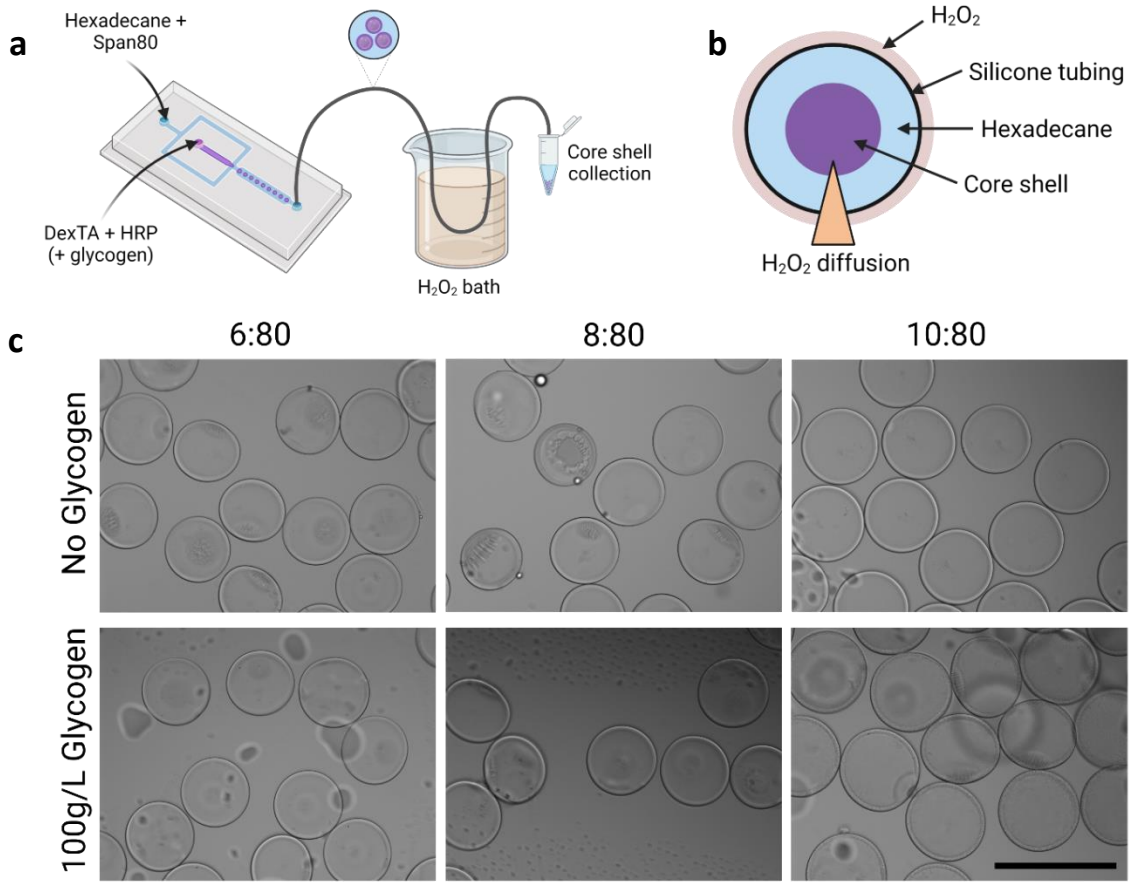

Figure 27: Core shell microgel production using microfluidics.. A) Schematic overview of the principle of core shell microgel production. B) Cross section of microgel inside tubing when in the H_2O_2 bath. C) Bright filed images of empty and glycogen-loaded core shell microgels (100 g/L encapsulated glycogen) at three different polymer solution to oil flow rate ratios. Abbreviations: DexTA: dextran tyramine, HRP: horseradish peroxidase, H_2O_2: hydrogen peroxide. Scale bar: 400 µm

At a fixed oil flow rate of 80 µl/min, the core shell microgels were characterized in terms of their diameter, shell thickness, stiffness, and degree of crosslinking. The diameter of the core shell microgels increased with higher polymer solution flow rates. Figure 28a depicts the diameter increase for empty core shell microgels, while Figure 28b shows the same trend for glycogen-loaded core shell microgels. As the total flow rate for microgel production increased, the crosslinking time of the core shell

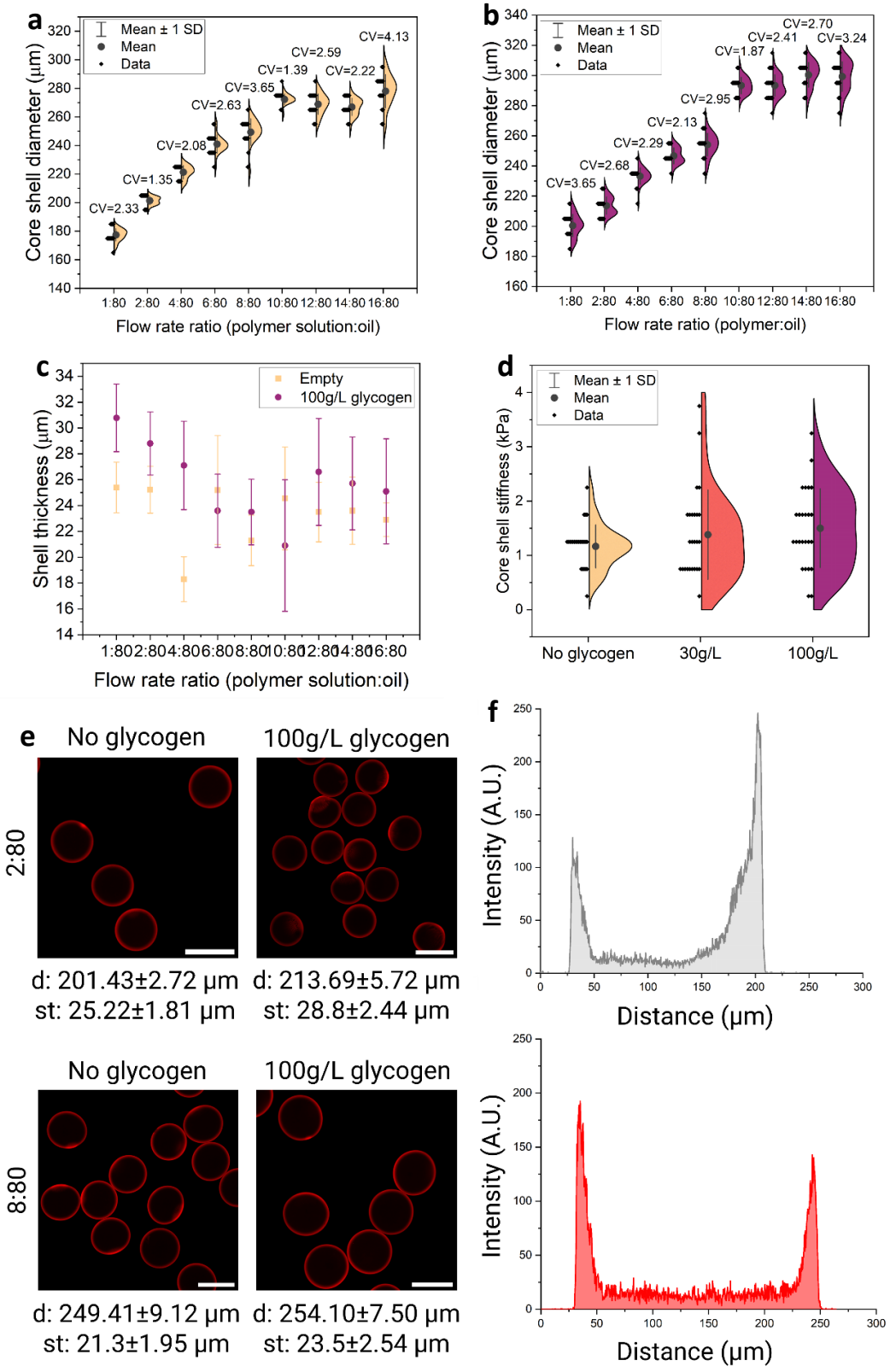

Figure 28: Characterization of core shell microgels. A) Diameter of core shell microgels at different polymer solution flow rates. B) Diameter of core shell microgels loaded with 100 g/L glycogen at different polymer solution flow rates. CV: coefficient of variation, SD: standard deviation. C) Shell thickness of empty and glycogen-loaded core shell microgels at different polymer solution flow rates. D) Stiffness of core shell microgels (polymer solution to oil flow rate: 10:80) with different glycogen content. E) Core shell microgels stained with ethidium homodimer-1. d: diameter, st: shell thickness. F) Intensity graphs of a microgel made with flow rate ratio 2:80 (above) and with 8:80 (below). Scale bar: 200 µm. Values presented in A), B) and D) are given in half-violin plots with the means ± SD and with the corresponding coefficient of variation (CV). Values presented in C) are given as means ± SD. For A) and B) n=30, for C) n=10 and for D) n=25.

microgels decreased, which explains the increase in core shell microgel diameter with increasing flow rates. Notably, the glycogen-loaded core shell microgels consistently exhibited a diameter of approximately 20 µm larger than their empty counterparts [62, 63]. In some studies it has been described that a higher solution viscosity can lead to the formation of larger droplets. In the case of producing glycogen-loaded core shell microgels, 100 g/L of glycogen is added to the polymer solution. Adding a high amount of glycogen to a solution has the same effect as adding a large amount of table sugar to a small volume of water: the solution becomes a lot more viscous. This could thus explain the larger core shell microgels formed when glycogen is encapsulated. The coefficient of variation (CV) value was calculated for all conditions and was less than 5%, indicating that the core shell microgels produced using the specified parameters is reproducible.

By staining the core shell microgels with ethidium homodimer-1, and imaging them with a confocal microscope, the shell thickness could be easily determined using ImageJ software. The resulting graph for the shell thickness did not exhibit a clear trend between the empty and glycogen-loaded core shell microgels, unlike the diameter measurements (Figure 28c). For most flow rate ratios, the glycogen-loaded core shell microgels exhibited a thicker shell. This can be explained solely by the presence of an extra component in the polymer solution, which in this case is the glycogen added. Upon the introduction of cells for example, it was observed that the crosslinking of the core shell microgels increased, resulting in the formation of soft core shell microgels rather than conventional core shell microgels [42]. Similarly, the introduction of glycogen to the polymer solution, demonstrated a comparable outcome, where the presence of glycogen led to an increase in crosslinking of the core shell microgels, which was however limited to an increased thickness of the crosslinked shell. It is important to highlight that considerable variability in size was observed within each condition, and the size distributions of empty and glycogen-loaded core shell microgels frequently overlapped.

To further characterize the core shell microgels, nanoindentation tests were performed to assess their stiffness. In general, the encapsulation of glycogen in the core shell microgels did not alter their stiffness (Figure 28d). Similar results were obtained in another study, where the glucose content did not alter the nanostructure of calcium-alginate gels [64]. As glycogen is a polymer of numerous glucose molecules it might have the same effect on gel characteristics as glucose does. It should be noted that, as the concentration of encapsulated glycogen increased, greater deviations in stiffness were observed among the core shell microgels.

Since the core shell microgels undergo crosslinking in an H_2O_2 bath, their degree of crosslinking was evaluated to determine if only the shell or also (part of) the core was affected. This was achieved again by staining the core shell microgels with ethidium homodimer-1 and by analyzing the fluorescent intensity across the core shell microgel. Figure 28d demonstrates that a core shell microgel containing 100 g/L glycogen, produced with a flow rate ratio of 2:80 (polymer solution to oil), exhibited crosslinking not only in the shell, but also partially in the core. This could be explained by the longer crosslinking time these core shell microgels undergo, leading to more crosslinking of the core shell microgel. On the other hand, when a flow rate ratio of 8:80 was utilized, the core shell microgels exhibited a distinct shell structure with no crosslinking in the core of the microgel (Figure 28h).

Having successfully produced the core shell microgels both with and without glycogen, the next step involved the evaluation of glycogen release from the glycogen-loaded core shell microgels. Microgels loaded with 100 g/L glycogen were monitored over time for glycogen release. Figure 29c presents the glycogen release profile for three different polymer solution to oil flow rate ratios (6:80, 8:80, and

10:80). No significant release of glycogen was observed over the course of one week due to the crosslinked DexTA shell (refer to section 5.6 for more information).

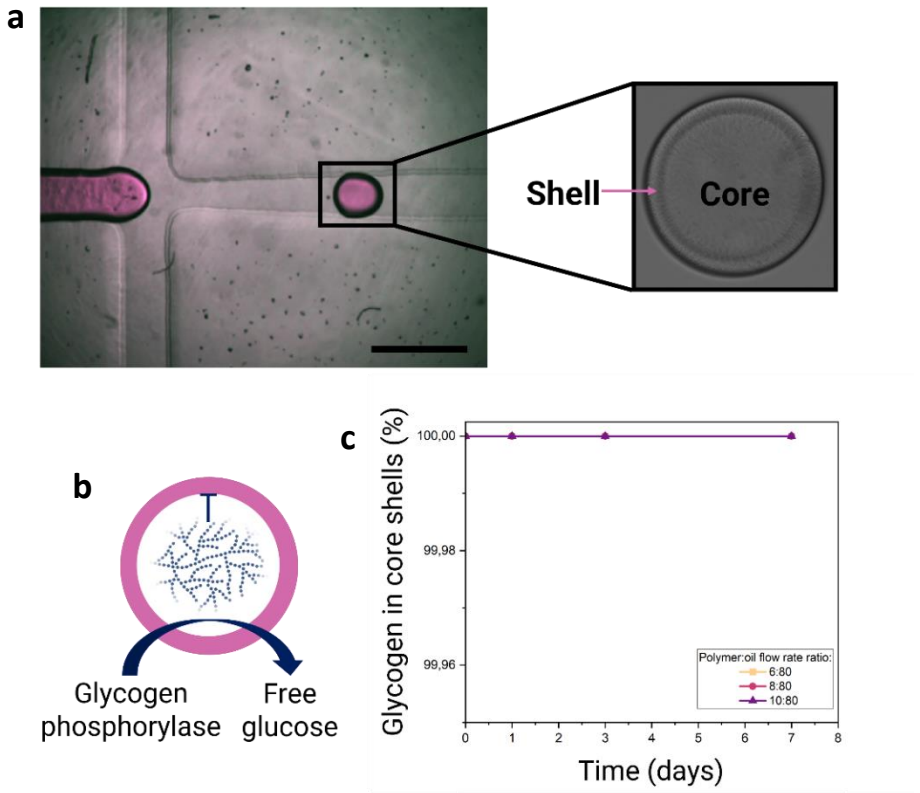

Figure 29: Glycogen can be encapsulated in core shell microgels. A) Core shell microgel production on chip. B) Core shell microgels present a liquid core containing glycogen in solution. Glycogen phosphorylase released by the cells is able to enter the microgel, where it can degrade glycogen to glucose, after which glucose is able to leave the core shell microgel. C) Glycogen remains inside the core shell microgels, indicating that release of glucose/glycogen will only take place in the presence of cells. Scale bar: 400 µm. Values in C) are presented as means ± SD, n=3.

Additional experiments were conducted to characterize the core shell microgels. In supplementary material 13, Figure 49, results regarding microgel morphology, diameter and glycogen release profile, are shown for core shell microgels produced with an oil flow rate of 48 µl/min and encapsulated glycogen concentrations of 30, 50, and 100 g/L. Furthermore, supplementary material 14 presents an overview of core shell microgels produced at an oil flow rate of 80 µl/min encompassing various concentrations of oyster glycogen (30, 50, and 100 g/L), as well as core shell microgels encapsulating bovine glycogen and glucose, both at a concentration of 100 g/L.

5.8 Glycogen-loaded core shell microgels are able to maintain cell viability and metabolic activity

To assess the impact of glycogen-loaded core shell microgels on hMSC viability, transwell cell inserts were utilized. The hMSCs were cultured in a well plate, with transwell cell inserts containing either empty or glycogen-loaded core shell microgels. The use of cell inserts aimed to avoid potential shear stress from the microgels on the 2D cultured cells. On day 7, cell viability, cell metabolic activity, vascular endothelial growth factor (VEGF) release, and glycogen concentration in the medium were analyzed and are presented in Figure 30.

The results demonstrate that hMSCs maintained a high cell viability when cultured with glycogen-loaded core shell microgels containing both 30 and 100 g/L of encapsulated glycogen. The respective cell viabilities were measured as 92.69 ± 2.01% and 96.64 ± 1.04%. Similarly, when hMSCs were cultured with free glycogen, their viability remained high, consistent with earlier findings (refer to section 5.3 for more information). As expected due to nutrient and oxygen deprivation, the negative control exhibited very low cell viability of 12.08 ± 0.87%. The most interesting finding is the cell viability of hMSCs cultured with empty core shell microgels, which reached 38.19 ± 5.69%. This level of viability is relatively high for cells cultured under nutrient and oxygen deprivation. Under these circumstances, one would expect results similar to those of the negative control. It is possible to hypothesize that cells may be able to break down free dextran molecules that could be present in the core shell microgels. Supplementary material 15 provides results regarding hMSCs cultured with free dextran in anoxic conditions to test this hypothesis. However, hMSCs were unable to survive in the presence of free dextran, indicating that there must be another reason for the observed viability in the case of empty core shell microgels. Another possibility could be that hMSCs enter a senescent or quiescent state, making them resistant to cell death [65].

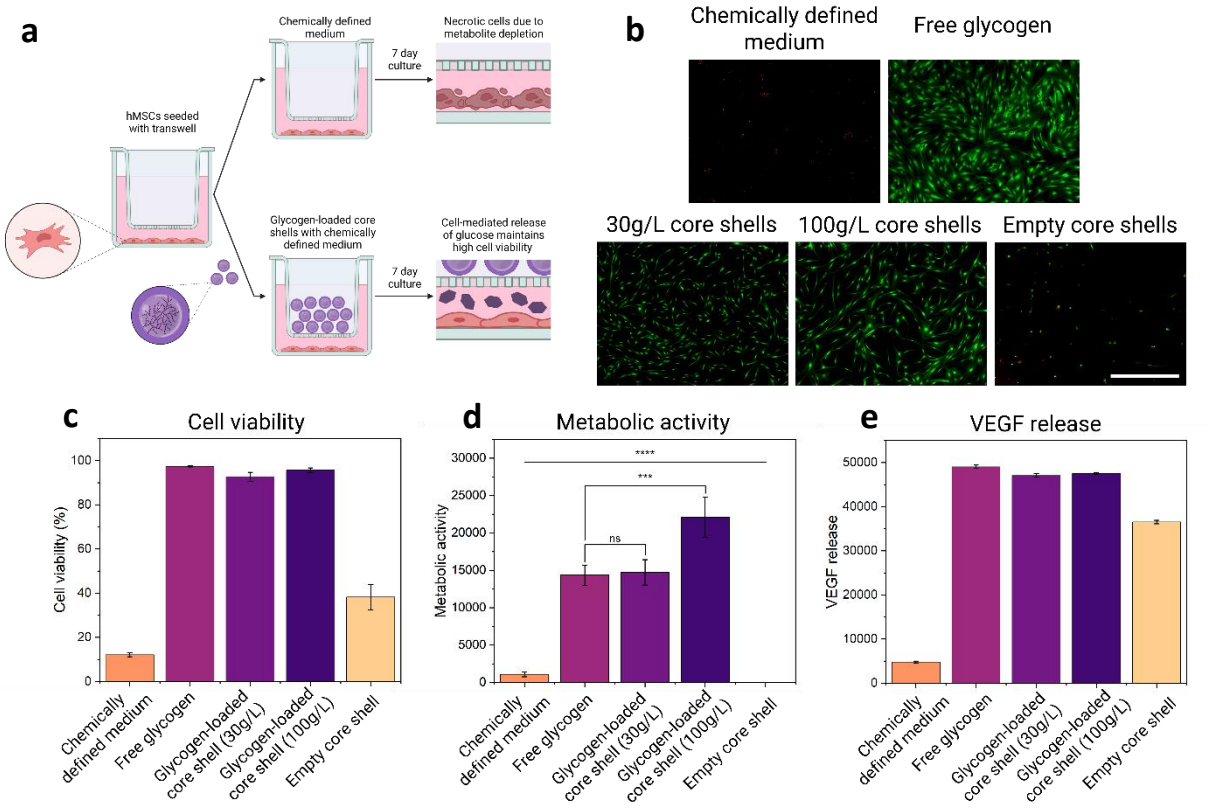

*Figure 30: Human mesenchymal stem cells (hMSCs) cultured with glycogen-loaded core shell microgels using transwell cell inserts. A) Schematic representation of the experimental set up. B) Live/dead images of hMSCs with the different culture conditions. Live: green (calcein AM), dead: red (ethidium homodimer-1). Scale bar: 1000 µm. hMSCs were evaluated on day 7 based on the C) viability, Mann-Whitney test D) metabolic activity, Pair-sample t-test, and E) VEGF release. Ns: non-significant, ***: p≤0.001, ****: p≤0.0001, n=3. Mann-Whitney test. Values presented in C), D) and E) are given as means ± SD. When not indicated, conditions are ns.*

It is important to note that this experiment once again demonstrates that glycogen breakdown is a cell-driven process. As illustrated in supplementary material 14, Figure 50, glycogen-loaded core shells with 100 g/L of encapsulated glycogen exhibit glycogen release over time in the absence of cells, while core shells containing 30 g/L of encapsulated glycogen show no glycogen release over a two-week period. However, as shown in Figure 30, hMSCs are capable of surviving when cultured with core shells

containing 30 g/L of encapsulated glycogen, indicating that hMSCs are able to utilize the encapsulated glycogen even when it is not released. This finding supports the notion that the process of glycogen breakdown is cell-driven.

The results for the metabolic activity of hMSCs raise some questions. hMSCs cultured with core shell microgels containing 100 g/L encapsulated glycogen exhibit the highest metabolic activity, whereas those cultured with free glycogen demonstrate the lowest metabolic activity, which is however similar to the metabolic activity of hMSCs cultured with core shell microgels containing 30 g/L encapsulated glycogen (Figure 30). Considering the results presented in supplementary material 14, Figure 50, the release of glycogen/glucose from the core shell microgels containing 30 g/L glycogen is entirely reliant on cellular processes, as no detectable glycogen release occurs from the core shell microgels in the absence of cells. In the other two conditions, namely cells cultured with free glycogen and with core shell microgels containing 100 g/L encapsulated glycogen, glycogen is readily detectable in the culture medium. This suggests that similar metabolic activities between these two conditions would be reasonable. However, contrary to this assumption, this was not the case and a justification for this has yet to be found. Notably, hMSCs cultured with empty core shell microgels, show a metabolic activity close to zero, indicating that, considering their viability, hMSCs might have become quiescent in this condition [66].

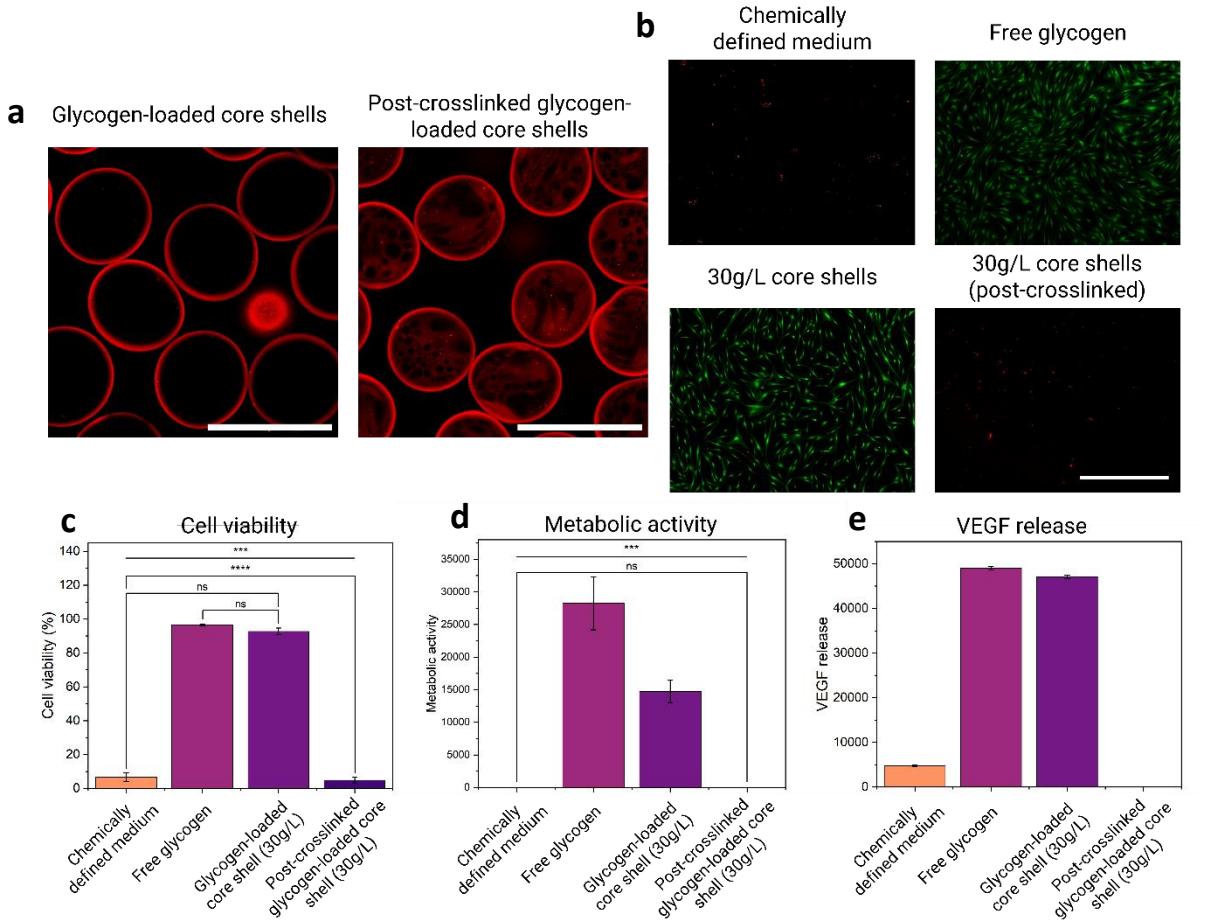

*Figure 31: The effect of post-crosslinking glycogen-loaded core shells on human mesenchymal stem cells (hMSCs). A) Glycogen-loaded core shell microgels without and with post-crosslinking in an horseradish peroxidase (HRP) and hydrogen peroxide (H2O2) bath. Scale bar: 300 µm. B) Live/dead images of hMSCs cultured under the different conditions. Live: green (calcein AM), dead: red (ethidium homodimer-1). Scale bar: 1000 µm. hMSCs were evaluated on day 7 based on their C) viability, Pair-Sample t-test, D) metabolic activity, Pair-Sample t-test, and E) VEGF release. Ns: non-significant, ***: p≤0.001, ****: p≤0.0001, n=3. Values presented in C), D) and E) are given as means ± SD. When not indicated, conditions are ns.*

The observed VEGF release results deviate from expectations. Notably, hMSCs cultured with empty core shell microgels exhibited an unexpectedly high VEGF release, despite their metabolic activity being close to zero. The reason for this remains unclear, particularly considering that cells cannot survive in the presence of dextran, as previously explained. However, it is worth noting that hMSCs cultured with free glycogen and glycogen-loaded core shell microgels demonstrate a substantial VEGF release, which can be attributed to their high viability and metabolic activity. On day 7, the glycogen concentration in the supernatant was also measured. These results can be found in supplementary material 22.

When hMSCs are cultured with glycogen-loaded core shell microgels containing 30 g/L of glycogen, they exhibit sustained viability, metabolic activity, and a notable release of VEGF over a one-week period. However, when these glycogen-loaded core shell microgels undergo post-crosslinking for 15 min in an H_2O_2 and HRP bath, hMSCs are unable to maintain their viability and die within a week. Consequently, no metabolic activity or VEGF release is observed in this scenario. Figure 31a illustrates the presence of a DexTA mesh within the post-crosslinked core shell microgels (shown by ethidium homodimer-1 staining of DexTA). It is thought that this phenomenon produces a similar effect to the one explained in section 5.6, where hMSCs are hindered to enzymatically break down the glycogen present in the core shell microgel due to the limited space for the enzymes to function properly caused by the crosslinked DexTA molecules in the microgel core.

5.9 Tissue engineered constructs using glycogen-loaded core shells

In order to investigate the impact of glycogen and glycogen-loaded core shell microgels within a 3D environment, tissue engineered constructs were developed using a diverse range of hydrogel materials.

5.9.1 Glycogen-loaded core shells in GelMA and DexTA hydrogel

Human mesenchymal stem cells (hMSCs) were cultured within a 3D environment using cell-laden hydrogels composed of GelMA (5 and 7.5% w/v) and DexTA (10% w/v). The results are presented in Figure 32. Based on the metabolic activity, hMSC-laden GelMA hydrogels containing 5% w/v GelMA exhibited the most promising outcomes when cultured with either free glycogen or glycogen-loaded core shell microgels incorporated into the gel. In contrast, the metabolic activity of hMSCs was significantly lower within 7.5% w/v GelMA hydrogels, particularly when glycogen-loaded core shell microgels were integrated into the gel matrix. In the case of DexTA hydrogel, minimal metabolic activity was observed in hMSCs when glycogen-loaded core shell microgels were incorporated, which can be attributed to the dense nature of Dextran-based hydrogels. The limited space within these DexTA hydrogels may hinder the proper functioning of the enzymes secreted by hMSCs for glycogen breakdown, ultimately leading to cell death, as discussed previously in section 5.6.

The difference in metabolic activity between hMSCs cultured in 5% w/v and 7.5% w/v GelMA hydrogels can be attributed to differences in stiffness between the two hydrogel formulations. An increase in GelMA content leads to increased covalent crosslinking between gelatin chains though methacryolyl group bonds, resulting in a stiffer hydrogel matrix. However, previous studies have reported that an increase in matrix stiffness leads to an increase in cell proliferation and viability, which contradicts the findings presented in Figure 32b [67, 68].

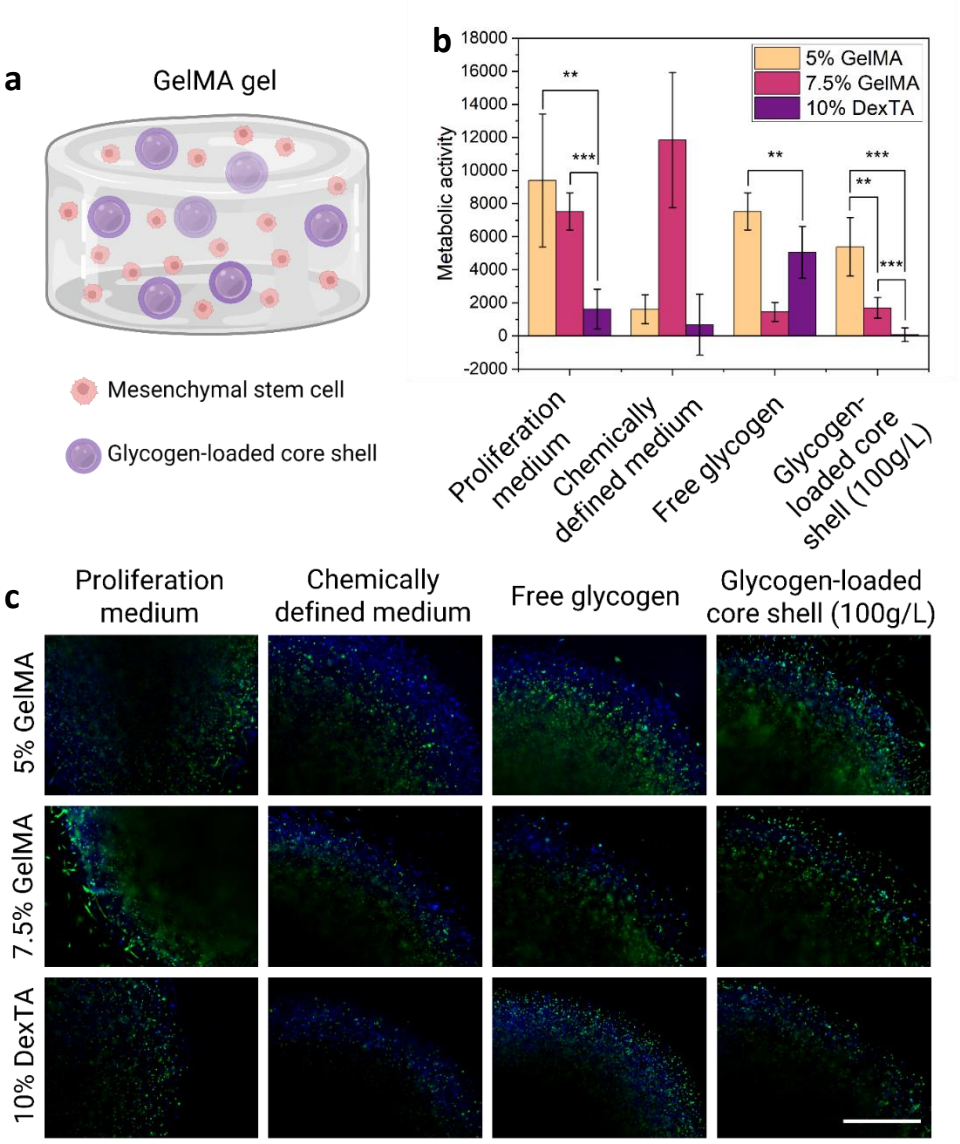

*Figure 32: Human mesenchymal stem cell (hMSC)-laden hydrogels with glycogen-loaded core shell microgels. A) Schematic representation of GelMA hydrogel containing hMSCs and glycogen-loaded core shell microgels. B) Metabolic activity of hMSC-laden GelMA hydrogel (5 and 7.5% w/v) and DexTA hydrogel (10% w/v) on day 7. C) Images of hMSCs in the different types of hydrogels on day 7. Green: live cells (calcein AM). Blue: nuclei (Hoechst staining). Scale bar: 1000 µm. Ns: non-significant, **: p≤0.01, ***: p≤0.001, n=2. Normally distributed data: Pair-Sample t-test. Non-normal data: Mann-Whitney test. Values presented in C), D) and E) are given as means ± SD. When not indicated, conditions are ns.*

Interestingly, hMSCs cultured in a 7.5% w/v GelMA hydrogel with chemically defined medium exhibited even higher metabolic activity compared to the positive control (hMSCs in hydrogel with proliferation medium). The underlying reason for this remains unknown, and the reliability of this result should be questioned, particularly due to the anomalous high metabolic activity measured in a condition where cells are cultured within a nutrient-deprived environment. Additionally, when hMSCs are cultured in chemically defined medium using a 5% GelMA hydrogel they exhibit a very low metabolic activity, which can be attributed to the harsh culture conditions. Consequently, the question arises as to how an elevation in GelMA concentration can account for the observed exceptionally high metabolic activity.

It is important to acknowledge certain limitations in this experiment. Each condition was tested in duplicate, and due to the inclusion of a DexTA hydrogel, ethidium homodimer-1 staining (for dead cell

detection) could not be used. Instead, a Hoechst staining was conducted to visualize the cell nuclei. However, in a 3D context, distinguishing the signals from Hoechst staining becomes challenging, making accurate determination of the cell viability nearly impossible. These results should be interpreted with caution and should not serve as the basis for definitive conclusions, but rather provide indicative insights. Additionally, it is important to note that despite multiple repetitions of this experiment, only the one depicted in Figure 32 yielded positive results regarding cell viability and metabolic activity. Consequently, the reproducibility of this experiment requires optimization.

5.9.2 Glycogen-loaded core shells in collagen hydrogel

To address the issue of reproducibility with hMSC-laden GelMA hydrogels, the utilization of collagen hydrogels was explored as an alternative. While the experimental setup remained mostly the same, there were modifications involving the addition of either 1% FBS and 9% ITS or 10% FBS to the chemically defined medium. The primary objective of these modifications was to prevent collagen degradation by the gels and to facilitate quicker acclimation of hMSCs to the 3D environment, thereby preventing excessive cell death caused by stress. The incorporation of glycogen-loaded core shell microgels within the collagen gel yielded positive outcomes for the cell viability. The hMSCs were able to adapt to the new culture conditions and sustained viabilities of 85.27 ± 1.27 % and 91.06 ± 1.47% for 1% FBS and 10% FBS, respectively, on day 7. The negative control group did not survive, exhibiting viabilities of only 4.08 ± 0.56% and 4.22 ± 3.29% for 1% and 10% FBS, respectively. Interestingly, hMSCs cultured with free glycogen displayed lower cell viability compared to those cultured with the glycogen-loaded core shell microgels. This is in contrast with earlier obtained results described in section 5.8, and might be attributed to the presence of collagen. However, this should be evaluated further in future experiments.

It is important to note that the cell viability was determined in a single plane of the hydrogels, and thus the results presented in the graphs may deviate from the overall state of the hydrogels. Additionally, when incorporating core shell microgels into the bulk hydrogel, fewer cells were visible in the hydrogel during imaging with a confocal microscope. This can be attributed to the core shell microgels basically obstructing the view, making the visualization of cells within the hydrogel nearly impossible. Consequently, the viability of hMSCs in collagen gels with core shell microgels could be questioned, and may not be fully representative of the entire hydrogel.

Furthermore, hMSCs cultured in collagen gel with chemically defined medium exhibited no detectable metabolic activity, which is consistent with the low cell viability observed under these conditions. The metabolic activity results for hMSCs cultured with free glycogen and glycogen-loaded core shell microgels appear contradicting when compared to the obtained cell viability data. However, this could potentially be explained by the readily available glycogen for the hMSCs cultured with free glycogen, which cells can easily sense, thereby stimulating them to degrade more glycogen and becoming more metabolically active. In the case of glycogen-loaded core shell microgels, cells may encounter difficulty in sensing the glycogen and thus could potentially enter a quiescent state to maintain viability, which would explain the decreased metabolic activity observed [66, 69, 70]. hMSCs also tend to enter a quiescent state when cultured in 3D, like when cultured in a collagen hydrogel. Whether this is actually happening should be examined during further research.

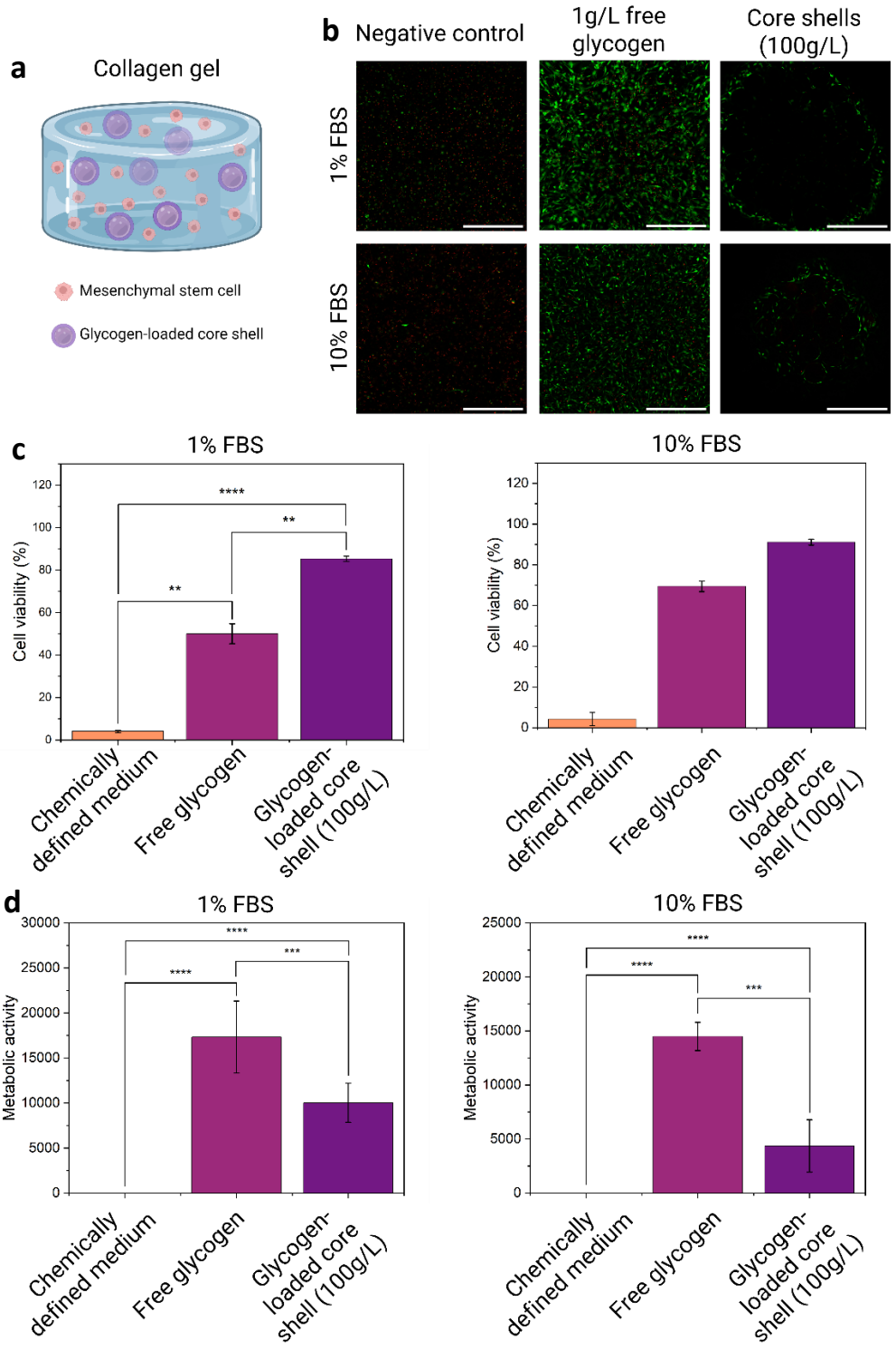

*Figure 33: Human mesenchymal stem cell (hMSC)-laden collagen bulk hydrogels with glycogen-loaded core shell microgels (100 g/L). A) Schematic representation. B) Live/Dead images of the conditions tested. Live: green (calcein AM), dead: red (ethidium homodimer-1). Scale bar: 500 µm. C) Cell viability results on day 7 for hMSCs cultured with 1% fetal bovine serum (FBS) (left, Pair-Sample t-test) and 10% FBS (right, Mann-Whitney test). D) Cell metabolic activity on day 7 for hMSCs cultured with 1% FBS (left, Mann-Whitney test) and 10% FBS (right, Mann-Whitney test). **: p≤0.01, ***: p≤0.001, ****: p≤0.0001, n=3. Values presented in C) and D) are given as means ± SD. When not indicated, conditions are non-significant.*

5.9.3 Glycogen-loaded core shells and hyaluronic acid blocks in collagen hydrogels

Subsequently, hMSC-laden collagen hydrogels were prepared with glycogen-loaded core shell microgels and hydroxyapatite (HA) block fragments incorporated. HA block fragments were

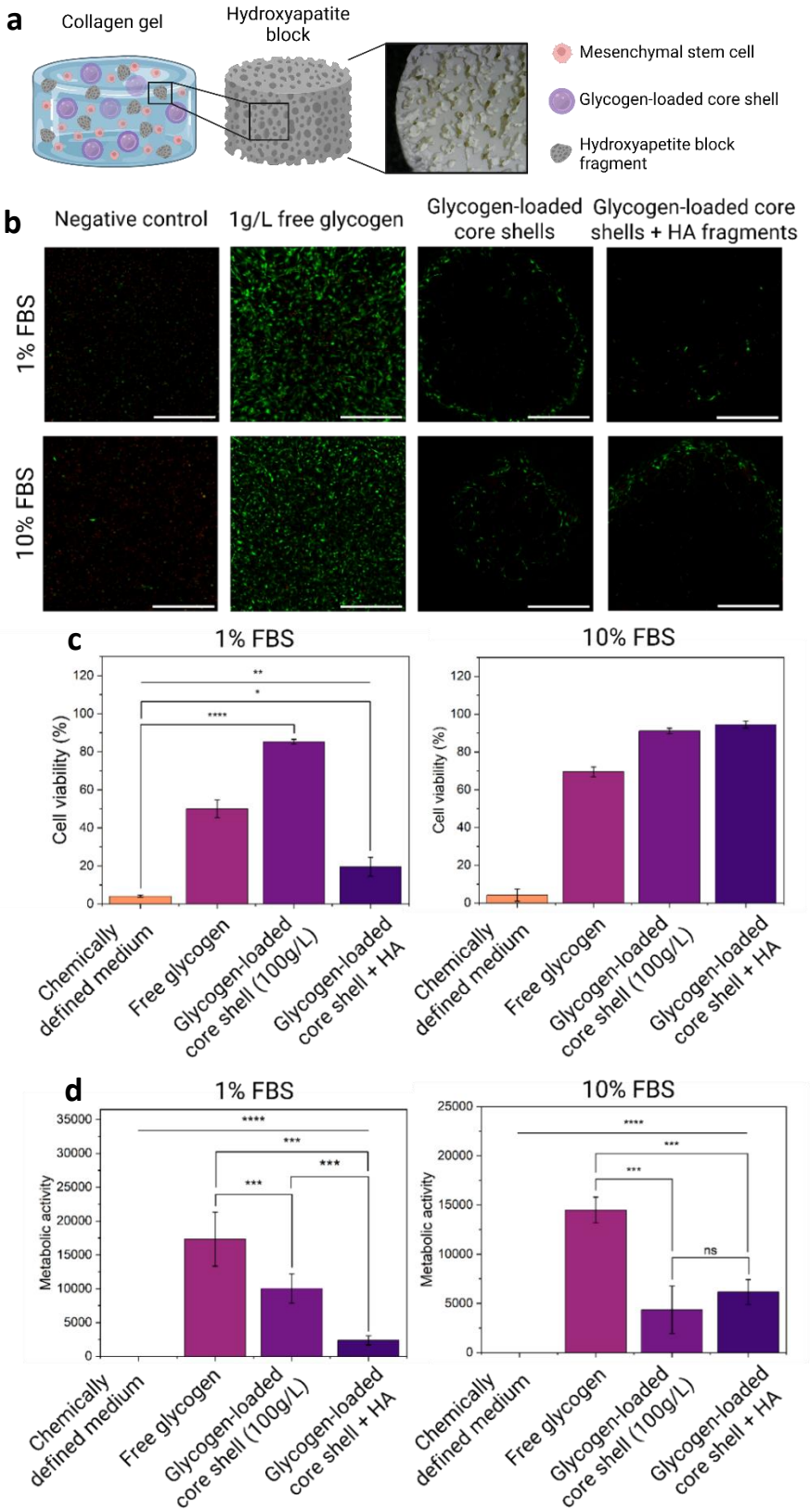

*Figure 34: Human mesenchymal stem cell (hMSC)-laden collagen bulk gel with glycogen-loaded core shell microgels (100 g/L) and hydroxyapatite (HA) block fragments. A) Schematic representation of the experimental set up. B) Live/dead images of the conditions tested. Live: green (calcein AM), dead: red (ethidium homodimer-1). Scale bar: 500 µm. C) Cell viability graphs of tested conditions on day 7 for hMSCs cultured with 1% fetal bovine serum (FBS) (left, Pair-Sample t-test) and 10% FBS (right, Mann-Whitney test). D) Metabolic activity of hMSCs on day 7 cultured with 1% FBS (left, Mann-Whitney test) and 10% FBS (right, Mann-Whitney test). *: p≤0.05, **: p≤0.01, ***: p≤0.001, ****: p≤0.0001, n=3. Values presented in C) and D) are given as means ± SD. When not indicated, conditions are non-significant.*

incorporated to study their impact on both hMSCs and glycogen-loaded core shell microgels. This investigation was undertaken to assess the feasibility of conducting an in vivo study in collaboration with prof. dr. M.C. Kruijt. The experimental conditions included a negative control group cultured with chemically defined medium, a positive control group cultured with 1 g/L free glycogen, the incorporation of glycogen-loaded core shell microgels, and the incorporation of both core shell microgels and HA block fragments. The cell viability and metabolic activity were assessed on day 7, and the results are presented in Figure 34.

As expected, hMSCs cultured in chemically defined medium exhibited a very low cell viability and no detectable metabolic activity for both cells cultured with 1% and 10% FBS. hMSCs cultured in medium containing free glycogen exhibited a viability of 50.05 ± 4.66% and 69.44 ± 2.62% when cultured with 1% and 10% FBS, respectively. Notably, the metabolic activity of cells cultured with 1% FBS was highest amongst all the evaluated conditions, while for 10% FBS the conditions involving core shell microgels exhibited a higher metabolic activity. These findings are in accordance with the results obtained and described in section 5.9.2.

Upon culture with 1% FBS, hMSCs are unable to maintain their viability in the presence of HA block fragments. Moreover, the metabolic activity here was extremely low. When hMSCs were cultured in collagen gel with glycogen-loaded core shells a high cell viability is maintained. Surprisingly, the viability is higher compared to the hMSCs cultured with free glycogen, while the metabolic activity is lower.

Supplementation of the medium with 10% FBS yielded positive results for the cell viability, both in the presence of glycogen-loaded core shells and in the presence of core shells together with HA block fragments. However, the metabolic activity under these conditions was significantly lower compared to hMSCs cultured with free glycogen.

The exact explanation for these findings has yet to be found. Initially, it was hypothesized that the HA blocks were toxic for hMSCs. However, in the presence of 10% FBS, the HA blocks did not induce any toxicity, and cells maintained a high viability.

6. Conclusion

This study presents the successful encapsulation of glycogen within core shell microgels, which effectively maintained high cell viability and metabolic activity of hMSCs in both a 2D monolayer and 3D hydrogel matrices. The following key findings and conclusions were drawn:

- Glycogen exhibited promising results in sustaining high cell viability under anoxic conditions, even at lower concentrations (Figure 22), and it did not induce any toxic effects on human mesenchymal stem cells (hMSCs) at higher concentrations (Figure 23). Surprisingly, this suggests that hMSCs can utilize exogenous glycogen. The secretion of glycogen phosphorylase by hMSCs (Figure 38) enables the degradation of exogenous glycogen into glucose, which can be utilized by the cells.
- Glycogen was characterized successfully in terms of size, charge, and osmolarity (Figure 25a, b, c). Oyster glycogen exhibited the largest size, while oyster and bovine glycogen displayed similar osmolarity, indicating a denser structure for bovine glycogen in terms morphology. However, morphology has not been confirmed yet through transmission electron microscopy (TEM) imaging.
- Release profiles of glycogen and glucose from GelMA and DexTA bulk hydrogels were obtained over a two week period (Figure 25e). DexTA hydrogel encapsulation of oyster glycogen showed the most promising outcome for long-term glycogen encapsulation, while glucose was readily released within 24 hours.
- Upon encapsulation of glycogen within a DexTA bulk gel, extensive cell death was observed after 7 days of culture. In contrast, when glycogen was present in soluble form in the culture medium, cell viability was maintained (Figure 24). This suggests that glycogen needs to be in soluble form for cells to utilize it, likely due to limited space within the dense DexTA hydrogel matrix for successful glycogen breakdown.
- DexTA was employed for the fabrication of core shell microgels. Core shell microgels were successfully produced, and glycogen encapsulation was achieved (Figure 27). Glycogen remained within the core shell microgels for at least two weeks (Figure 29).
- Culture of hMSCs in a 2D monolayer with transwell cell inserts containing glycogen-loaded core shell microgels, resulted in high cell viability up to day 7, sustained metabolically activity, and continued VEGF secretion essential for vasculature formation (Figure 30).
- Incorporation of glycogen-loaded core shell microgels into hMSC-laden GelMA hydrogels was challenging, as gelatin degradation by cells occurred rapidly in a nutrient- and oxygen-deprived environment. The addition of insulin transferrin selenium (ITS) prevented GelMA hydrogel degradation, but reproducible results regarding viability and metabolic activity were not achieved in the majority of the experiments.
- Encapsulation of glycogen-loaded core shell microgels within hMSC-laden collagen hydrogels yielded promising and reproducible results in terms of cell viability (>90% on day 7) and metabolic activity (Figure 33).

In conclusion, glycogen-loaded core shell microgels demonstrated promising outcomes in maintaining high cell viability and metabolic activity in both 2D- and 3D-culture environments. Cell survival relied on glycogen phosphorylase, which could penetrate the highly crosslinked shell of the core shell microgel, facilitating glycogen degradation and the release of glucose. The small size of glucose molecules enabled their diffusion out of the core shell microgels, providing an adequate energy source for hMSCs. This mechanism ensured high cell viability, metabolic activity, and substantial VEGF release by hMSCs. The findings of this study contribute novel insights into the characterization and

degradation of glycogen. Additionally, the encapsulation of glycogen within core shell microgels shows promise in bridging the prevascular phase in tissue engineered constructs.

7. Future Outlook

7.1 The promising role of glycogen-loaded core shell microgels in tackling organ shortage

The only solution for end-stage organ failure is organ transplantation [71]. However, due to a severe shortage of organs, only a limited number of patients are fortunate to receive a transplant. Organ transplantations pose various risks, and post-transplantation, patients must undergo lifelong immunosuppressant therapy. Tissue engineering has emerged as a field aiming to address the challenges associated with organ transplantation by the development of patient-specific tissues and organs [72]. Utilizing patient-specific cells eliminates the need for immunosuppressants, while the fabrication of new organs offers a potential solution for the organ shortage crisis. However, several challenges remain, with the inability to develop vascularized tissues being one of them.

We believe that glycogen-loaded core shell microgels, capable of providing adequate nutrients to tissue engineered constructs, can sustain their viability until the host vascular network can invade it, ensuring the supply of oxygen and nutrients. Our ongoing in vivo study, conducted in collaboration with dr. S. R. Shin (Brigham and Women's Hospital, Harvard Medical School, Boston, USA), focuses on evaluating the impact of glycogen-loaded core-shell microgels on the viability and behavior of human mesenchymal stem cells (hMSCs). This study involves the implantation of hMSC-laden GelMA hydrogels with incorporated glycogen-loaded core-shell microgels in mice.

Furthermore, we are discussing an additional in vivo study in collaboration with prof. dr. M.C. Kruijt from UMC Utrecht, the Netherlands, which explores the incorporation of glycogen-loaded core-shell microgels and hydroxyapatite (HA) constructs into cell-laden hydrogels. These studies aim to provide valuable insights into the application of core-shell microgels in the field of tissue engineering.

7.2 The application of glycogen in neurodegenerative diseases

Neurodegenerative diseases often exhibit a metabolic shift towards glycolysis as a survival mechanism for neurons under stressful and energy-deficient conditions. In Parkinson's disease (PD), increased glycolysis appears to have neuroprotective effects on both neurons and glial cells [73]. Similarly, Alzheimer's disease (AD) is associated with enhanced glucose metabolism, which serves as a protective mechanism for neuronal tissue. The progression of AD is correlated with elevated blood glucose levels and increased brain glucose levels, indicating that augmented glycolysis may compensate for dysfunctional mitochondria in this disease [74]. In amyotrophic lateral sclerosis (ALS), a high sugar diet has shown promise in extending lifespan in certain models, suggesting that enhanced glycolysis is neuroprotective [73].

The promotion of glycolysis appears to be beneficial in neurodegenerative diseases such as PD, AD, and ALS. However, this would lead to a rapid depletion of the body's glycolytic reserves. Here, the application of glycogen-loaded core-shell microgels holds promise as a potential solution. By introducing these microgels, a sustainable supply of glucose can be provided to the brain, satisfying the heightened demand for enhanced glycolysis.

7.3 Evaluating the role of glycogen in tumors and tumor metastasis

Hypoxic conditions commonly developed within tumors trigger an upregulation of glycogen degradation as an adaptive mechanism to sustain tumor survival. Furthermore, glycogen has been implicated in facilitating crosstalk with cancer-associated fibroblasts, promoting cancer metastasis

[75]. Figure 35 provides a schematic representation of the involvement of glycogen in tumor processes. The utilization of exogenous glycogen in cancer models offers a valuable approach to enhance our comprehension of glycogen metabolism within tumors. Moreover, it holds the potential to serve as a means to target glycogen metabolism, thereby attenuating tumor progression and impeding metastasis.

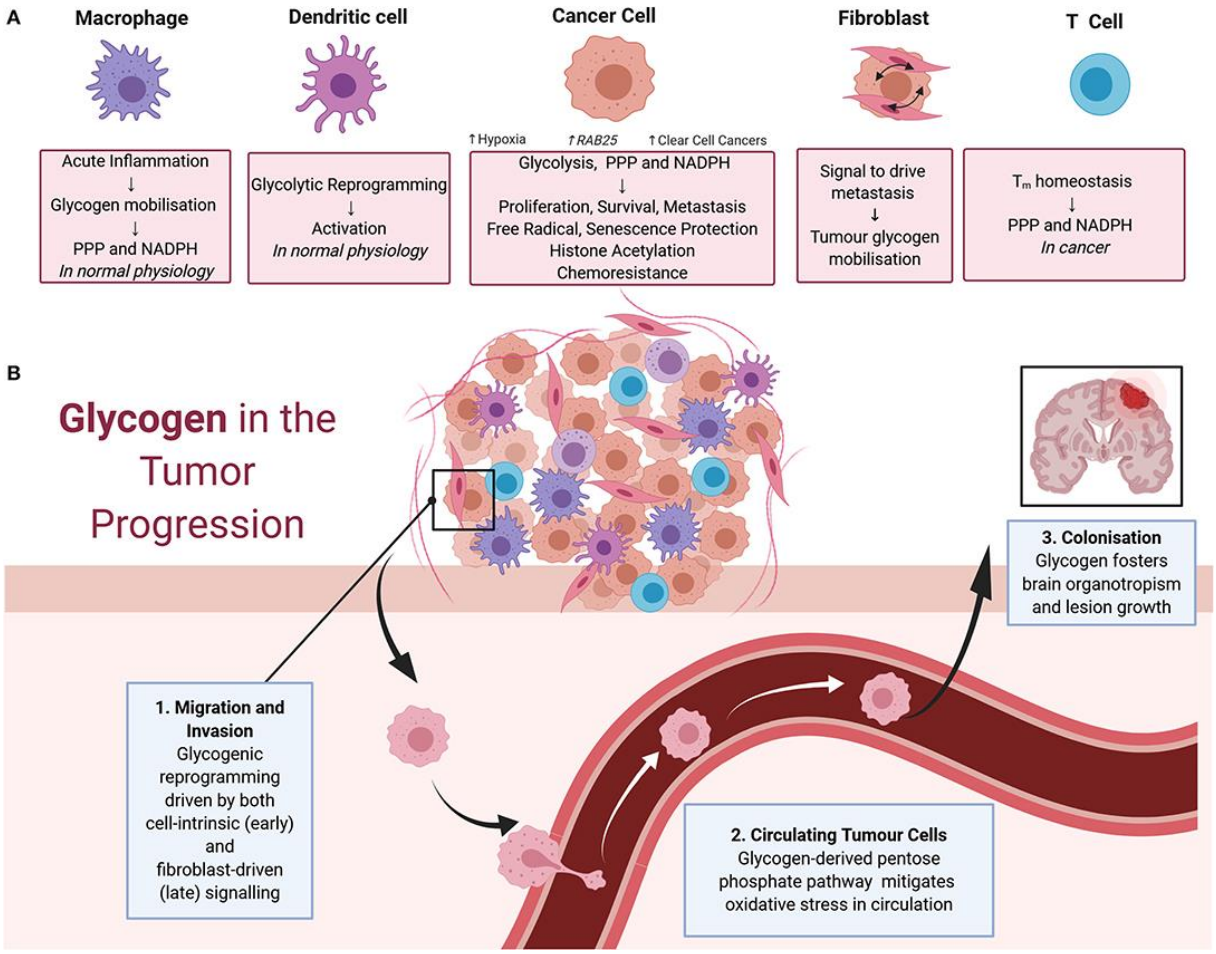

Figure 35: The role of glycogen in tumor progression and metastasis [75].

7.4 Glycogen in GSD modeling

As outlined in section 3.1.7 and supplementary material 2, glycogen storage disorders (GSDs), which arise from defects in enzymes involved in glycogen breakdown or synthesis, cause a wide variety of symptoms. Presently, there is no known cure for GSDs [76]. In this thesis, we have demonstrated the ability of human mesenchymal stem cells (hMSCs) to utilize exogenous glycogen. This finding suggests that exogenous glycogen can serve as a valuable tool for modeling GSDs, enabling the investigation of their impact on cells and tissues and the development of novel therapeutic approaches for disease management and symptom mitigation.

In this thesis, certain GSDs have already been (accidently) partially modelled through the cultivation of hMSCs in a glycogen-enriched medium supplemented with a phosphorylase inhibitor. This approach inhibits glycogen breakdown and subsequent glucose release, mimicking conditions observed in GSD1A, GSD3, GSD6, GSD15, and Fanconi-Bickel syndrome. Numerous other disorders are characterized by glycogen accumulation. By culturing human-derived cells within a tissue-engineered

construct that provides a constant supply of glycogen or glucose, it may be possible to replicate similar conditions and mimic the pathophysiological characteristics associated with these disorders.

7.5 Glycogen-loaded core shell microgels as functional building blocks

As presented in supplementary material 24, glycogen-loaded core shell microgels have demonstrated potential for bottom-up tissue engineering approaches. However, due to the larger size of the core shell microgels, successful aggregate formation requires a substantial number of cells. Therefore, the exploration of strategies to produce smaller glycogen-loaded core shell microgels represents a promising avenue for bottom-up tissue engineering.

Upon achieving the fabrication of cell-sized glycogen-loaded core shell microgels, they can be further customized to serve as smart building blocks, as described by Kamperman & Willemen *et al.* [41]. By tuning the characteristics of smart building blocks, functional tissues can be constructed. By incorporating glycogen within the microgels, it becomes feasible to fabricate larger tissues that maintain their viability over extended periods. Kamperman & Willemen *et al.* also showed the that these smart building blocks, upon modification, can steer stem cell fate towards the adipogenic (soft building blocks) or osteogenic (stiff building blocks) lineage. As described in section 3.1.5.1, ESG had the ability to enhance the osteogenic differentiation. This suggests for the evaluation of osteogenic differentiation of hMSCs in the presence of stiff smart building blocks loaded with glycogen.

7.6 Further characterization of glycogen-loaded core shell microgels

Despite all the promising outcomes presented in this thesis, further experimentation is still required to better understand the mechanisms involved in producing the core shell microgels, and to fully evaluate the potential of glycogen-loaded core shell microgels in bridging the prevascular phase of tissue engineered constructs.

7.6.1 Glycogen characterization

A variety of analyses for the characterization of glycogen have already been performed (section 5.5). However, additional analyses could provide valuable insights into the glycogen molecule and its encapsulation within core shell microgels. The application of transmission electron microscopy (TEM) imaging to examine oyster and bovine glycogen molecules would offer valuable information regarding their size and morphological structure. Moreover, this analysis could provide insights into the potential entanglement of glycogen molecules within different hydrogel formulations, thereby further elucidating the understanding of glycogen breakdown within specific hydrogel matrices.

Additionally, visualizing the distribution of glycogen molecules within core shell microgels and hydrogel matrices can provide valuable information on the distribution of the glycogen particles throughout the gel. Successful visualization of glycogen molecules has already been demonstrated (Figure 25f). Encapsulating these stained glycogen molecules in a gel formulation would provide useful insights. Alternative visualization techniques could also be explored, taking into consideration that commercially available stains may not be suitable due to their affinity for staining the dextran moieties present. Nie et al. successfully stained glycogen particles with Patent blue V, although initial attempts to stain oyster glycogen with Patent blue V [77], although initial attempts to stain oyster glycogen with Patent blue V were unsuccessful. Protocol optimization could be considered in this regard. Another potential option is the labeling of glycogen using FITC, as described by Besford *et al*. [78].

7.6.2 Glycogen characterization and breakdown within bulk hydrogel and core shell microgels

Based on the findings presented in section 5.6, it was assumed that upon encapsulation of glycogen within a DexTA bulk hydrogel, enzymatic breakdown of glycogen is hindered by limited space imposed by the dense hydrogel matrix. However, this hypothesis is based on the characteristics of the hydrogel, our understanding of the complicated enzymatic degradation process of glycogen, and the observed viability of hMSCs in the presence of freely available glycogen in solution. Despite these thoughts, experimental evidence supporting this assumption was not provided. Therefore, it is crucial to investigate the precise mechanisms occurring within the hydrogel and elucidate the specific steps of degradation that are impeded by the dense matrix. Further research should be undertaken to verify this hypothesis.

7.6.3 Optimizing the incorporation of core shell microgels into cell-laden hydrogels

The utilization of GelMA hydrogel did not yield consistent and reproducible results, after which the transition to collagen gels was made. The use of collagen gels demonstrated greater reproducibility, although certain outcomes appeared contradictory and currently lack a comprehensive explanation. Consequently, further investigation is required to examine the impact of collagen gels with and without core shell microgels on the viability and metabolic activity of hMSCs.

Thus far, viability assessment within the hydrogel constructs has been conducted in a single specific plane, which may not accurately represent the overall state of the entire hydrogel. Therefore, it is advised to assess the viability by analyzing multiple planes or the entirety of the hydrogel. Moreover, the inclusion of core shell microgels obstructs the transmission of light necessary for cell visualization, thereby raising concerns about the validity of viability assessments under these conditions. As a result, it could be considered to analyze the viability of cells throughout the entire construct, although this approach will require additional time and effort.

7.6.4 Explore the full potential of glycogen-loaded core shell microgels for bridging the prevascular phase

The results obtained in section 5.8 and 5.9 have demonstrated the promising potential of glycogen-loaded core shell microgels in sustaining cell viability and metabolic activity. However, it is important to note that these experiments were conducted over a relatively short duration of 7 days, which is insufficient for proper vascularization of tissue constructs. Consequently, the next step should involve investigating cell viability, metabolic activity, VEGF release, and phosphorylase secretion over an extended period of at least 14 days, preferably up to 21 days. After 21 days, the tissue engineered construct should have achieved complete vascularization, at which point the glycogen-loaded core shell microgels become unnecessary for cell survival.

Thus, glycogen-loaded core shell microgels are required for a maximum period of 21 days until the construct is fully vascularized and capable of supplying the tissue with adequate nutrients and oxygen. Hence, it would be valuable to explore the utilization of degradable materials that can be tailored to degrade only after full vascularization of the construct has been achieved. A variety of degradable materials can be considered, such as gelatin-based materials [79], the crosslinking of chitosan with carboxymethyl cellulose using Schiff base chemistry [80], the crosslinking of vinyl ether acrylate-functionalized polyvinyl alcohol (PVA-VEA) with thiolated PVA-VEA (PVA-VEA-SH) through a Michael addition reaction [81], the combination of polyethylene glycol polylactic acid (PEG-PLA) and PEG-PLA diacrylate (PEG-PLA-DA) microgels [82], the crosslinking of maleimide-functionalized PEG with thiol-terminated, ester-containing molecules [83], and much more.

Subsequent to the degradation of the core shell microgels, the remaining glycogen content will be released following a burst release profile. Therefore, it is essential to assess the potential toxicity of high levels of released glycogen to hMSCs, particularly considering that the toxicity evaluation in section 5.3 was limited to a maximum glycogen concentration of 10 g/L.

7.6.5 Shelf-life of glycogen-loaded core shell microgels

Building upon the dehydration and rehydration experiment described in supplementary material 15, it would be valuable to investigate the shelf-life of glycogen-loaded core shell microgels. These microgels can be produced and stored in PBS for extended periods (weeks to months) before their utilization in cell experiments. Alternatively, dehydrating the core shell microgels and subsequently rehydrating them after several weeks would provide insights into their ability to maintain high cell viability.

Acknowledgements

First of all I would like to express my gratitude to my two daily supervisors, Niels Willemen and Melvin Gurian, for their guidance and support throughout my master thesis. You were both always available and ready to help me with any questions I had. Besides showing me new techniques and tricks in the lab, you taught me how to set up my own experiments, interpret the obtained data critically, and learn how to think and act like a scientist. But most of all, I had a very good time with both of you during my thesis, and I already miss our random encounters in the lab that turned out to great discussions about the project.

I would also like to extend my appreciation to the other members of the examination committee. I would like to thank dr. Jeroen Leijten for giving me the opportunity to work under his supervision and for believing in me throughout the whole project, that started during my internship. Although we didn't have that many meetings, you were always extremely excited about the project and shared your thoughts and suggestions. On top of that, you provided me with feedback to help me become a better researcher. Thanks to Tom Kamperman for being the external member of the examination committee, and for taking the time to evaluate my thesis and provide me with new insights and suggestions on the project.

Lastly, I would like to thank the members of the DBE group for always being eager to help in the lab. A special thanks to Malin Becker for helping me with the compression measurements and for her insights in the possibilities for encapsulation, Maik Schot for explaining the microfluidic set up for core shell production, and Jacqueline Plass for helping me out with any questions and troubles encountered with the XVivo system. Also many thanks to Tom Knop for taking the time to help me out taking images with the Zeiss Confocal. Thanks to all the DBE students at the student table for the support and the many fun coffee breaks.

References

[1] Caddeo S, Boffito M, Sartori S. Tissue engineering approaches in the design of healthy and pathological in vitro tissue models. Front Bioeng Biotechnol 2017;5:272273. https://doi.org/10.3389/FBIOE.2017.00040/BIBTEX.

[2] Griffith CK, Miller C, Sainson RCA, Calvert JW, Jeon NL, Hughes CCW, et al. Diffusion Limits of an in Vitro Thick Prevascularized Tissue. Https://HomeLiebertpubCom/Ten 2005;11:257–66. https://doi.org/10.1089/TEN.2005.11.257.

[3] Moysidou CM, Barberio C, Owens RM. Advances in Engineering Human Tissue Models. Front Bioeng Biotechnol 2021;8:620962. https://doi.org/10.3389/FBIOE.2020.620962/BIBTEX.

[4] Rouwkema J, Koopman BFJM, Blitterswijk CAV, Dhert WJA, Malda J. Supply of nutrients to cells in engineered tissues. Biotechnol Genet Eng Rev 2009;26:163–78. https://doi.org/10.5661/BGER-26-163.

[5] Rizzo SA, Bartley O, Rosser AE, Newland B. Oxygen-glucose deprivation in neurons: implications for cell transplantation therapies. Prog Neurobiol 2021;205. https://doi.org/10.1016/J.PNEUROBIO.2021.102126.

[6] Farzin A, Hassan S, Moreira Teixeira LS, Gurian M, Crispim JF, Manhas V, et al. Self-Oxygenation of Tissues Orchestrates Full-Thickness Vascularization of Living Implants. Adv Funct Mater 2021;31:2100850. https://doi.org/10.1002/ADFM.202100850.

[7] McMurtrey RJ. Analytic models of oxygen and nutrient diffusion, metabolism dynamics, and architecture optimization in three-dimensional tissue constructs with applications and insights in cerebral organoids. Tissue Eng - Part C Methods 2016;22:221–49. https://doi.org/10.1089/TEN.TEC.2015.0375/ASSET/IMAGES/LARGE/FIGURE12.JPEG.

[8] Adeva-Andany MM, González-Lucán M, Donapetry-García C, Fernández-Fernández C, Ameneiros-Rodríguez E. Glycogen metabolism in humans. BBA Clin 2016;5:85–100. https://doi.org/10.1016/J.BBACLI.2016.02.001.

[9] Kanungo S, Wells K, Tribett T, El-Gharbawy A. Glycogen metabolism and glycogen storage disorders. Ann Transl Med 2018;6:474–474. https://doi.org/10.21037/ATM.2018.10.59.

[10] Murray B, Rosenbloom C. Fundamentals of glycogen metabolism for coaches and athletes. Nutr Rev 2018;76:243–59. https://doi.org/10.1093/NUTRIT/NUY001.

[11] Willemen NGA, Hassan S, Gurian M, Li J, Allijn IE, Shin SR, et al. Oxygen-Releasing Biomaterials: Current Challenges and Future Applications. Trends Biotechnol 2021;39:1144–59. https://doi.org/10.1016/J.TIBTECH.2021.01.007.

[12] Willemen NGA, Hassan S, Gurian M, Jasso-Salazar MF, Fan K, Wang H, et al. Enzyme Mediated Alleviation of Peroxide Toxicity in Self-Oxygenating Biomaterials. Adv Healthc Mater 2022;11:2102697. https://doi.org/10.1002/ADHM.202102697.

[13] Newland H, Eigel D, Rosser AE, Werner C, Newland B. Oxygen producing microscale spheres affect cell survival in conditions of oxygen-glucose deprivation in a cell specific manner: implications for cell transplantation. Biomater Sci 2018;6:2571–7. https://doi.org/10.1039/C8BM00490K.

[14] Hall JE, Hall ME. Cerebral Blood Flow, Cerebrospinal Fluid, and Brain Metabolism, Guyton and Hall Textbook of Medical Physiology, Fourteenth Edition, Chapter 62, 777-784, ISBN: 0323597122.

[15] Deschepper, M., Oudina, K., David, B., Myrtil, V., Collet, C., Bensidhoum, M., LogeartAvramoglou, D., Petite, H., 2011. Survival and function of mesenchymal stem cells (MSCs) depend on glucose to overcome exposure to long-term, severe and continuous hypoxia. Journal of Cellular and Molecular Medicine 15 (7), 1505–1514.

[16] Deschepper, M., Manassero, M., Oudina, K., Paquet, J., Monfoulet, L.-E., Bensidhoum, M., Logeart-Avramoglou, D., Petite, H., 2013. Proangiogenic and prosurvival functions of glucose in human mesenchymal stem cells upon transplantation. Stem Cells 31 (3), 526–535.

[17] Moya A, Paquet J, Deschepper M, Larochette N, Oudina K, Denoeud C, et al. Human Mesenchymal Stem Cell Failure to Adapt to Glucose Shortage and Rapidly Use Intracellular Energy Reserves Through Glycolysis Explains Poor Cell Survival After Implantation. Stem Cells 2018;36:363–76. https://doi.org/10.1002/STEM.2763.

[18] Zhang H, Ma J, Tang K, Huang B. Beyond energy storage: roles of glycogen metabolism in health and disease. FEBS J 2021;288:3772–83. https://doi.org/10.1111/FEBS.15648.

[19] Testoni G, Duran J, Vilaseca M, Muñ Oz-Cá P, Guinovart Correspondence JJ. Lack of Glycogenin Causes Glycogen Accumulation and Muscle Function Impairment. Cell Metab 2017;26:256–66. https://doi.org/10.1016/j.cmet.2017.06.008.

[20] Nawaz A, Zhang P, Li E, Gilbert RG, Sullivan MA. The importance of glycogen molecular structure for blood glucose control. IScience 2021;24:101953. https://doi.org/10.1016/J.ISCI.2020.101953.

[21] Sullivan MA, Forbes JM. Glucose and glycogen in the diabetic kidney: Heroes or villains? EBioMedicine 2019;47:590–7. https://doi.org/10.1016/J.EBIOM.2019.07.067.

[22] Liu QH, Tang JW, Wen PB, Wang MM, Zhang X, Wang L. From Prokaryotes to Eukaryotes: Insights Into the Molecular Structure of Glycogen Particles. Front Mol Biosci 2021;8:673315. https://doi.org/10.3389/FMOLB.2021.673315/BIBTEX.

[23] Besford QA, Cavalieri F, Caruso F. Glycogen as a Building Block for Advanced Biological Materials. Adv Mater 2020;32:1904625. https://doi.org/10.1002/ADMA.201904625.

[24] Gopinath V, Saravanan S, Al-Maleki AR, Ramesh M, Vadivelu J. A review of natural polysaccharides for drug delivery applications: Special focus on cellulose, starch and glycogen. Biomed Pharmacother 2018;107:96–108. https://doi.org/10.1016/J.BIOPHA.2018.07.136.

[25] Gálisová A, Jirátová M, Rabyk M, Sticová E, Hájek M, Hrubý M, et al. Glycogen as an advantageous polymer carrier in cancer theranostics: Straightforward in vivo evidence. Sci Reports 2020 101 2020;10:1–11. https://doi.org/10.1038/s41598-020-67277-y.

[26] Prats C, Graham TE, Shearer J. The dynamic life of the glycogen granule. J Biol Chem 2018;293:7089. https://doi.org/10.1074/JBC.R117.802843.

[27] Zeqiraj E, Tang X, Hunter RW, García-Rocha M, Judd A, Deak M, et al. Structural basis for the recruitment of glycogen synthase by glycogenin. Proc Natl Acad Sci U S A 2014;111:E2831–40. https://doi.org/10.1073/PNAS.1402926111/SUPPL_FILE/PNAS.1402926111.SAPP.PDF.

[28] Ryu JH, Drain J, Kim JH, McGee S, Gray-Weale A, Waddington L, et al. Comparative structural analyses of purified glycogen particles from rat liver, human skeletal muscle and commercial preparations. Int J Biol Macromol 2009;45:478–82. https://doi.org/10.1016/J.IJBIOMAC.2009.08.006.

[29] Deng B, Sullivan MA, Chen C, Li J, Powell PO, Hu Z, et al. Molecular Structure of Human-Liver Glycogen. PLoS One 2016;11:e0150540. https://doi.org/10.1371/JOURNAL.PONE.0150540.

[30] Zhou Y, van Zijl PCM, Xu X, Xu J, Li Y, Chen L, et al. Magnetic resonance imaging of glycogen using its magnetic coupling with water. Proc Natl Acad Sci U S A 2020;117:3144–9. https://doi.org/10.1073/PNAS.1909921117/-/DCSUPPLEMENTAL.

[31] Obel LF, Müller MS, Walls AB, Sickmann HM, Bak LK, Waagepetersen HS, et al. Brain glycogen—new perspectives on its metabolic function and regulation at the subcellular level. Front Neuroenergetics 2012;4. https://doi.org/10.3389/FNENE.2012.00003.

[32] Liu QH, Tang JW, Wen PB, Wang MM, Zhang X, Wang L. From Prokaryotes to Eukaryotes: Insights Into the Molecular Structure of Glycogen Particles. Front Mol Biosci 2021;8:673315. https://doi.org/10.3389/FMOLB.2021.673315/BIBTEX.

[33] Kajiura H, Kakutani R, Akiyama T, Takata H, Kuriki T. A novel enzymatic process for glycogen production. Http://DxDoiOrg/101080/10242420701789411 2009;26:133–40. https://doi.org/10.1080/10242420701789411.

[34] Takata H, Kajiura H, Furuyashiki T, Kakutani R, Kuriki T. Fine structural properties of natural and synthetic glycogens. Carbohydr Res 2009;344:654–9. https://doi.org/10.1016/J.CARRES.2009.01.008.

[35] Ida-Yonemochi H, Nakagawa E, Takata H, Furuyashiki T, Kakutani R, Tanaka M, et al. Extracellular enzymatically synthesized glycogen promotes osteogenesis by activating osteoblast differentiation via Akt/GSK-3β signaling pathway. J Cell Physiol 2019;234:13602–16. https://doi.org/10.1002/JCP.28039.

[36] Minarich LA, Kirpich A, Fiske LM, Weinstein DA. Bone mineral density in glycogen storage disease type Ia and Ib. Genet Med 2013;14:737. https://doi.org/10.1038/GIM.2012.36.

[37] Jacoby JT, Bento Dos Santos B, Nalin T, Colonetti K, Farret Refosco L, de Souza CFM, et al. Bone mineral density in patients with hepatic glycogen storage diseases. Nutrients 2021;13. https://doi.org/10.3390/NU13092987/S1.

[38] Mogahed EA, El-Moslemany M, Aboueleyoun I, Musa N, Abo-Elsoud M, El-Raziky MS. A high prevalence of low bone mineral density in children with glycogen storage disease type III. Arch Med Sci 2021. https://doi.org/10.5114/AOMS/141986.

[39] Osteoporosis as a major risk for patients with glycogen storage disease | SFEBES2009 | Society for Endocrinology BES 2009 | Endocrine Abstracts n.d. https://www.endocrine-abstracts.org/ea/0019/ea0019p14 (accessed June 15, 2023).

[40] Chen M, Bolognesi G, Vladisavljević GT. Crosslinking Strategies for the Microfluidic Production of Microgels. Molecules 2021;26. https://doi.org/10.3390/MOLECULES26123752.

[41] Kamperman T, Willemen NGA, Kelder C, Koerselman M, Becker M, Lins L, et al. Steering Stem Cell Fate within 3D Living Composite Tissues Using Stimuli-Responsive Cell-Adhesive Micromaterials. Adv Sci 2023;10:2205487. https://doi.org/10.1002/ADVS.202205487.

[42] van Loo B, Salehi SS, Henke S, Shamloo A, Kamperman T, Karperien M, et al. Enzymatic outside-in cross-linking enables single-step microcapsule production for high-throughput three-dimensional cell microaggregate formation. Mater Today Bio 2020;6:100047. https://doi.org/10.1016/J.MTBIO.2020.100047.

[43] Shieh H, Saadatmand M, Eskandari M, Bastani D. Microfluidic on-chip production of microgels using combined geometries. Sci Reports 2021 111 2021;11:1–10. https://doi.org/10.1038/s41598-021-81214-7.

[44] Whitesides GM. The origins and the future of microfluidics. Nat 2006 4427101 2006;442:368–73. https://doi.org/10.1038/nature05058.

[45] Fatehifar M, Revell A, Jabbari M. Non-Newtonian Droplet Generation in a Cross-Junction Microfluidic Channel. Polym 2021, Vol 13, Page 1915 2021;13:1915. https://doi.org/10.3390/POLYM13121915.

[46] Moreira Teixeira LS, Bijl S, Pully V V., Otto C, Jin R, Feijen J, et al. Self-attaching and cell-attracting in-situ forming dextran-tyramine conjugates hydrogels for arthroscopic cartilage repair. Biomaterials 2012;33:3164–74. https://doi.org/10.1016/J.BIOMATERIALS.2012.01.001.

[47] Jin R, Moreira Teixeira LS, Dijkstra PJ, van Blitterswijk CA, Karperien M, Feijen J. Enzymatically-crosslinked injectable hydrogels based on biomimetic dextran–hyaluronic acid conjugates for cartilage tissue engineering. Biomaterials 2010;31:3103–13. https://doi.org/10.1016/J.BIOMATERIALS.2010.01.013.

[48] Kamperman T, Henke S, Crispim JF, Willemen NGA, Dijkstra PJ, Lee W, et al. Tethering Cells via Enzymatic Oxidative Crosslinking Enables Mechanotransduction in Non-Cell-Adhesive Materials. Adv Mater 2021;33:2102660. https://doi.org/10.1002/ADMA.202102660.

[49] Kamperman T, Teixeira LM, Salehi SS, Kerckhofs G, Guyot Y, Geven M, et al. Engineering 3D parallelized microfluidic droplet generators with equal flow profiles by computational fluid dynamics and stereolithographic printing. Lab Chip 2020;20:490–5. https://doi.org/10.1039/C9LC00980A.

[50] Kamperman T, Koerselman M, Kelder C, Hendriks J, Crispim JF, de Peuter X, et al. Spatiotemporal material functionalization via competitive supramolecular complexation of avidin and biotin analogs. Nat Commun 2019 101 2019;10:1–11. https://doi.org/10.1038/s41467-019-12390-4.

[51] Estrada JC, Albo C, Benguría A, Dopazo A, López-Romero P, Carrera-Quintanar L, et al. Culture of human mesenchymal stem cells at low oxygen tension improves growth and genetic stability by activating glycolysis. Cell Death Differ 2012 195 2011;19:743–55. https://doi.org/10.1038/cdd.2011.172.

[52] Lee DY, Lee SY, Yun SH, Jeong JW, Kim JH, Kim HW, et al. Review of the Current Research on Fetal Bovine Serum and the Development of Cultured Meat. Food Sci Anim Resour 2022;42:775. https://doi.org/10.5851/KOSFA.2022.E46.

[53] Coster J, Mccauley R, Hall J. Glutamine: metabolism and application in nutrition support. Asia Pac J Clin Nutr 2004.

[54] Higuera GA, Schop D, Spitters TWGM, Van Dijkhuizen-Radersma R, Bracke M, De Bruijn JD, et al. Patterns of Amino Acid Metabolism by Proliferating Human Mesenchymal Stem Cells. Tissue Eng Part A 2012;18:654. https://doi.org/10.1089/TEN.TEA.2011.0223.

[55] Barot S, Abo-Ali EM, Zhou DL, Palaguachi C, Dukhande V V. Inhibition of glycogen catabolism induces intrinsic apoptosis and augments multikinase inhibitors in hepatocellular carcinoma cells. Exp Cell Res 2019;381:288–300. https://doi.org/10.1016/J.YEXCR.2019.05.017.

[56] Koeppen BM, Stanton BA. Physiology of Body Fluids. Ren Physiol 2013:1–14. https://doi.org/10.1016/B978-0-323-08691-2.00001-6.

[57] Dibartola SP. Fluid, Electrolyte and Acid-Base Disorders in Small Animal Practice. Fluid, Electrolyte Acid-Base Disord Small Anim Pract 2006. https://doi.org/10.1016/B0-7216-3949-6/X5001-2.

[58] Annabi N, Nichol JW, Zhong X, Ji C, Koshy S, Khademhosseini A, et al. Controlling the porosity and microarchitecture of hydrogels for tissue engineering. Tissue Eng - Part B Rev 2010;16:371–83. https://doi.org/10.1089/TEN.TEB.2009.0639/ASSET/IMAGES/LARGE/FIGURE7.JPEG.

[59] Krishnamoorthy S, Noorani B, Xu C. Effects of Encapsulated Cells on the Physical–Mechanical Properties and Microstructure of Gelatin Methacrylate Hydrogels. Int J Mol Sci 2019, Vol 20, Page 5061 2019;20:5061. https://doi.org/10.3390/IJMS20205061.

[60] Ferreira L, Figueirecio MM, Gil MH, Ramos MA. Structural analysis of dextran-based hydrogels obtained chemoenzymatically. J Biomed Mater Res Part B Appl Biomater 2006;77B:55–64. https://doi.org/10.1002/JBM.B.30394.

[61] Size of glucose molecule - Generic - BNID 106979 n.d. https://bionumbers.hms.harvard.edu/bionumber.aspx?id=106979&ver=1 (accessed June 16, 2023).

[62] Xue CD, Chen XD, Li YJ, Hu GQ, Cao T, Qin KR. Breakup Dynamics of Semi-dilute Polymer Solutions in a Microfluidic Flow-focusing Device. Micromachines 2020;11. https://doi.org/10.3390/MI11040406.

[63] Gaillard A, Sijs R, Bonn D. What determines the drop size in sprays of polymer solutions? J Nonnewton Fluid Mech 2022;305:104813. https://doi.org/10.1016/J.JNNFM.2022.104813.

[64] Lopez-Sanchez P, Assifaoui A, Cousin F, Moser J, Bonilla MR, Ström A. Impact of Glucose on the Nanostructure and Mechanical Properties of Calcium-Alginate Hydrogels. Gels 2022;8:71. https://doi.org/10.3390/GELS8020071/S1.

[65] Wiley CD, Campisi J. The metabolic roots of senescence: mechanisms and opportunities for intervention. Nat Metab 2021 310 2021;3:1290–301. https://doi.org/10.1038/s42255-021-00483-8.

[66] Wiley CD, Campisi J. From ancient pathways to aging cells - Connecting metabolism and cellular senescence. Cell Metab 2016;23:1013. https://doi.org/10.1016/J.CMET.2016.05.010.

[67] Luo T, Tan B, Zhu L, Wang Y, Liao J. A Review on the Design of Hydrogels With Different Stiffness and Their Effects on Tissue Repair. Front Bioeng Biotechnol 2022;10. https://doi.org/10.3389/FBIOE.2022.817391.

[68] Xu Y, Gaillez MP, Zheng K, Voigt D, Cui M, Kurth T, et al. A Self-Assembled Matrix System for Cell-Bioengineering Applications in Different Dimensions, Scales, and Geometries. Small 2022;18:2104758. https://doi.org/10.1002/SMLL.202104758.

[69] Regmi S, Raut PK, Pathak S, Shrestha P, Park PH, Jeong JH. Enhanced viability and function of mesenchymal stromal cell spheroids is mediated via autophagy induction. Autophagy 2021;17:2991. https://doi.org/10.1080/15548627.2020.1850608.

[70] Lemons JMS, Coller HA, Feng XJ, Bennett BD, Legesse-Miller A, Johnson EL, et al. Quiescent Fibroblasts Exhibit High Metabolic Activity. PLOS Biol 2010;8:e1000514. https://doi.org/10.1371/JOURNAL.PBIO.1000514.

[71] Sohn S, Van Buskirk M, Buckenmeyer MJ, Londono R, Faulk D. Whole Organ Engineering: Approaches, Challenges, and Future Directions. Appl Sci 2020, Vol 10, Page 4277 2020;10:4277. https://doi.org/10.3390/APP10124277.

[72] Kurniawan NA. The ins and outs of engineering functional tissues and organs: Evaluating the in-vitro and in-situ processes. Curr Opin Organ Transplant 2019;24:590–7. https://doi.org/10.1097/MOT.0000000000000690.

[73] Tang BL. Glucose, glycolysis, and neurodegenerative diseases. J Cell Physiol 2020;235:7653–62. https://doi.org/10.1002/JCP.29682.

[74] Bell SM, Burgess T, Lee J, Blackburn DJ, Allen SP, Mortiboys H. Peripheral Glycolysis in Neurodegenerative Diseases. Int J Mol Sci 2020;21:1–19. https://doi.org/10.3390/IJMS21238924.

[75] Khan T, Sullivan MA, Gunter JH, Kryza T, Lyons N, He Y, et al. Revisiting Glycogen in Cancer: A Conspicuous and Targetable Enabler of Malignant Transformation. Front Oncol 2020;10:592455. https://doi.org/10.3389/FONC.2020.592455.

[76] Pritchard JC, Center SA. Glycogen Storage Disease. Blackwell's Five-Minute Vet Consult Clin Companion Small Anim Gastrointest Dis 2023:729–33. https://doi.org/10.1002/9781119376293.ch111.

[77] Nie J, Chen Z. A generic method for fluorescence monitoring glycogen through patent blue V triggered supramolecular switching. Sensors Actuators B Chem 2022;359:131630. https://doi.org/10.1016/J.SNB.2022.131630.

[78] Besford QA, Wojnilowicz M, Suma T, Bertleff-Zieschang N, Caruso F, Cavalieri F. Lactosylated Glycogen Nanoparticles for Targeting Prostate Cancer Cells. ACS Appl Mater Interfaces 2017;9:16869–79. https://doi.org/10.1021/ACSAMI.7B02676/ASSET/IMAGES/LARGE/AM-2017-02676H_0008.JPEG.

[79] Rashid TU, Sharmeen S, Biswas S, Ahmed T, Mallik AK, Shahruzzaman M, et al. Gelatin-Based Hydrogels 2018:1–41. https://doi.org/10.1007/978-3-319-76573-0_53-1.

[80] Newsom JP, Payne KA, Krebs MD. Microgels: Modular, Tunable Constructs for Tissue Regeneration. Acta Biomater 2019;88:32. https://doi.org/10.1016/J.ACTBIO.2019.02.011.

[81] Hou Y, Xie W, Achazi K, Cuellar-Camacho JL, Melzig MF, Chen W, et al. Injectable degradable PVA microgels prepared by microfluidic technology for controlled osteogenic differentiation of mesenchymal stem cells. Acta Biomater 2018;77:28–37. https://doi.org/10.1016/J.ACTBIO.2018.07.003.

[82] Zhou W, Stukel J, Alniemi A, Willits RK. Novel microgel-based scaffolds to study the effect of degradability on human dermal fibroblasts. Biomed Mater 2018;13:055007. https://doi.org/10.1088/1748-605X/AACA57.

[83] Coronel MM, Martin KE, Hunckler MD, Kalelkar P, Shah RM, García AJ, et al. Hydrolytically Degradable Microgels with Tunable Mechanical Properties Modulate the Host Immune Response. Small 2022;18:2106896. https://doi.org/10.1002/SMLL.202106896.

[84] Low Blood Sugar (Hypoglycemia) | Diabetes | CDC n.d. https://www.cdc.gov/diabetes/basics/low-blood-sugar.html (accessed June 15, 2023).

[85] Low blood sugar (hypoglycaemia) - NHS n.d. https://www.nhs.uk/conditions/low-blood-sugar-hypoglycaemia/ (accessed June 15, 2023).

[86] Information for parents and carers n.d. https://www.royalberkshire.nhs.uk/media/enckebmf/hypoglycaemia-ketotic-hypoglycaemia_nov20.pdf (accessed June 15, 2023).

[87] Vaillant AAJ, Zito PM. Neutropenia. Autoimmune Dis Fourth Ed 2022:585–9. https://doi.org/10.1016/B978-012595961-2/50046-9.

[88] Hypotonia | National Institute of Neurological Disorders and Stroke n.d. https://www.ninds.nih.gov/health-information/disorders/hypotonia (accessed June 15, 2023).

[89] Enlarged liver - Symptoms and causes - Mayo Clinic n.d. https://www.mayoclinic.org/diseases-conditions/enlarged-liver/symptoms-causes/syc-20372167 (accessed June 15, 2023).

[90] Cirrhosis - NIDDK n.d. https://www.niddk.nih.gov/health-information/liver-disease/cirrhosis (accessed June 15, 2023).

[91] Martinez-Hervas S, Ascaso JF. Hypercholesterolemia. Encycl Endocr Dis 2023:320–6. https://doi.org/10.1016/B978-0-12-801238-3.65340-0.

[92] Torres PA, Helmstetter JA, Kaye AM, Kaye AD. Rhabdomyolysis: Pathogenesis, Diagnosis, and Treatment. Ochsner J 2015;15:58.

[93] Bockman CS, Eckerson J, McCarson KE. Myalgia. Ref Modul Biomed Sci 2015. https://doi.org/10.1016/B978-0-12-801238-3.05161-8.

[94] Diabetic Retinopathy | National Eye Institute n.d. https://www.nei.nih.gov/learn-about-eye-health/eye-conditions-and-diseases/diabetic-retinopathy (accessed June 15, 2023).

[95] Sun SZ, Empie MW. Fructose metabolism in humans – what isotopic tracer studies tell us. Nutr Metab (Lond) 2012;9:89. https://doi.org/10.1186/1743-7075-9-89.

[96] Nikolits I, Nebel S, Egger D, Kreß S, Kasper C. Towards Physiologic Culture Approaches to Improve Standard Cultivation of Mesenchymal Stem Cells. Cells 2021, Vol 10, Page 886 2021;10:886. https://doi.org/10.3390/CELLS10040886.

[97] Sun SZ, Empie MW. Fructose metabolism in humans – what isotopic tracer studies tell us. Nutr Metab (Lond) 2012;9:89. https://doi.org/10.1186/1743-7075-9-89.

[98] Sharma V, Ichikawa M, Freeze HH. MANNOSE METABOLISM: MORE THAN MEETS THE EYE. Biochem Biophys Res Commun 2014;453:220. https://doi.org/10.1016/J.BBRC.2014.06.021.

[99] Sharma V, Smolin J, Nayak J, Ayala JE, Scott DA, Peterson SN, et al. Mannose Alters Gut Microbiome, Prevents Diet-Induced Obesity and Improves Host Metabolism. SSRN Electron J 2018. https://doi.org/10.2139/SSRN.3205404.

[100] Wheaton WW, Chandel NS. Hypoxia. 2. Hypoxia regulates cellular metabolism. Am J Physiol - Cell Physiol 2011;300:C385. https://doi.org/10.1152/AJPCELL.00485.2010.

[101] Cucchi D, Camacho-Muñoz D, Certo M, Pucino V, Nicolaou A, Mauro C. Fatty acids - from energy substrates to key regulators of cell survival, proliferation and effector function. Cell Stress 2020;4:9. https://doi.org/10.15698/CST2020.01.209.

[102] Smith AN, Muffley LA, Bell AN, Numhom S, Hocking AM. Unsaturated fatty acids induce mesenchymal stem cells to increase secretion of angiogenic mediators. J Cell Physiol 2012;227:3225. https://doi.org/10.1002/JCP.24013.

[103] Legrand P, Rioux V. The Complex and Important Cellular and Metabolic Functions of Saturated Fatty Acids. Lipids 2010;45:941. https://doi.org/10.1007/S11745-010-3444-X.

[104] Leschelle X, Delpal S, Goubern M, Blottière HM, Blachier F. Butyrate metabolism upstream and downstream acetyl-CoA synthesis and growth control of human colon carcinoma cells. Eur J Biochem 2000;267:6435–42. https://doi.org/10.1046/J.1432-1327.2000.01731.X.

[105] Xie J, Lou Q, Zeng Y, Liang Y, Xie S, Xu Q, et al. Single-Cell Atlas Reveals Fatty Acid Metabolites Regulate the Functional Heterogeneity of Mesenchymal Stem Cells. Front Cell Dev Biol 2021;9:653308. https://doi.org/10.3389/FCELL.2021.653308/BIBTEX.

[106] dos Santos GG, Hastreiter AA, Sartori T, Borelli P, Fock RA. L-Glutamine in vitro Modulates some Immunomodulatory Properties of Bone Marrow Mesenchymal Stem Cells. Stem Cell Rev Reports 2017;13:482–90. https://doi.org/10.1007/S12015-017-9746-0/FIGURES/5.

[107] Rubin H. Deprivation of glutamine in cell culture reveals its potential for treating cancer. Proc Natl Acad Sci U S A 2019;116:6964–8. https://doi.org/10.1073/PNAS.1815968116/ASSET/7D240977-2EB5-4CB6-B5CB-95F1F88EC79E/ASSETS/GRAPHIC/PNAS.1815968116FIG06.JPEG.

[108] Chinopoulos C. Which way does the citric acid cycle turn during hypoxia? The critical role of α-ketoglutarate dehydrogenase complex. J Neurosci Res 2013;91:1030–43. https://doi.org/10.1002/JNR.23196.

[109] Fujisawa K, Hara K, Takami T, Okada S, Matsumoto T, Yamamoto N, et al. Evaluation of the effects of ascorbic acid on metabolism of human mesenchymal stem cells. Stem Cell Res Ther 2018;9:1–12. https://doi.org/10.1186/S13287-018-0825-1/FIGURES/6.

[110] Santacruz L, Arciniegas AJL, Darrabie M, Mantilla JG, Baron RM, Bowles DE, et al. Hypoxia decreases creatine uptake in cardiomyocytes, while creatine supplementation enhances HIF activation. Physiol Rep 2017;5. https://doi.org/10.14814/PHY2.13382.

[111] Chamberlain KA, Chapey KS, Nanescu SE, Huang JK. Creatine Enhances Mitochondrial-Mediated Oligodendrocyte Survival After Demyelinating Injury. J Neurosci 2017;37:1479. https://doi.org/10.1523/JNEUROSCI.1941-16.2016.

[112] Spillane M, Schoch R, Cooke M, Harvey T, Greenwood M, Kreider R, et al. The effects of creatine ethyl ester supplementation combined with heavy resistance training on body

composition, muscle performance, and serum and muscle creatine levels. J Int Soc Sports Nutr 2009;6. https://doi.org/10.1186/1550-2783-6-6.

[113] Eales KL, Hollinshead KER, Tennant DA. Hypoxia and metabolic adaptation of cancer cells. Oncog 2016 51 2016;5:e190–e190. https://doi.org/10.1038/oncsis.2015.50.

[114] TeSlaa T, Chaikovsky AC, Lipchina I, Escobar SL, Hochedlinger K, Huang J, et al. α-Ketoglutarate Accelerates the Initial Differentiation of Primed Human Pluripotent Stem Cells. Cell Metab 2016;24:485–93. https://doi.org/10.1016/J.CMET.2016.07.002.

Supplementary Material

S1. Glycogen Storage Disorders (GSDs)

S1.1 Short explanation of main conditions caused by GSDs

Table 1: Short explanation of main conditions caused by glycogen storage disorders.

Condition	Explanation
Hypoglycemia	Low blood sugar level, typically below 70 mg/dL (normal levels are between 72 and 99 mg/dL) [18, 84, 85].
Ketonic hypoglycemia	Recurrent episodes of hypoglycemia [86].
Neutropenia	Lower number of neutrophils present in blood (less than 1.5x10/L) leasing to decreased capabilities of the immune system [87].
Hypotonia	Muscles show a small amount of contraction and muscle tone is decreased [88].
Hepatomegaly	The liver is enlarged, which can be an indication of liver disease, cancer, or heart failure [89].
Liver cirrhosis	The liver shows presence of scar tissue, preventing it from functioning normally [90]. In this case, the liver is permanently damaged.
Hypercholesterolemia	Uptake of cholesterol by the liver is not possible increasing the risk of developing heart disease even at a young age [91].
Rhabdomyolysis	The rapid disintegration of skeletal muscle that has been damaged [92].
Myalgia	Muscle pain, caused by injury, infection, overuse, drugs and by breakdown of muscle tissue [93].
Retinopathy	Condition in the eye that can cause loss of vision and even blindness [94].

S1.2 Overview of GSDs

In the table below, an overview is given on the GSDs identified in humas, the enzyme each GSD affects and the consequences of this for patients.

Table 2: Overview of glycogen storage disorders. Information derived from [9].

Disorder	Enzyme defect	Consequences
GSD01 – Liver GSD 0	Liver glycogen synthase	Liver unable to maintain glucose homeostasis → ketotic hypoglycemia. No glycogen storage in liver possible.
GSD0B – Muscle GSD 0	Muscle glycogen synthase	Fatigue, exercise intolerance, sudden cardiac death.
GSD1A – Von Gierke/Hepatorenal	Glucose-6-phophatase	Free glucose can not be set available → glycogen accumulation in kidney → chronic kidney disease, renal cancer, polycystic cancer Muscle fatigue, risk of cardiac arrest in childhood.
GSD1B – G6P transport defect	Glucose-6-phosphate translocase	Neutropenia due to disruption in myeloid cell energy homeostasis.
GSD2 – Pompe/Cardiac GSD	Acid maltase (alpha 1,4-glucosidase)	Hypotonia, weakness in muscles and diaphragm, arrythmias.

GSD3 – Forbes/Cori/IIIa/IIIb	Glycogen debrancher (amylo-1,6 glucosidase)	Glycogen can not be broken down → accumulation. Symptoms similar to GSD1 (growth delay, hepatomegaly, hypoglycemia). Higher chance of liver failure later in life.
GSD4 – Andersen/Amylopectinosis/ Neuromuscular/Polyglucosan	Glycogen brancher [amylo(1,4 to 1,6) transglucosidase]	Abnormal glycogen (limited branch points). Failure to thrive, liver cirrhosis, eventually liver failure → death by age of 5.
GSD5 – McArdle	Myophosphorylase	Exercise intolerance, weak muscles, cramps.
GSD6 – Hers	Liver glycogen phosphorylase	Excessive amounts of glycogen in liver, hepatomegaly, ketotic hypoglycemia. *Considered a mild disease.*
GSD7 – Tarui	Muscle phosphofructokinase	Exercise intolerance, muscle cramps, pain, fatigue, weak muscles.
GSD9A1 – XLG1	Alpha-2 subunit of liver phosphorylase kinase (in liver or erythrocytes)	More prevalent in males. Delays in growth and motor development, hepatomegaly, hypercholesterolemia. Symptoms present during childhood, most resolve during puberty.
GSD9B/GSDIXb	Beta subunit of liver and muscle phosphorylase kinase	Hepatomegaly and muscle weakness.
GSD9C/GSDIXc	Hepatic and testis isoform – gamma subunit of phosphorylase kinase	Hypoglycemia, hepatomegaly, end stage liver disease, motor delay, weak muscles, seizures and intellectual disability.
GSD9D/GSDIXd	Alpha subunit of muscle phosphorylase kinase	Muscle weakness, pain and stiffness due to exercise.
GSD10/GSDX – PGAMM deficiency	Muscle phosphoglycerate mutase	Muscle cramps, rhabdomyolysis.
GSD11/GSDXI – LDHA deficiency	Lactate dehydrogenase A	Fatigue, uterine pain and stiffness during pregnancy.
GSD12/GSDXII – Aldolase deficiency	Fructose-1,6-bisphosphate aldolase A in red cell	Anemia and myopathy.
GSD13/GSDXIII – Enolase 3 deficiency	Beta-enolase	Inability to exercise, myalgia, rhabdomyolysis.
GSD14/GSDXIV – PGM1 deficiency	Phosphoglucomutase-1	Myopathy, congenital anomalies.
GSD15/GSDXV – GYG1 deficiency	Glycogenin-1	Glycogen depletion in skeletal muscle → weak muscles. Abnormal glycogen storage in heart → arrythmia, cardiomyopathy.

Fanconi-Bickel syndrome	*Glucose transport defect*	Glycogen accumulation in liver and kidney. Defective utilization of glucose and galactose.
GSD heart, lethal congenital	Gamma-2 subunit of AMP-activated protein kinase/cardiac muscle phosphorylase kinase	Hypoglycemia and heart failure, can be fatal for infants.
Danon disease/lysosomal-associated membrane protein-2 deficiency	Lysosomal-associated membrane protein-2 def-cy	Cardio- and skeletomyopathy, arrhythmia, retinopathy, intellectual disability.
Brain GSD – Laforin deficiency	Laforin, E3 ligase	Epilepsy, dementia, hallucinations.

S2. Metabolic Library

S2.1 Explanation on the selection of metabolites tested

Carbohydrates (Sugars)

Glucose and galactose are commonly present in standard culture media, while maltose and fructose may also be included in certain media [95].

Glucose

Glucose serves as the primary energy source for cells and is involved in essential processes like protein and lipid synthesis [96]. Consequently, glucose plays an important role in cell survival, metabolism, and overall cell function. Overall, hMSCs show a glycolytic phenotype, making them more susceptible to fast glucose depletion and its subsequent consequences on cellular processes compared to other nutrients or serum [96].

Fructose

Fructose is primarily found in fruits and, to a lesser extent, in certain vegetables. Thus, fructose has been consumed by humans since forever [97]. Additionally, approximately half of the added sugars in food products consist of fructose. There are some common steps between the glucose and fructose degradation pathways. Glucose is initially converted to diphosphorylated fructose, which is then transformed into glyceraldehyde-3-phosphate and dihydroxy acetone phosphate. However, fructose itself is monophosphorylated before being converted to the same two types of phosphates as glucose. This difference in metabolic pathways may result in increased fatty acid synthesis in the presence of fructose, potentially playing a determinant role in obesity.

Mannose

Mannose is found in plants, animals, fruits, and in humans and animal plasma [98]. The GLUT transporters located in the plasma membrane that facilitate glucose and fructose transport, also facilitate the transport of mannose. Mannose is then phosphorylated to mannose-6-phosphate. From here it can follow different pathways depending on the ratio of specific enzymes present in the cell. One potential pathway involves its conversion to fructose-6-phosphate by the enzyme phosphomannose isomerase (MPI), allowing fructose-6-phosphate to enter the glycolytic pathway. However, mannose alone does not provide the cells with a sufficient amount of energy [99].

Sucrose

Sucrose, commonly known as table sugar, consists of a glucose molecule bonded to a fructose molecule, and is readily available in grocery stores [97].

Glycogen

Glycogen is a molecule composed of numerous glucose molecules (see also section 3.1 for more details).

Glyceraldehyde & Pyruvate as part of the glycolysis pathway

Looking at the glycolysis pathway, it is observed that glucose can be converted to Glyceraldehyde-3-phosphate, which is then able to generate energy. Pyruvate, as illustrated in Figure 5 (section 2.1), is considered the last step of glycolysis, resulting in the production of 30-36 ATP molecules (alongside H_2O and CO_2) under aerobic conditions, while in an anaerobic environment, it yields 2 ATP molecules and lactate [100].

Fatty acids

Fatty acids, also known as lipids, are one of the major biomolecules playing important roles in cell metabolism, structure and signaling [96]. These lipids are present in culture media due to the addition of serum. Lipids that are essential for cells, such as Linoleic acid and Linolenic acid, are produced by themselves. Even though these two are considered essential, culture medium without them still allows cell proliferation, but their addition to the medium significantly improves this process. The catabolism of fatty acids represents an efficient way of generating energy for the cell [101].

Linoleic & Linolenic acid

These two fatty acids play an essential role in the structure and diversity of the lipids found in the cell membrane [101]. They can be metabolized to meet the cellular energy requirements and can be metabolized to hormone-like mediators that are involved in immune responses. However, at a concentration of 20µM, linoleic acid inhibits hMSC proliferation, and exposure of cells to linoleic acid leads to a decreased cell viability on days 3, 5 and 7 [102]. This negative effect of linoleic acid on hMSCs is likely due to its interference with DNA synthesis.

Oleic acid

Oleic acid has similar effects on cell viability compared to linoleic acid [102]. At a concentration of 20µM, it inhibits cell proliferation, and cell viability decreases on days 3, 5 and 7.

Palmeate

Palmeate, also known as palmitic acid, is found in natural fats, and has demonstrated to play a significant role in signal transduction processes [103]. Its presence in the liver enhances the transcription of the glucose-6-phoshpatase gene and recruits various transcription factors.

Butyrate

In the human body, butyrate is predominantly found in the colon [104]. High doses of butyrate reduce cell growth in HT-29 (cancer cell line). In cell culture, butyrate increases the rate of apoptosis, while also suppressing the self-renewal and differentiation potential of MSCs [105].

Amino acids

The 20 amino acids that occur in nature can be divided in essential (essential AAs) and non essential (NEAAs) [96]. Thus, culture media are generally supplemented with essential AAs, as cells possess the capacity to synthesize the non essential ones internally. However, supplying cells with both essential and non essential AAs can improve cell proliferation, although an excessive supply of NEAAs can reduce the proliferation rate. The most used amino acid in culture media is L-glutamine [106].

Glutamine

While glutamine is typically classified as a NEAAs, it can become essential under specific stressful conditions such as cancer [106, 107]. Depriving cancer cells of glutamine leads to a reduction in their growth rate [107]. At high concentrations (10mM), glutamine has the capacity to promote MSC proliferation [106].

Aspartic acid

Under anoxic conditions, aspartic acid (also known as aspartate) can have a positive influence on cells, but only in the presence of alpha-ketoglutarate [108]. The coexistence of these metabolites triggers a sequence of metabolic reactions in the maltase-aspartate shuttle eventually leading to ATP production. This implies however that the metabolites on their own are incapable of maintaining cell viability.

Vitamins

Vitamins are often present in the serum that is added to the culture media (FBS). Ascorbic acid, commonly known as Vitamin C, has been found to promote hMSC proliferation, specifically for hMSCs derived from bone marrow [96, 109]. Additionally, it eliminates reactive oxygen species (ROS) caused by oxidative stress, like for example in hypoxic and anoxic conditions [109]. Ascorbic acid can enhance proliferation of MSCs (concentration of 250 µM) but in excessively high concentrations (500µM) it hinders proliferation [96].

Other

Creatine

Creatine can be useful for cellular adaptation to hypoxic conditions [110]. Studies have demonstrated that creatine can regulate the metabolic activity of neurons, offering protection against oxidative damage, thus acting as a sort ATP buffer [111]. However, creatine itself cannot be converted to ATP [111, 112]. ATP production involves the conversion of phosphocreatine to creatine, and ATP is required to convert creatine to phosphocreatine. Hence, phosphocreatine may serve as a more suitable nutrient for energy supply.

Acetate

Cancer cells are able to metabolize acetate to get sufficient amounts of acetyl-CoA to produce lipids [113].

α-ketoglutarate

Alpha-ketoglutarate, in combination with alanine, can generate glutamate and pyruvate, suggesting that in combination it can probably contribute to ATP formation. However, on its own cannot serve as an independent energy source [108]. Similarly, when combined with aspartic acid. Increased levels of alpha-ketoglutarate within cells have been shown to promote self-renewal of mouse-derived embryonic stem cells [114].

S2.2 Other important information on the metabolic library experiment

Use of chemically defined medium

To investigate the impact of individual metabolites on cell viability, a chemically defined medium was used. This ensures that the culture medium used does not contain any unidentified factors like serum (e.g. FBS) or other supplements that may influence the cell viability [96]. It is important to note that a chemically defined medium differs from serum free medium, as the latter lacks serum but may still contain metabolites or nutrients. For the metabolic library experiment, the chemically defined medium was supplemented sodium bicarbonate acting as a buffer to maintain pH stability, as well as 100 U/ml penicillin and 100mg/ml streptomycin to minimize the risk of infections.

Concentrations used

In human plasma, glucose levels within the range of 700 and 1000 mg/L are considered healthy [96]. In cell culture media, typical glucose concentrations range from 1000 mg/L to resemble as closely as possible the glucose concentration measured *in vivo*, till up to 10,000 mg/L to simulate for example diabetic conditions. As a glucose concentration of 1000 mg/ml (=5.5mM) is within the normal physiological range, this concentration was chosen as the highest concentration to be tested. Additionally, lower concentrations were evaluated to determine which metabolites can sustain cell viability at reduced levels. Specifically, concentrations of 10-fold and 100-fold smaller than the standard glucose concentration were included in the analysis.

Culture conditions

All metabolites were tested both in normoxia (21% O_2) and anoxia (0.1% O_2).

Other

As a positive control, standard hMSC proliferation medium was used. The negative control was the culture of hMSCs in chemically defined medium without the addition of any metabolite. Each conditions was tested in triplo and viability was assessed on day 3, 5 and 7.

S3. hMSCs cultured with proliferation and chemically defined medium

Human mesenchymal stem cells (hMSCs) were cultured in standard proliferation and in chemically defined medium, and their viability was assessed on days 3, 5 and 7. Representative images illustrating the cell viability on day 3 and day 5 are presented in Figure 36, while the corresponding images for day 7 can be found in Figure 21, section 5.1. Generally, hMSCs maintained their viability when cultured in the proliferation medium. However, when exposed to chemically defined medium, the viability of hMSCs exhibited a drastic decrease as early as day 3 in both normoxic and anoxic conditions. This decrement in viability continued on days 5 and 7.

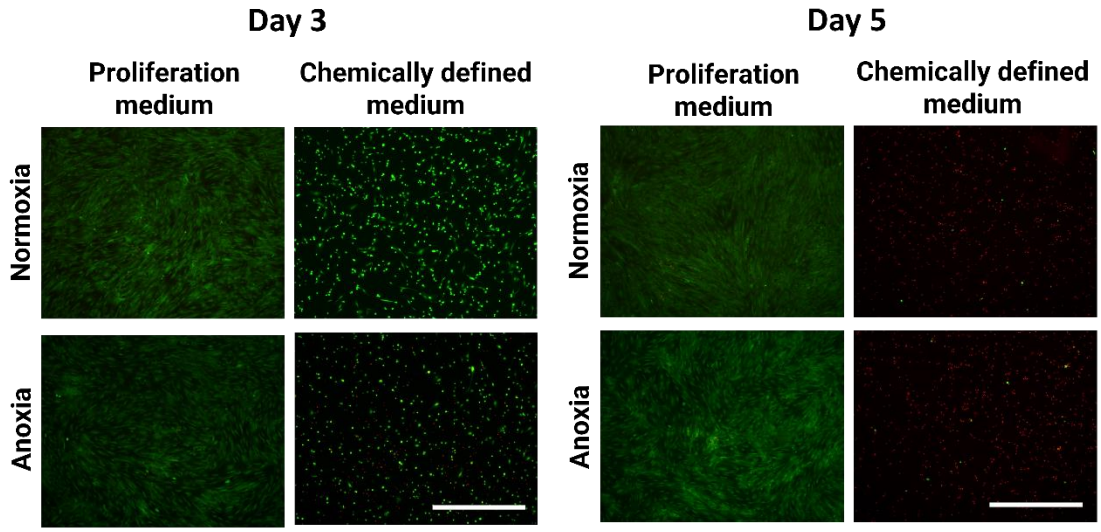

Figure 36: Live/Dead images of hMSCs cultured with standard proliferation medium and chemically defined medium under normoxic and anoxic conditions. Live: green (calcein AM), dead: red (ethidium homodimer-1). Scale bar: 1000 µm.

S4. Metabolic library – Cell viability results (0.55 and 0.055 mM)

The metabolic library, as explained in section 5.2, was established to investigate the effect of a variety of metabolites on the viability of hMSCs. The results obtained for a metabolite concentration of 5.5 mM are presented in section 5.2, Figure 22. The results for the remaining two metabolite concentrations, 0.55 and 0.055 mM are depicted in Figure 37.

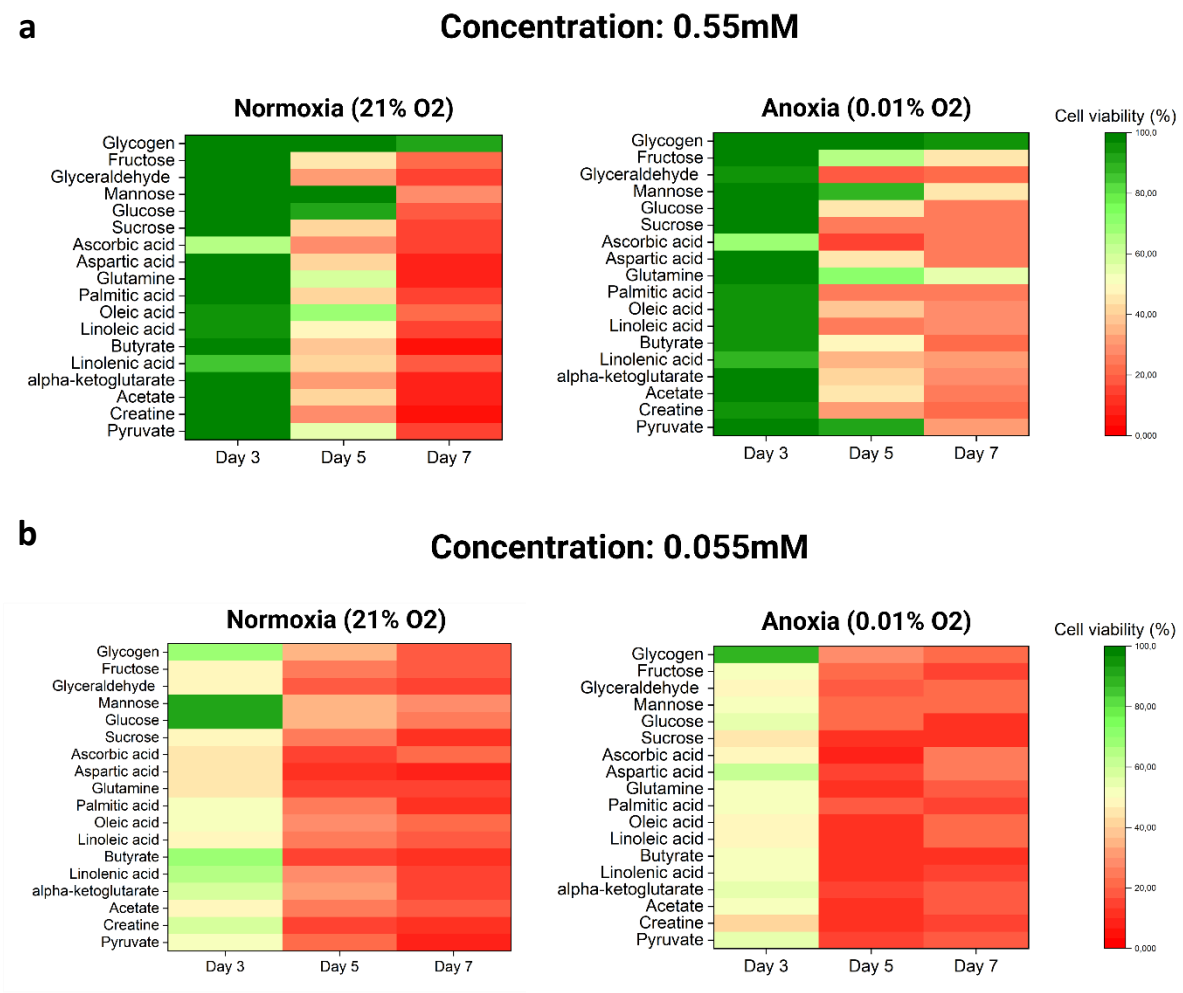

Figure 37: Cell viability results on day 3, 5, and 7 for all metabolites tested in normoxic and anoxic conditions at a concentration of A) 0.55mM and B) 0.055mM.

S5. Glycogen phosphorylase release by hMSCs upon culture with 1g/L glycogen

Human mesenchymal stem cells (hMSCs) were cultured with 1 g/L free glycogen in an anoxic environment for 7 days. Subsequently, the secretion of glycogen phosphorylase, specifically the liver form (PYGL), was quantified using a PYGL ELISA kit. Notably, hMSCs secreted glycogen phosphorylase, and phosphorylase secretion was increased with higher seeding density (initial cell count).

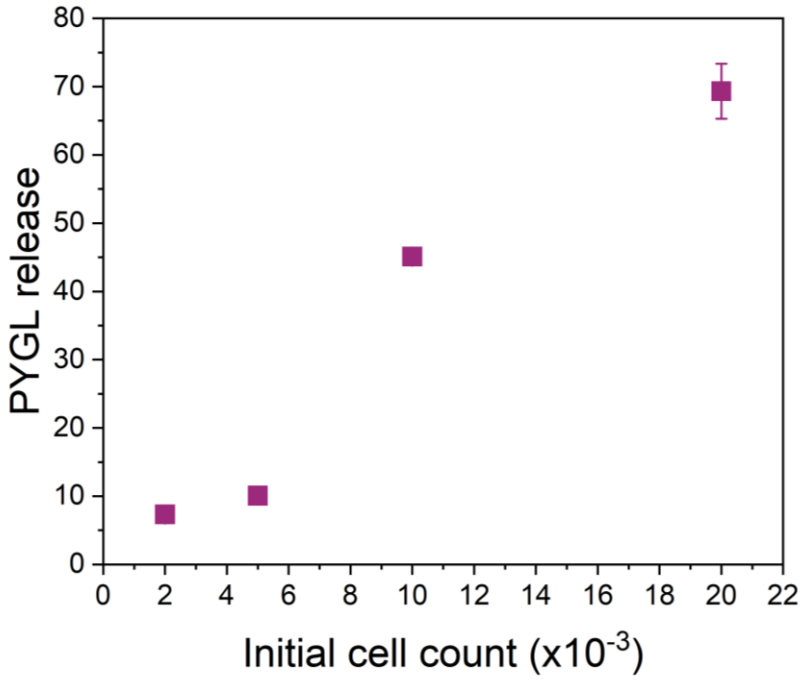

Figure 38: Glycogen phosphorylase liver form (PYGL) secretion on day 7 by human mesenchymal stem cells (hMSCs) cultured with 1 g/L glycogen with varying initial cell count. Values presented are given as means ± SD.

S6. Varying hMSC seeding density and culturing with 1 g/L glycogen

hMSCs were seeded at different densities and cultured with 1 g/L glycogen for two weeks. The hMSC viability was determined by staining the cells using a live/dead assay (live: calcein AM, dead: ethidium homodimer-1). Representative images for each condition at the different time points are presented in Figure 39.

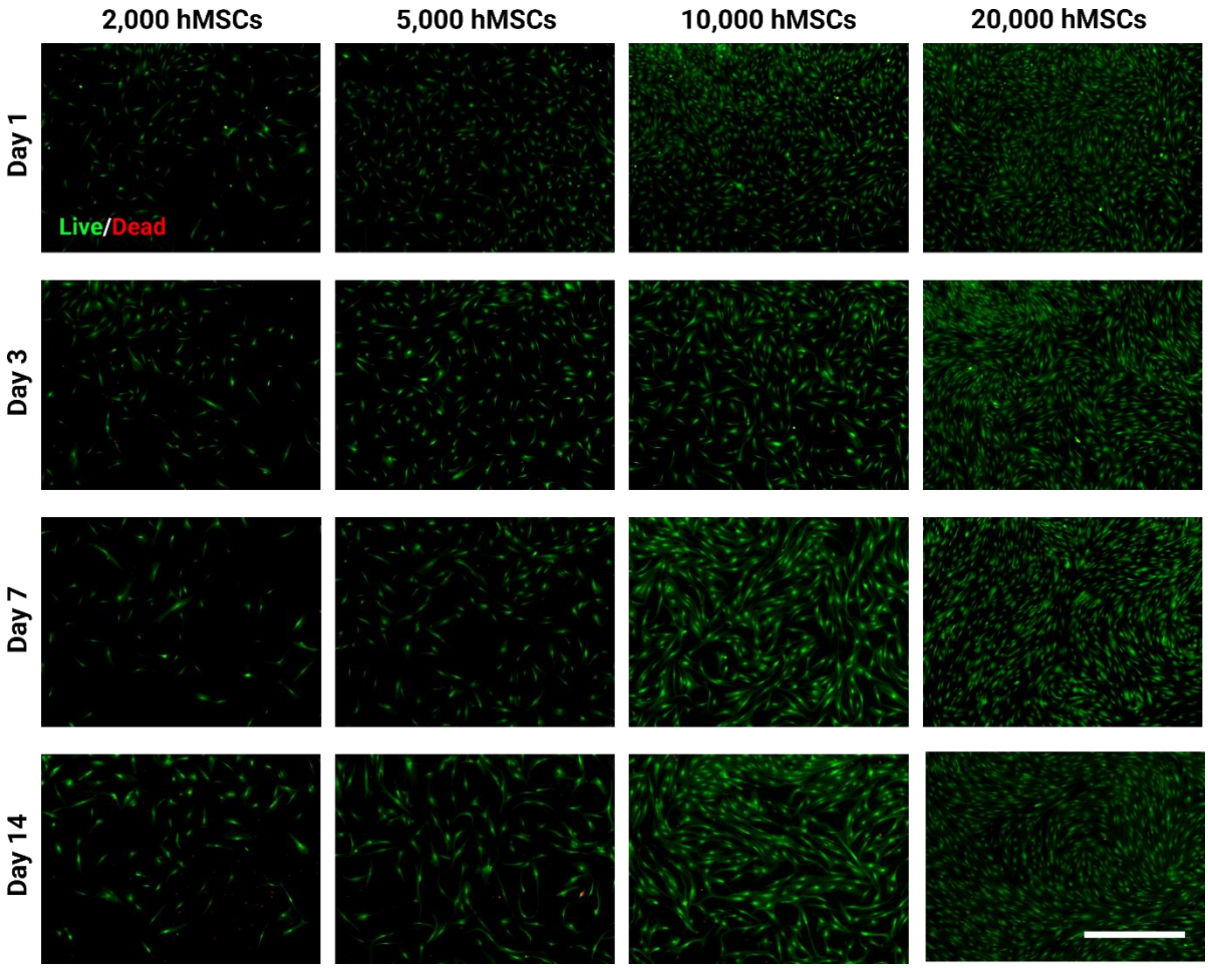

Figure 39: Live/dead images of hMSCs cultured at different seeding densities with 1g/L glycogen. Live/dead images were taken on days 1, 3, 7, and 14. Live: green (calcein AM), dead: red (ethidium homodimer-1). Scale bar: 1000 µm.

S7. Effect of different glycogen concentrations in anoxia on hMSC viability

hMSCs were seeded and cultured with different glycogen concentrations under anoxic conditions. Their viability was determined by doing a live/dead staining using calcein AM (live cells) and ethidium homodimer-1 (dead cells). Representative images of the stained cells for each condition at the two time points are given in Figure 40.

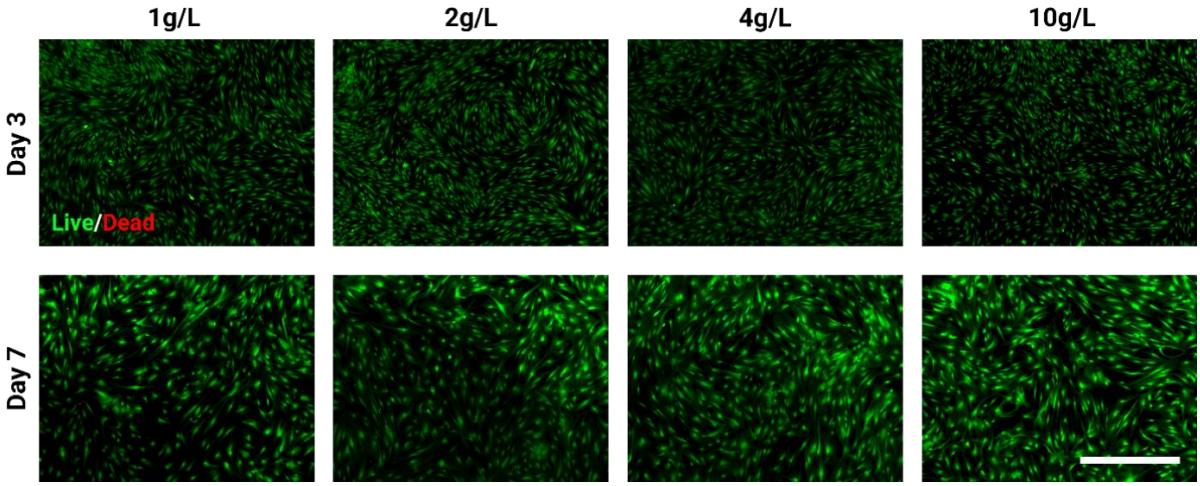

Figure 40: Live/dead images of hMSCs cultured at a fixed seeding density (20,000 cells/well) and different glycogen concentrations. Cell viability was assessed on day 1 and day 7. Live: green (calcein AM), dead: red (ethidium homodimer-1). Scale bar: 1000 µm.

S8: Viability of hMSCs cultured with various glycogen concentrations in normoxia

Human mesenchymal stem cells (hMSCs) were cultured with 1 and 10 g/L glycogen for 7 days. The viability of the cells was assessed on days 1, 3, and 7. Representative live/dead images are presented in Figure 41, and quantitative results for the cell viability are shown in Figure 42. As expected due to nutrient deprivation, hMSCs cultured with chemically defined medium were unable to maintain their viability after day 3 of culture. The other conditions were able to maintain a high cell viability over time.

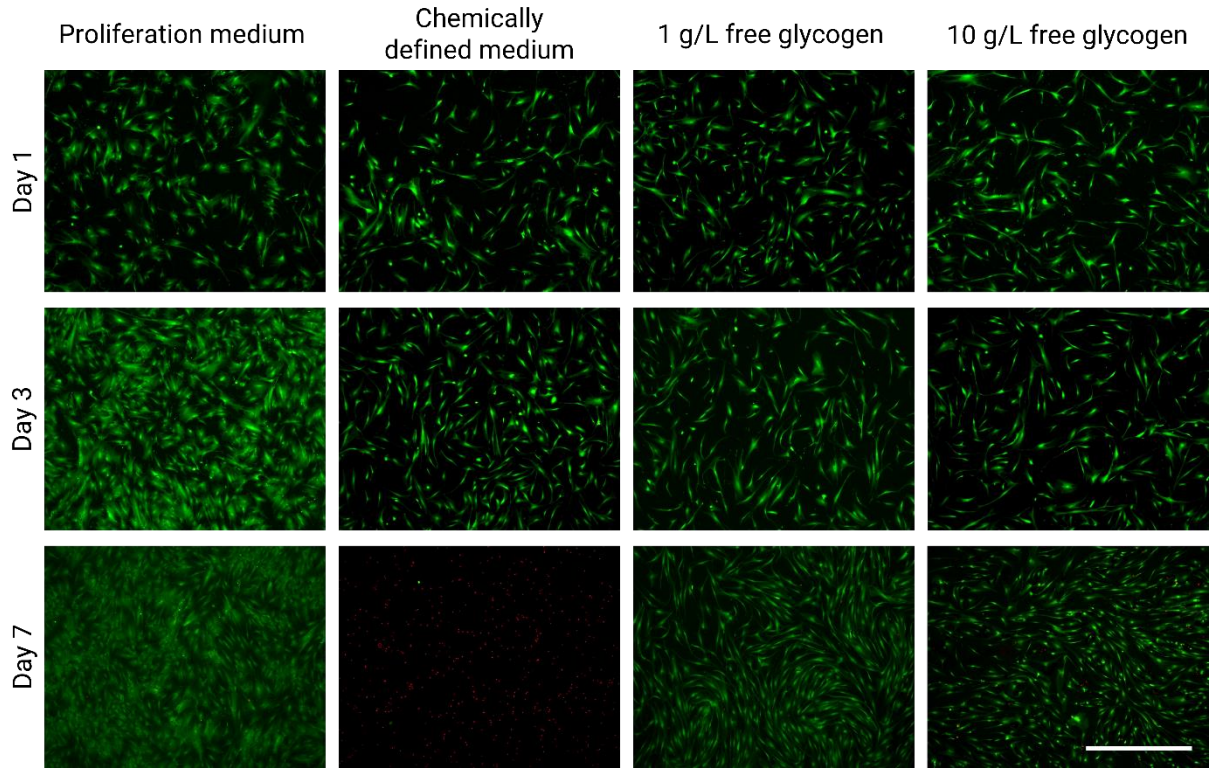

Figure 41: Live/dead images of human mesenchymal stem cells (hMSCs) cultured with different glycogen concentrations under normoxic conditions. Live: green (calcein AM), dead: red (ethidium homodimer-1). Scale bar: 1000 µm.

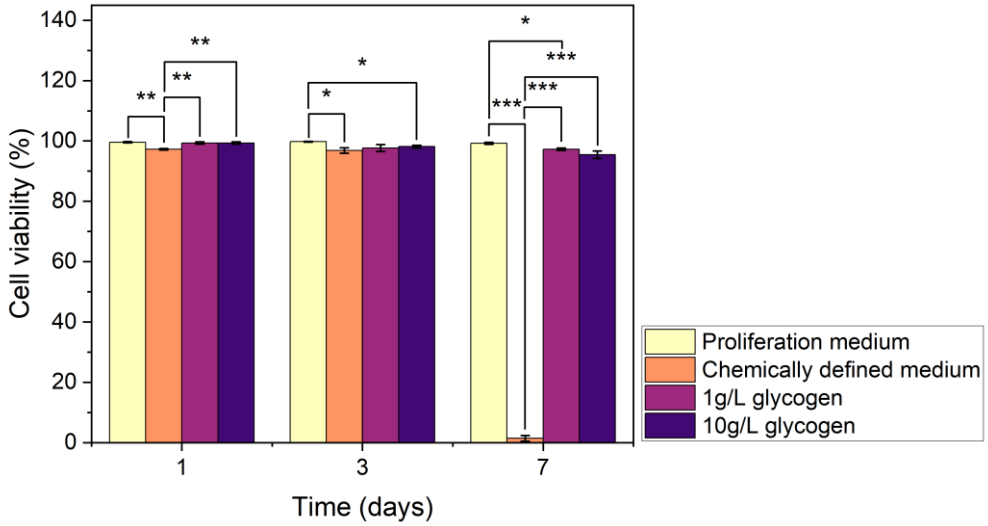

*Figure 42: Viability of human mesenchymal stem cells (hMSCs) cultured with different glycogen concentrations under normoxic conditions. *: p≤0.05, **: p≤0.01, ***: p≤0.001, ****: p≤0.0001, n=3, Pair-Sample t-test. Values presented are given as means ± SD. When not indicated, conditions are non-significant.*

S9. Effect of a phosphorylase inhibitor on hMSCs cultured with glycogen

hMSCs were cultured with different glycogen concentrations to which a phosphorylase inhibitor was added. Their viability was determined on day 3 by performing a live/dead staining (live: calcein AM, green, dead: ethidium homodimer-1, red). Representative images of the stained cells are given in Figure 43. hMSCs cultured with different glycogen concentrations and without the phosphorylases inhibitor served as a positive control.

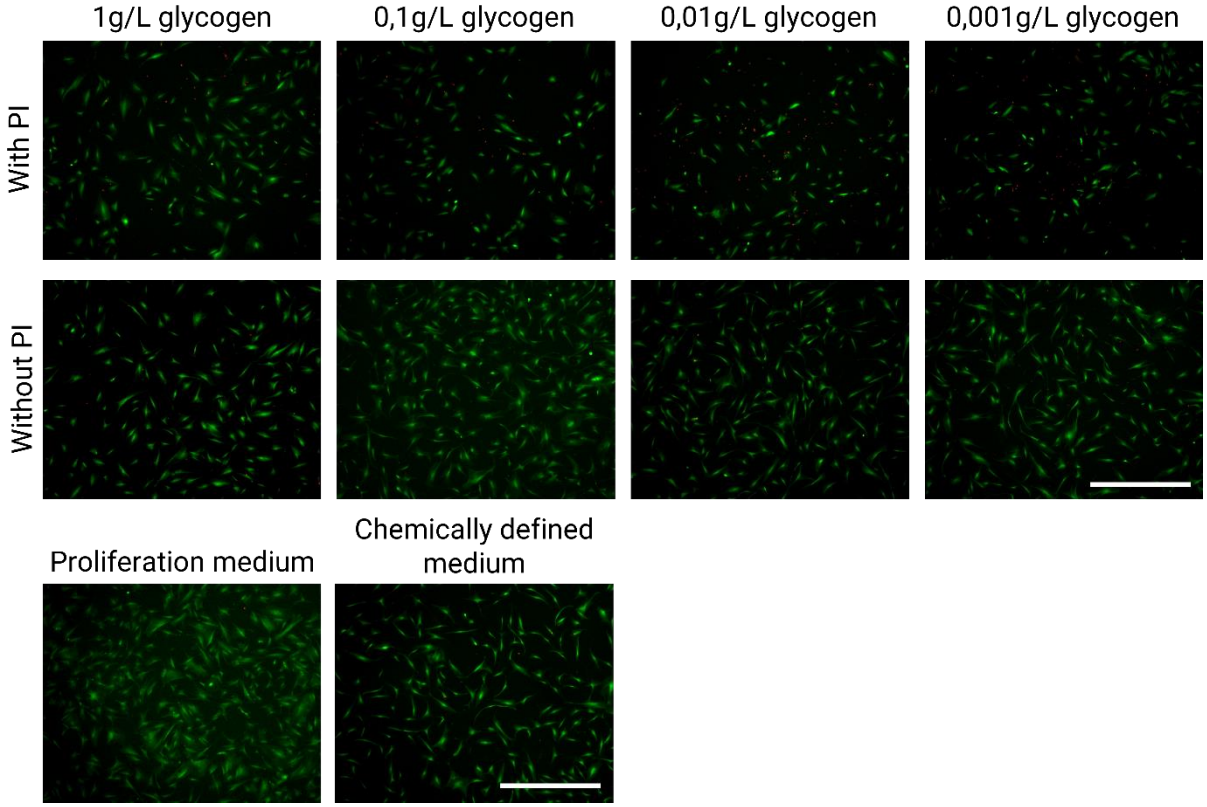

Figure 43: Live/dead images of human mesenchymal stem cells (hMSCs) cultured with different glycogen concentrations with and without phosphorylase inhibitor (PI). Proliferation medium and chemically defined medium were used as positive and negative control, respectively. Live: green (calcein AM), dead: red (ethidium homodimer-1). Scale bar: 1000 µm.

S10. Conjugation of oyster glycogen to Alexa-Fluor™ 647 tyramine reagent

The conjugation of glycogen to Alexa-Fluor™ 647 tyramine reagent was successful, and the tyramine reagent alone did not generate any detectable background signal.

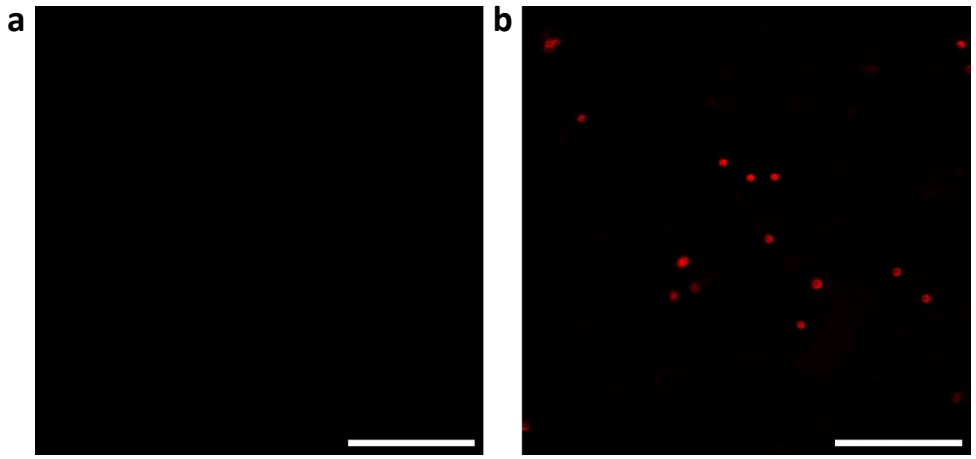

Figure 44: Conjugation of oyster glycogen to Alexa Fluor TM 647 (red) Tyramine Reagent for glycogen visualization. A) Alexa Fluor™ 647 (red) Tyramine Reagent, and B) Glycogen visualization using Alexa Fluor™ 647 (red) Tyramine Reagent. Scale bar: 200 µm.

S11. Core shell microgel optimization: finding the optimal polymer solution flow rate

After some trial and error experiments, an oil flow rate of 80 µl/min was determined to be optimal for the production of core shell microgels. However, some tuning could still be done by adjusting the flow rate of the polymer solution. In order to find the optimal polymer solution flow rate to the aforementioned oil flow rate, variations in the flow rate of the polymer solution were examined. The results are depicted in Figure 45Figure 45. Notably, well-defined core shell microgels were observed, with a slight increase in size as the polymer solution flow rate increased (see also section 5.7 for more information).

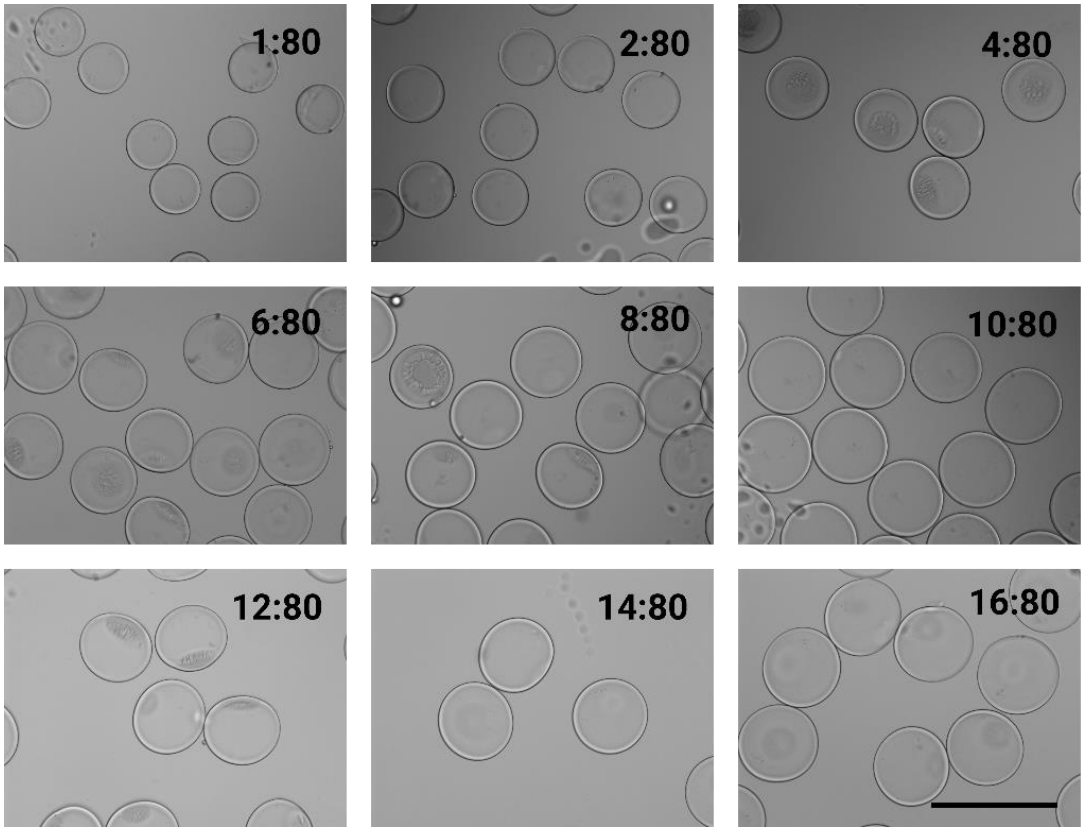

Figure 45: Empty core shell microgels produced with a fixed oil flow rate (80 µl/min) and a varying polymer solution flow rate. Scale bar: 400 µm.

Empty core shell microgels were produced successfully. To evaluate the formation of core shell microgels in the presence of glycogen, 100g/L glycogen was encapsulated. The results, considering different polymer solution flow rates, are presented in Figure 46. Once again, well-formed core shell microgels were observed, but do show the presence of some crosslinking in the core for certain flow rate ratios (specifically, 2:80, 4:80, 10:80, 12:80, 14:80, and 16:80).

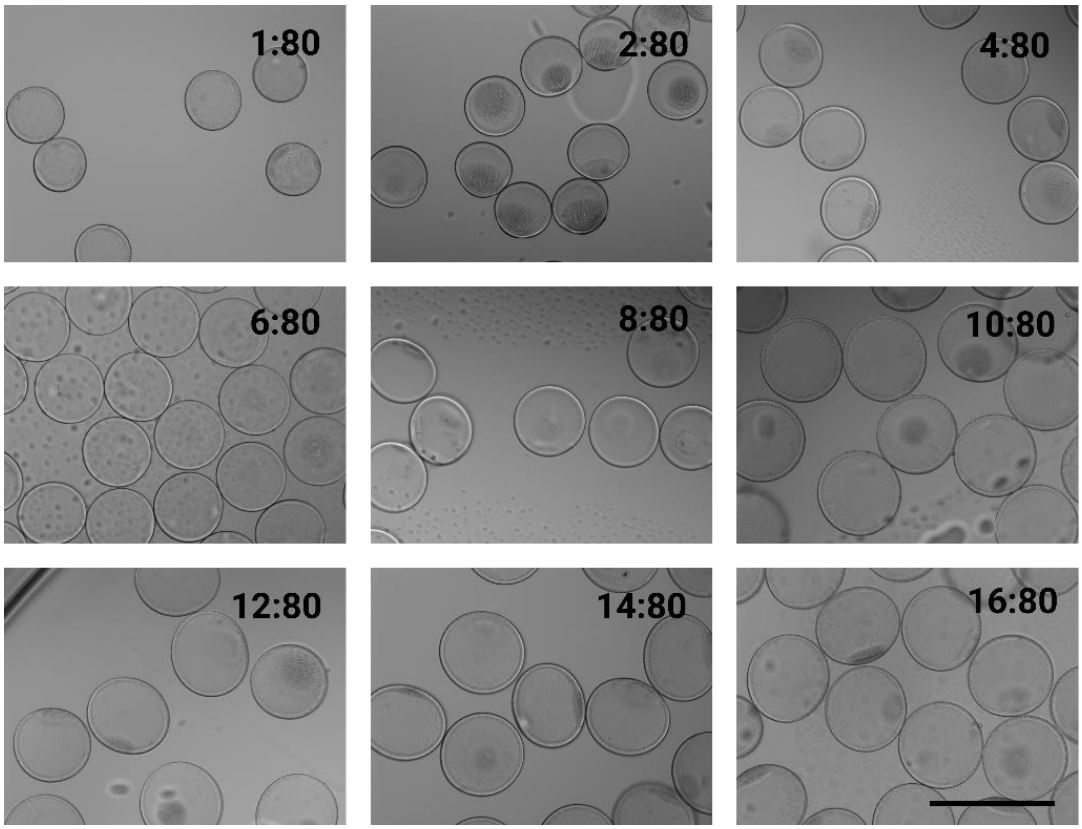

Figure 46: Glycogen-loaded core shell microgels (100 g/L) produced with a fixed oil flow rate (80 µl/min) and a varying polymer solution flow rate. Scale bar: 400 µm.

S12. Core shell microgel optimization: varying polymer flow rates

Prior to implementing the optimal oil flow rate of 80 µl/min, alternative flow rate ratios were examined. Specifically, various polymer flow rates were tested at an oil flow rate of 48 µl/min. The obtained results are presented in Figure 47. Although the visual inspection of the bright field images suggests the production of nicely-formed core shell microgels, an analysis of the diameter distribution reveals significant variations in size among them.

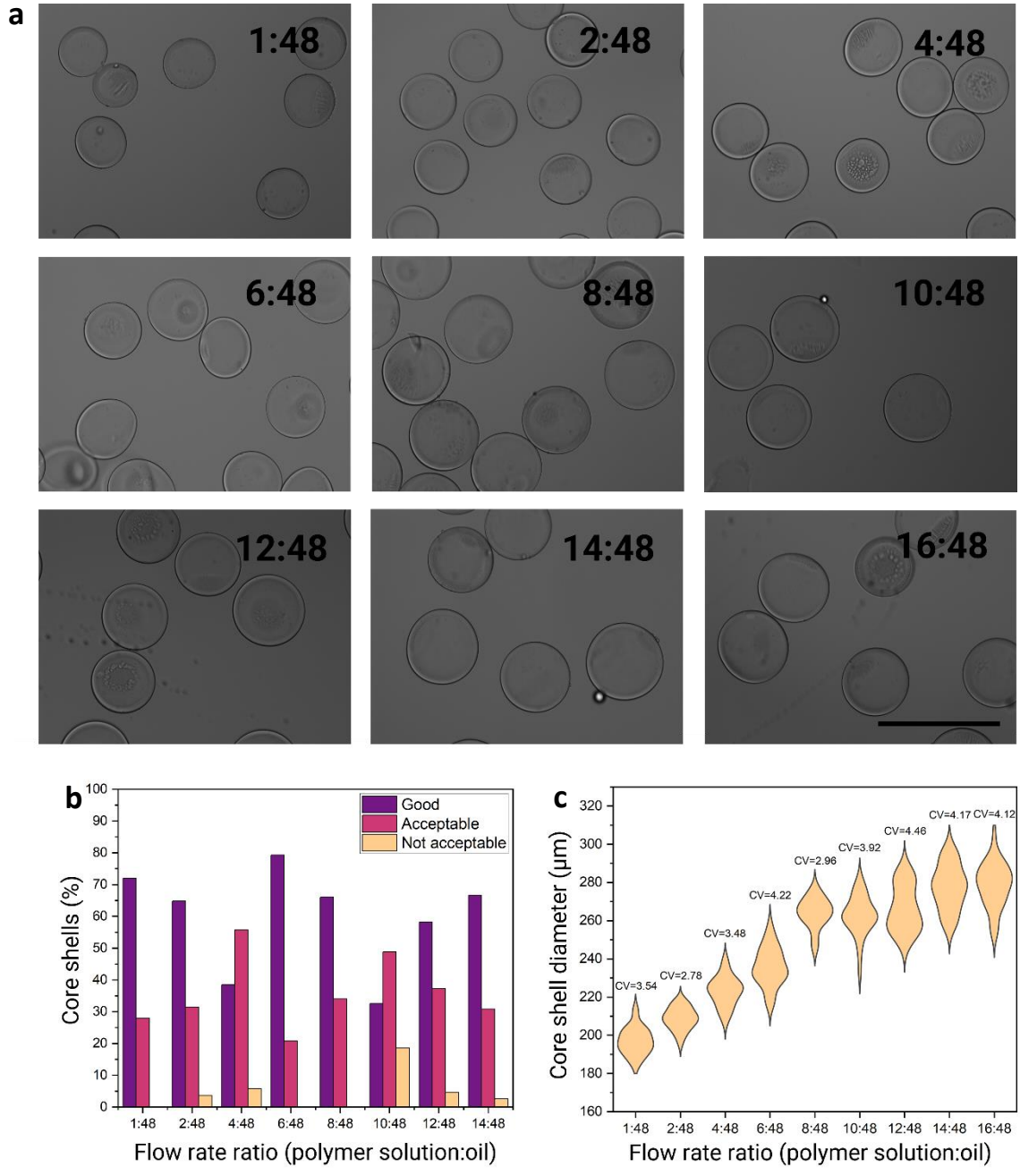

Figure 47: Optimization of core shell microgels with a fixed oil flow rate at 48 µl/min. A) Bright field images of core shell microgels produced with varying the polymer solution flow rate. B) Overview of how successful core shell microgels were produced based on core shell microgel morphology and on the degree of crosslinking of the core. C) Diameter of produced core shell microgels. Scale bar: 400 µm.

S13. Core shell microgel optimization: varying the polymer flow rates (with glycogen)

Following the successful formation of empty core shell microgels using an oil flow rate of 48 µl/min, glycogen encapsulation was performed. However, the resulting core shell microgels exhibited significant variations not only in diameter but also in the degree of crosslinking. Particularly, when a polymer flow rate exceeding 12 µl/min was used, the microgel production proved unsuccessful die to an extremely wide size distribution and incomplete crosslinking (see also Figure 48b for visual representation). Despite these challenges encountered at higher flow rates, the release of encapsulated glycogen remained extremely low, as demonstrated in Figure 48c.

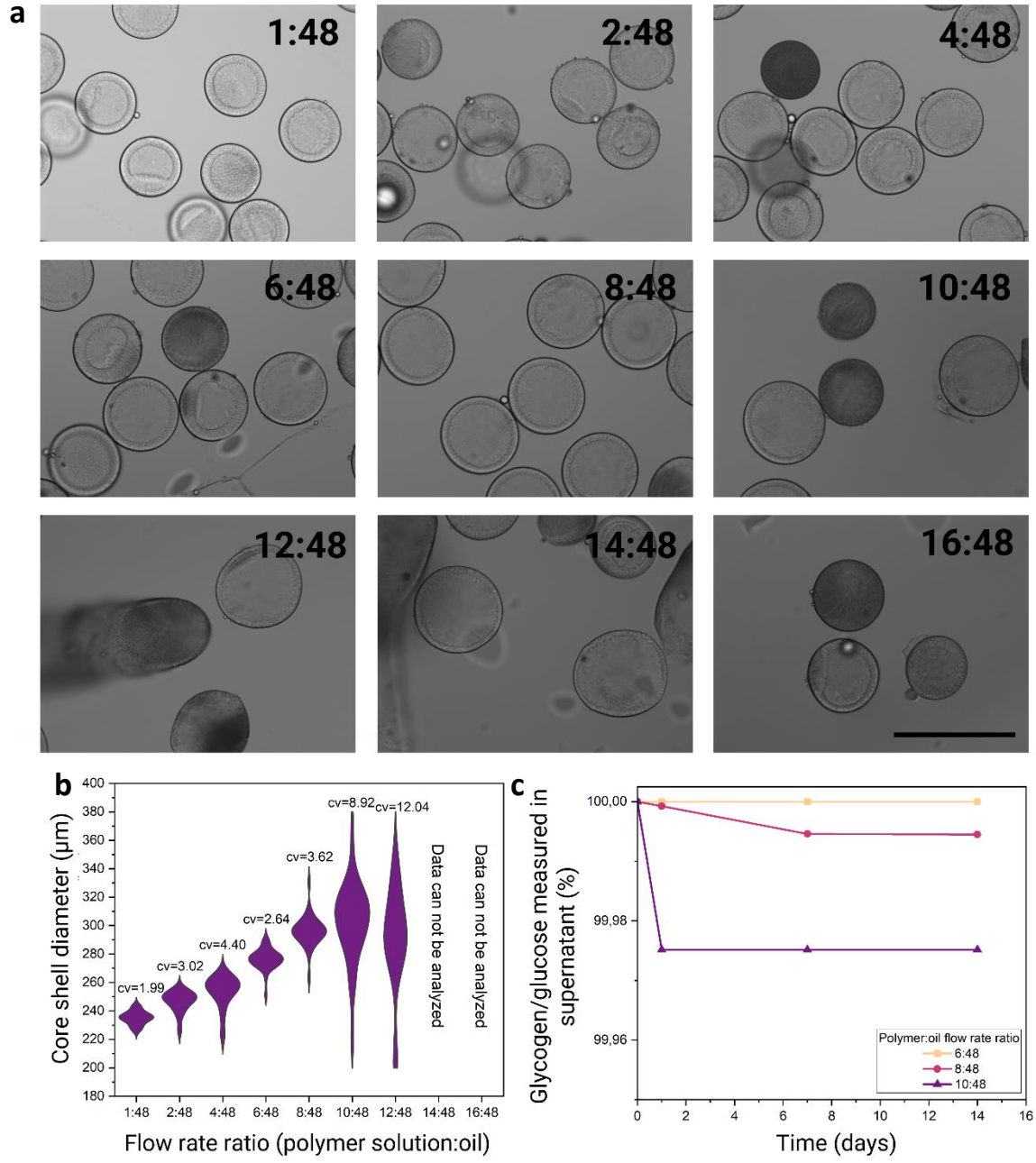

Figure 48: Optimization of glycogen-loaded core shell microgels with a fixed oil flow rate of 48 µl/min. A) Bright field images of glycogen-loaded core shell microgels produced with varying the polymer solution flow rate. B) Diameter of produced glycogen-loaded core shell microgels. Diameter of glycogen-loaded core shell microgels could not be determined for a polymer flow rate of 14 and 16 µl/min, and the CV values for most conditions are high. C) Glycogen release profile of glycogen-loaded core shell microgels (100 g/L encapsulated glycogen) for three different polymer flow rates. Values presented in C) are given as means ± SD. Scale bar: 400 µm.

With a flow rate ratio of 8 to 48 (8 µl/min for the polymer solution and 48 µl/min for the oil), various concentrations of glycogen were successfully encapsulated. Among the different glycogen concentrations, core shell microgels containing 50g/L encapsulated glycogen exhibited the most narrow diameter distribution. Conversely, core shell microgels with 100g/L displayed a (partially) crosslinked core. When encapsulating 30g/L glycogen, the resulting microgels exhibited the best characteristics visually, as determined through analysis of the bright field images. The underlying factors responsible for these observed effects of glycogen concentration on core shell microgel formation, size, and glycogen release remain unknown, as these trends were not observed in microgels formed using a flow rate ratio of 10 to 80 (additional information is available in supplementary material 14).

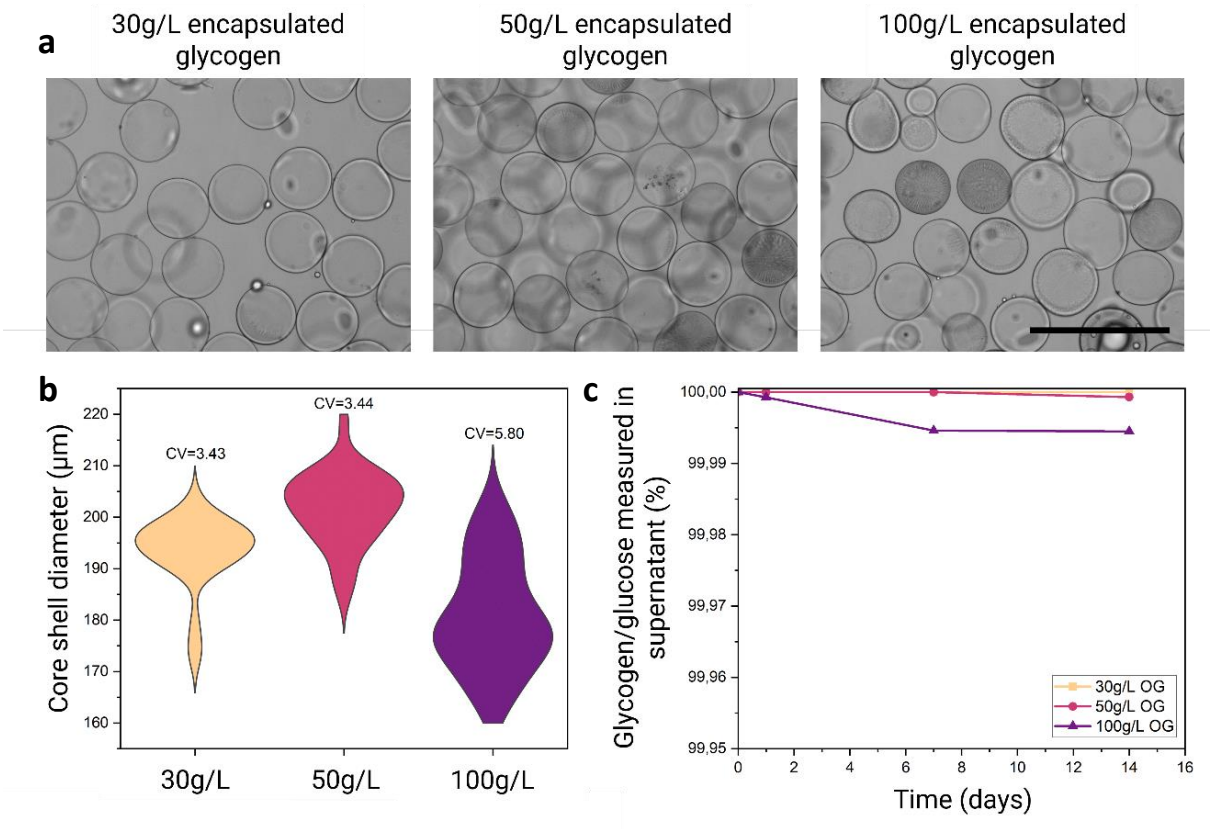

Figure 49: Optimization of glycogen-loaded core shell microgels with a fixed oil flow rate of 48 µl/min and a polymer solution flow rate of 8 µl/min. A) Bright field images of glycogen-loaded core shell microgels produced with different glycogen concentrations. B) Diameter of produced glycogen-loaded core shell microgels. C) Glycogen release profile over a two week period of glycogen-loaded core shell microgels with 30, 50, and 100 g/L encapsulated glycogen. Values presented in C) are given as means ± SD. Scale bar: 400 µm.

S14. Core shell microgel optimization: varying encapsulated molecule

Having established the optimal flow rate ratio (10:80, polymer solution to oil), the encapsulation of oyster glycogen was done at various concentrations, as well as the encapsulation of bovine glycogen and glucose. The results of these encapsulation experiments are presented in Figure 50. Encapsulation of the various molecules was successful, and core shell microgel diameter was determined, as well as the glycogen/glucose release profiles over time. Notably, the encapsulation of various oyster glycogen concentrations did not have an effect on core shell microgel diameter. When glucose was encapsulated, the diameter of the core shell microgels decreased with almost 30 µm compared to when oyster or bovine glycogen was encapsulated using the same concentration. This could be attributed to the smaller size of glucose molecules compared to the glycogen molecules derived from oyster and bovine sources (see section 5.5).

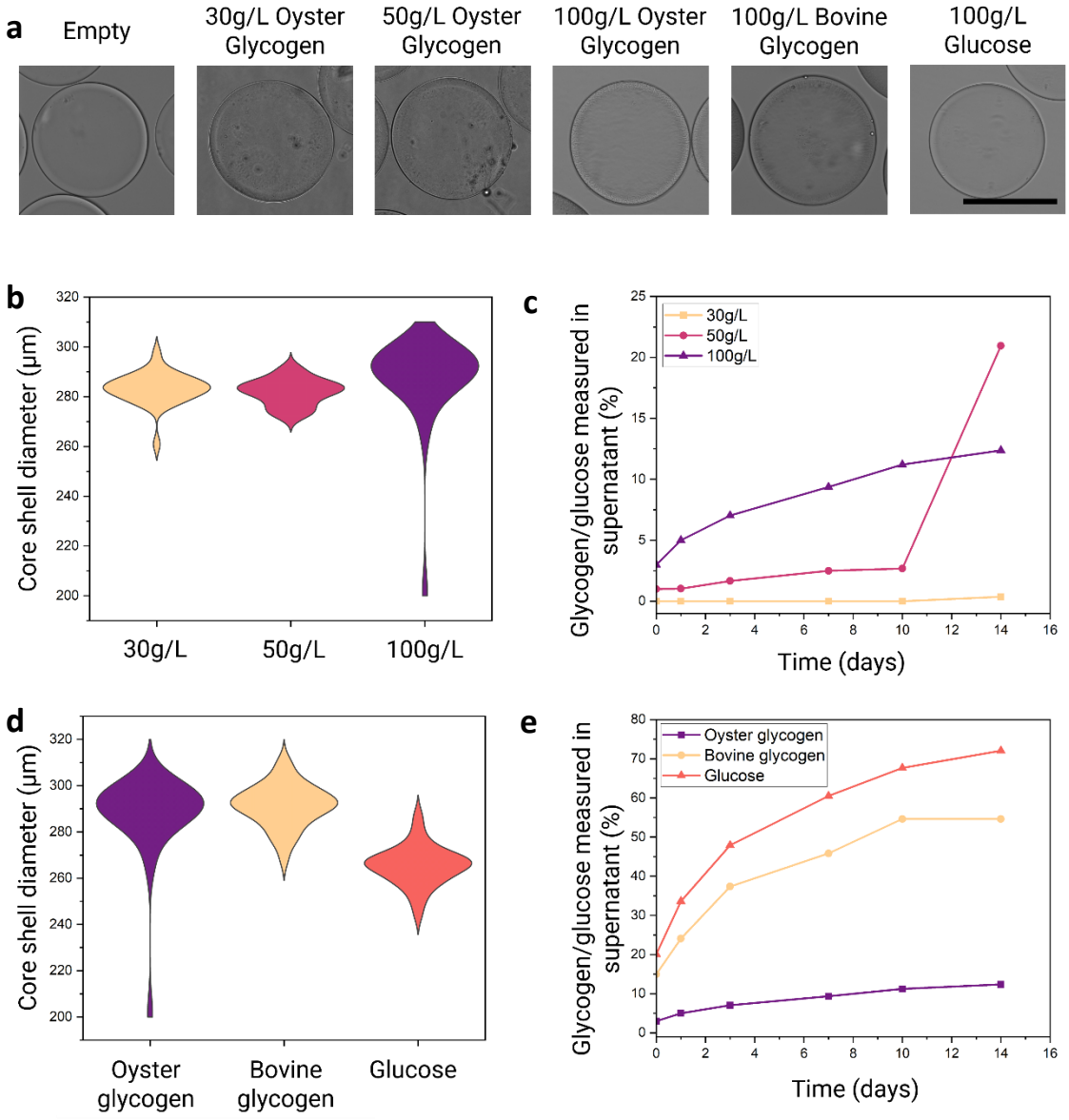

Figure 50: Optimization of glycogen-loaded core shell microgels with a fixed oil flow rate of 80 µl/min. A) Bright field images of glycogen/glucose-loaded core shell microgels. B) Diameter of produced glycogen-loaded core shell microgels with different concentrations of oyster glycogen (30, 50, and 100 g/L). C) Glycogen release profile from glycogen-loaded core shell microgels with different oyster glycogen concentrations over a two week period. D) Diameter of core shell microgels loaded with 100 g/L of oyster glycogen, bovine glycogen or glucose. E) Release profile from core shell microgels loaded with oyster glycogen, bovine glycogen or glucose over a two week period. Values presented in C) and E) are given as means ± SD. Scale bar: 200 µm.

As can be observed in Figure 50c, core shell microgels containing 30 g/L of encapsulated oyster glycogen exhibit minimal glycogen release over a two-week period. However, as the glycogen content increases, the release of glycogen is increased as well. Eventually, approximately 12.5% of the glycogen content is released from the core shell microgels containing 100 g/L of encapsulated glycogen after 14 days. The glycogen concentration measured in the supernatant of the 50 g/L glycogen-loaded core shell microgels on day 14 is surprisingly high compared to the other values measured on previous days. One possibility is that during the sampling for glycogen concentration analysis, core shell microgels were included, resulting in the measurement of the total glycogen content within these microgels rather than just the released glycogen. Another potential explanation is that some of the microgels ruptured, leading to the complete release of their glycogen content into the supernatant.

The release profiles of oyster glycogen, bovine glycogen and glucose, as presented in Figure 50e, can be attributed to the differences in the sizes of the encapsulated molecules. Glucose, sue to its smaller molecular size, exhibits a significantly faster release rate compared to both types of glycogen. Moreover, bovine glycogen demonstrates a faster release rate than oyster glycogen, which can be attributed to the larger size of oyster glycogen compared to bovine glycogen.

S15. Viability of hMSCs cultured with free dextran

In order to investigate the capacity of hMSCs to utilize dextran as an energy source, they were cultured with free dextran in chemically defined medium for 7 days. The viability of the cells was assessed on days 1, 3, and 7. Representative live/dead images are presented in Figure 51, and quantitative cell viability results are given in Figure 52. hMSCs remained alive upon culture with proliferation medium but were unable to maintain their viability when cultured with chemically defined medium with or without dextran. Consequently, it can be concluded that hMSCs are unable to utilize dextran as an energy source for sustaining their viability.

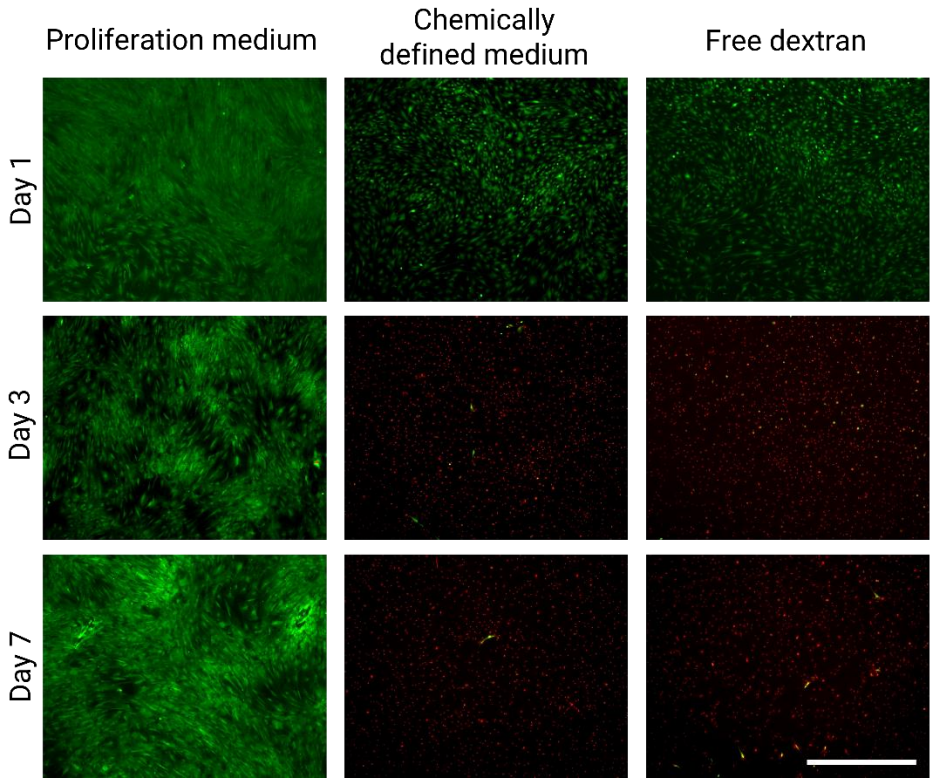

Figure 51: Live/dead images of human mesenchymal stem cells (hMSCs) cultured with free dextran in anoxic conditions. Live: green (calcein AM), dead: red (ethidium homodimer-1). Scale bar: 1000 µm.

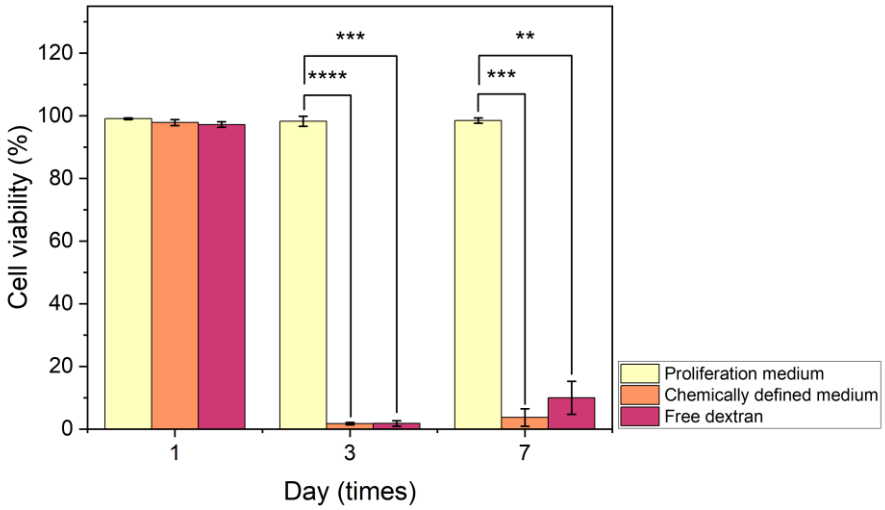

*Figure 52: Viability of human mesenchymal stem cells (hMSCs) cultured with free dextran in anoxic conditions. **: p≤0.01, ***: p≤0.001, ****: p≤0.0001, n=3, Pair-Sample t-test. Values presented are given as means ± SD. When not indicated, conditions are non-significant.*

S16. Dehydration and rehydration of glycogen-loaded core shell microgels

Glycogen-loaded core shell microgels have demonstrated to be promising for the maintenance of a high cell viability (refer to section 5.8 for more information). However, in the present study, the glycogen-loaded core shell microgels were used within one week after their production. To assess whether glycogen-loaded core shells can be utilized at a later time point (weeks to months later), core shell microgels underwent a dehydration process using an ethanol (EtOH) series with increasing ethanol concentration (Figure 53a). Subsequently, the core shell microgels were air-dried overnight and afterwards immersed in PBS. The release of glycogen from these rehydrated core shell microgels was then measured over time. As depicted in Figure 53c, the release profile of the dehydrated and again rehydrated glycogen-loaded core shell microgels, follows the same trend as the "fresh" glycogen-loaded core shell microgels, but the release is a magnitude 2.5 times lower. This could potentially be attributed to glycogen loss during the dehydration and rehydration process.

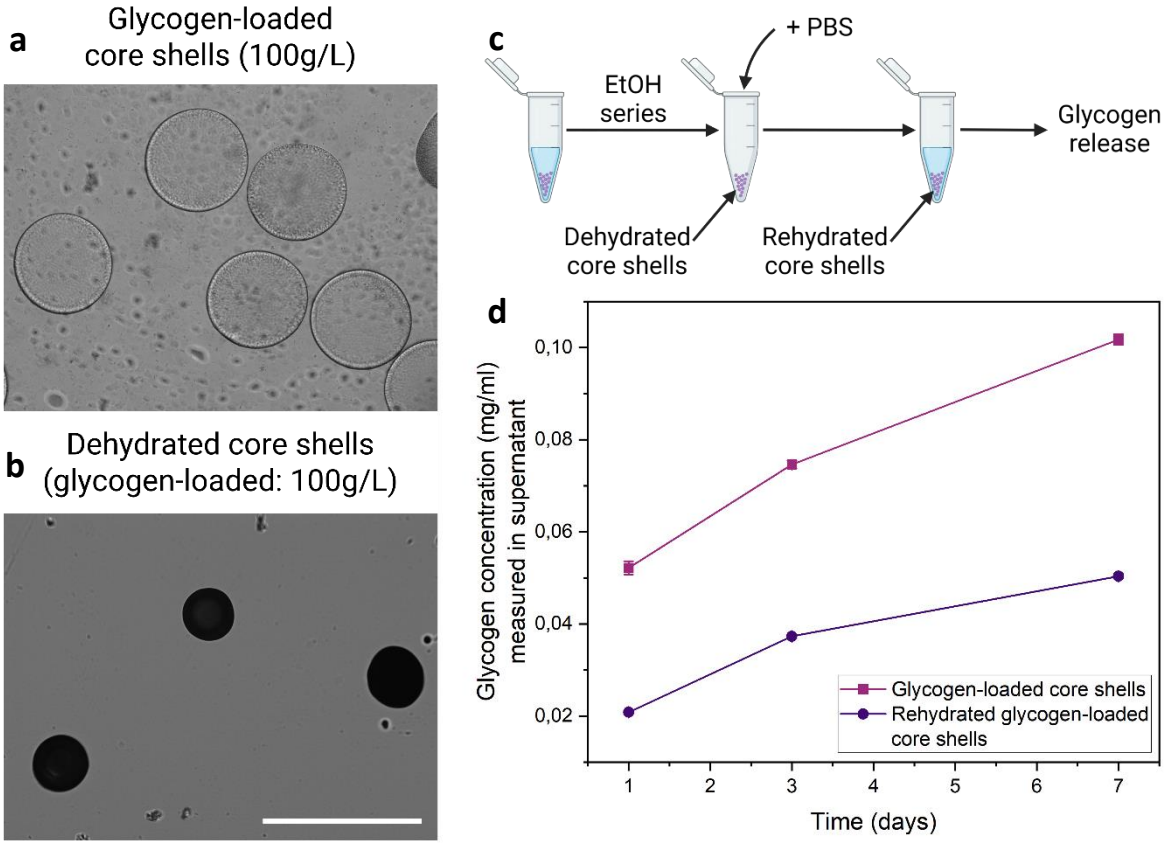

Figure 53: Dehydration and rehydration of glycogen-loaded core shell microgels. A) Glycogen-loaded core shell microgels before dehydration. B) Glycogen-loaded core shell microgels after dehydration and before rehydration. Scale bar: 400 µm. C) Schematic overview of the de- and rehydration process. D) Glycogen release profile of glycogen-loaded core shells after de- and rehydration compared to not dehydrated core shell microgels. Values presented are given as means ± SD.

S17. hMCs cultured with 30 and 100g/L glycogen-loaded core shell microgels

This supplementary material provides the complete data set of the experiment described in section 5.8, including the outcomes obtained for hMSCs cultured in standard proliferation medium. In addition to the findings described in section 5.8, the glycogen content in the culture medium was assessed on day 7. As illustrated in Figure 54e, only hMSCs cultured with free glycogen exhibited detectable levels of glycogen in the medium. This observation suggests that a concentration of 1g/L glycogen is more than adequate to sustain high cell viability up till day 7. Moreover, it indicates that hMSCs are capable of releasing glycogen/glucose form the core shell microgels at a rate equivalent to their consumption, thereby maintaining a high cell viability. As expected, the chemically defined medium did not show the presence of any glycogen. Furthermore, the proliferation medium exhibited no detectable glycogen or glucose in the medium after 7 days, yet the cell viability remained high. This observation may indicate that the proliferation medium can sustain the viability for approximately a week and that viability will decline within a few days due to metabolite depletion if the culture was to be extended.

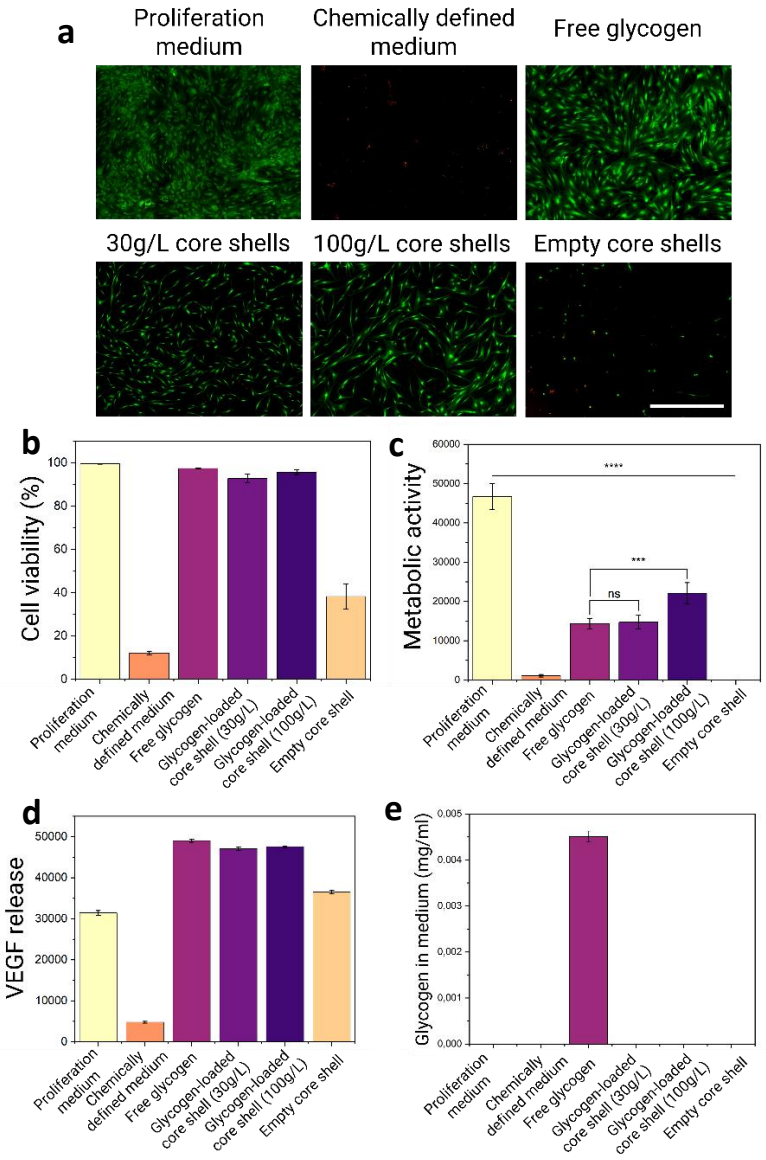

*Figure 54: Human mesenchymal stem cells (hMSCs) cultured with glycogen-loaded core shell microgels. A) Live/dead images of the different culture conditions on day 7. Live: green (calcein AM), dead: red (ethidium homodimer-1). Scale bar: 1000 µm. hMSCs were analyzed on day based on their: B) viability, Mann-Whitney test, C) metabolic activity, Pair-Sample t-test, D) VEGF release (no statistical analysis), and E) glycogen content in the medium (no statistical analysis). *: p≤0.05, **: p≤0.01, ***: p≤0.001, ****: p≤0.0001, n=3. Values presented are given as means ± SD. When not indicated, conditions are non-significant.*

S18. Effect of post-crosslinking of glycogen-loaded core shell microgels on hMSCs

For more information on the outcomes of this experiment, please refer to section 5.8. In this supplementary material the complete data set is provided, including the results obtained for hMSCs cultured in standard proliferation medium.

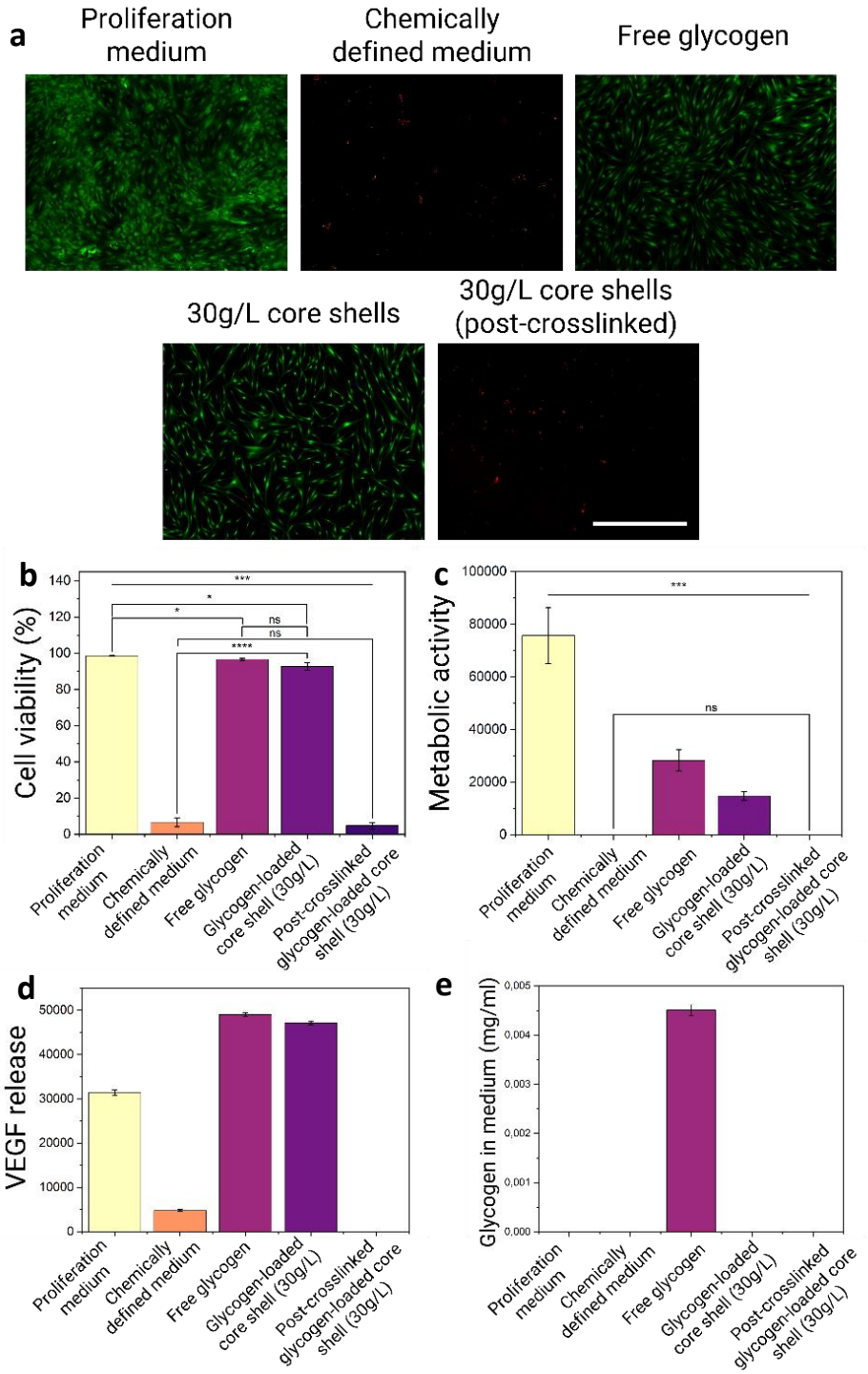

*Figure 55: The effect of post-crosslinked glycogen loaded core shell microgels on human mesenchymal stem cell (hMSC) viability. A) Live/dead images of hMSCs on day 7. Live: green (calcein AM), dead: red (ethidium homodimer-1). Scale bar: 1000 µm. hMSCs were analyzed based on their: B) viability, Pair-Sample t-test, C) metabolic activity, Pair-Sample t-test, D) VEGF release (no statistical analysis), and E) glycogen content in the medium (no statistical analysis). *: p≤0.05, **: p≤0.01, ***: p≤0.001, ****: p≤0.0001, n=3. Values presented are given as means ± SD. When not indicated, conditions are non-significant.*

The glycogen content in the medium was measured on day 7. The analysis observed the presence of glycogen exclusively in the condition where the cells were cultured with free glycogen, suggesting that the cells were cultured in an excess glycogen environment. Conversely, in the case of hMSCs cultured with glycogen-loaded core shell microgels, only the glycogen that is immediately utilized by the cells is degraded by the cells, leaving no glycogen behind in the medium for detection.

S19. Compression of core shell microgel-laden GelMA hydrogels

Gelatin methacrylate (GelMA) bulk hydrogels were prepared with varying the v/v percentages of glycogen-loaded core shell microgels to investigate their impact on the mechanical characteristics of the gel. The compression modulus of the GelMA hydrogels was assessed, as illustrated in Figure 56. The results indicate that the incorporation of glycogen-loaded core shell microgels does not yield a significant effect on the compression modulus of the GelMA hydrogel. This could be explained by the low stiffness exhibited by the glycogen-loaded core shell microgels (refer to section 5.7, Figure 28 for more information).

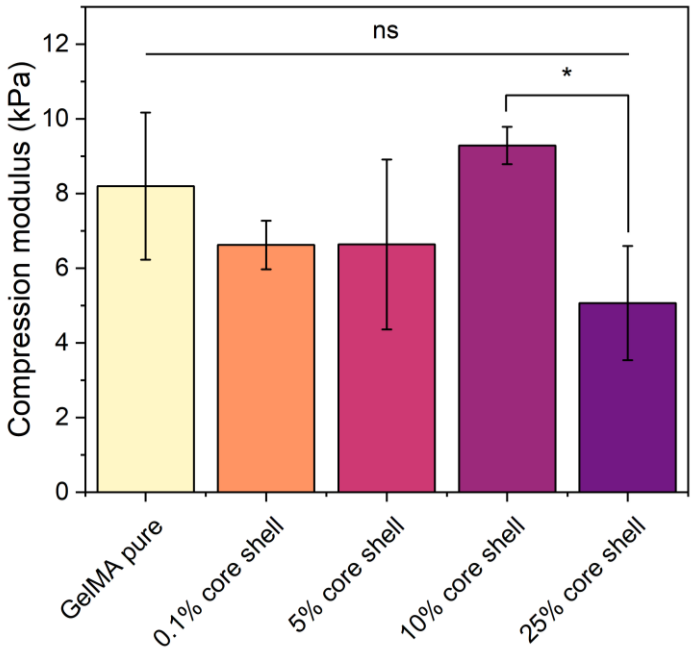

*Figure 56: Compression of GelMA bulk hydrogel with different v/v% of incorporated glycogen-loaded core shell microgels (100 g/L glycogen). One way Anova, *: p≤0.05, n=4. Values presented are given as means ± SD.*

S20. Effect of glycogen-loaded core shells and HA block fragments on hMSCs in GelMA

Hydroxyapatite (HA) block fragments were integrated into hMSC-laden GelMA hydrogels, along with incorporated core shell microgels (empty and containing 100 g/L glycogen). The hMSC viability was assessed on day 7. As can be observed in the images in Figure 57, it can be noted that the cell population is very small, while a relatively high number of dead cells is observed. Due to the extremely low cell count, determining the percentage viability was not feasible. This outcome raises some questions, considering the initial cell density of $3x10^6$ cells/ml that was used. Some of the cells might not be visible due to light obstruction by the presence of the HA block fragments.

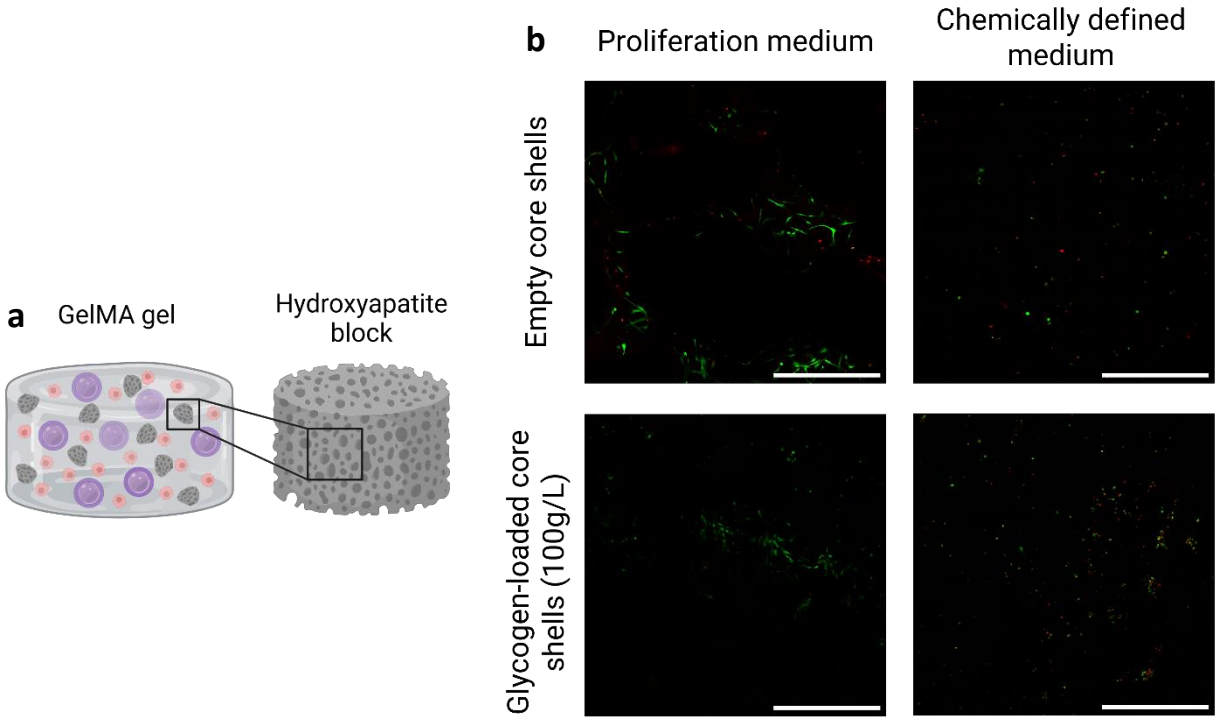

Figure 57: Human mesenchymal stem cell (hMSC)-laden GelMA hydrogel with glycogen-loaded core shells and hydroxyapatite (HA) block fragments. A) Schematic overview of the hydrogel containing hMSCs, glycogen-loaded core shells and HA block fragments. B) Live/dead images of the conditions tested. Live: green (calcein AM), dead: red (ethidium homodimer-1). Scale bar: 500 µm.

S21. Combining glycogen-loaded core shell microgels and HA constructs

A series of preliminary experiments were conducted to assess the feasibility of integrating free glycogen or glycogen-loaded core shell microgels within hydroxyapatite (HA) constructs. In the first experiment, glycogen-loaded core shells suspended in PBS were carefully applied onto the construct via pipetting. However, it was observed that the core shells were unable to penetrate the pores of the HA construct, remaining on the surface where they were deposited (Figure 58a). This outcome was surprising considering the significantly larger pore sizes of the construct. A possible explanation can be that the interconnective space between pores within the construct is narrower that the size of the core shell microgels, thereby physically hindering their entry into the construct.

Next, HA blocks were immersed in either PBS or PBS supplemented with 1 g/L glycogen for a designated period. Afterwards, the constructs were transferred to fresh PBS, and the release of glycogen over time was measured. As illustrated in Figure 58b, most of the glycogen is measured in the supernatant already after 24h, indicating that the HA constructs were unable to absorb the glycogen efficiently.

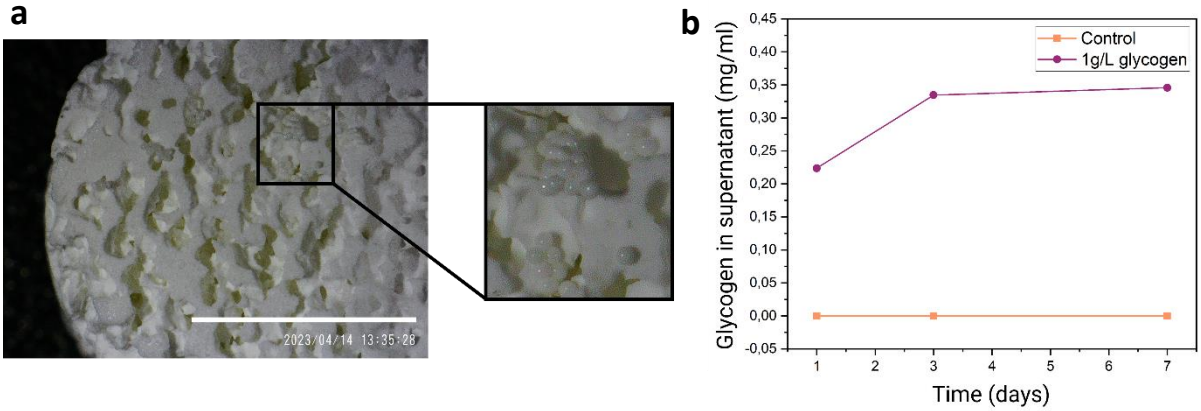

Figure 58: Possibility of core shell and glycogen uptake by the hydroxyapatite (HA) blocks. A) The core shells are not able to enter the pores of the HA construct and remain on top of the construct where they have been deposited. Scale bar: 4.5 mm. B) Glycogen release of HA blocks emerged in PBS containing glycogen. Values presented in b) are given as means ± SD.

S22. hMSC-laden collagen gel with glycogen-loaded core shell microgels

Human mesenchymal stem cells (hMSCs)-laden collagen gels were produced with incorporated glycogen-loaded core shell microgels. A detailed explanation of the results can be found in section 5.9.2. The complete data set is given in Figure 59, including the data obtained for hMSCs cultured with standard proliferation medium.

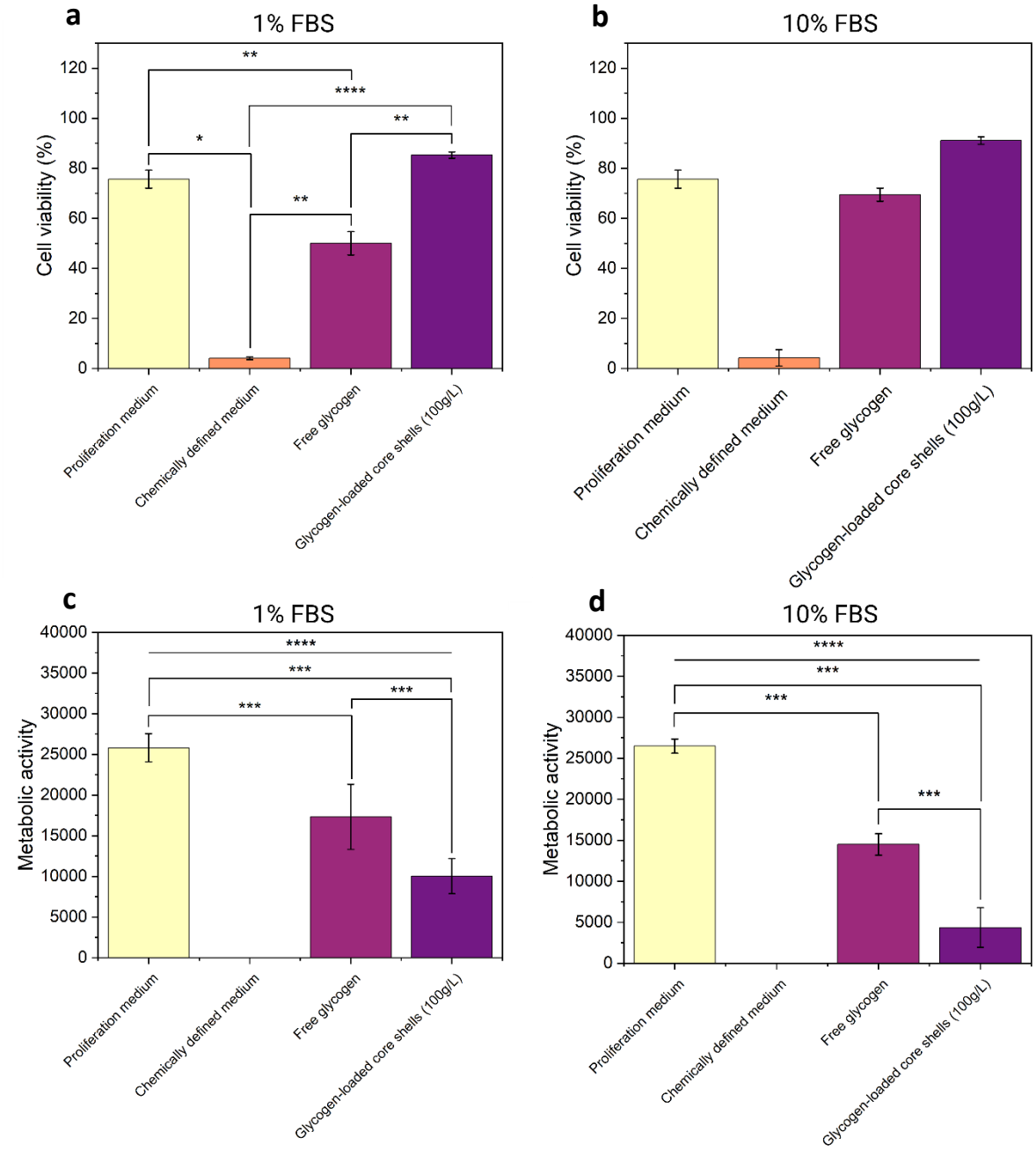

*Figure 59: Complete data set of hMSC-laden collagen gels with glycogen-loaded core shell microgels. A) Cell viability on day 7 when chemically defined medium was supplemented with 1% FBS and 9% ITS, Pair-Sample t-test. B) Cell viability on day 7 when chemically defined medium was supplemented with 10% FBS, Mann-Whitney test. C) Cell metabolic activity when chemically defined medium was supplemented with 1% FSB and 9% ITS, Mann-Whitney test. D) Cell metabolic activity when chemically defined medium was supplemented with 10% FBS, Mann-Whitney test. *: p≤0.05, **: p≤0.01, ***: p≤0.001, ****: p≤0.0001, n=3. Values presented are given as means ± SD. When not indicated, conditions are non-significant.*

S23. hMSC-laden collagen gel with glycogen-loaded core shells and HA block fragments

Human mesenchymal stem cells (hMSCs) were cultured within a collagen gel with incorporated glycogen-loaded core shell microgels and hydroxyapatite (HA) block fragments. Detailed information regarding the results can be found in section 5.9.3. This section provides the entire dataset, including the results obtained for the hMSCs cultured with standard proliferation medium.

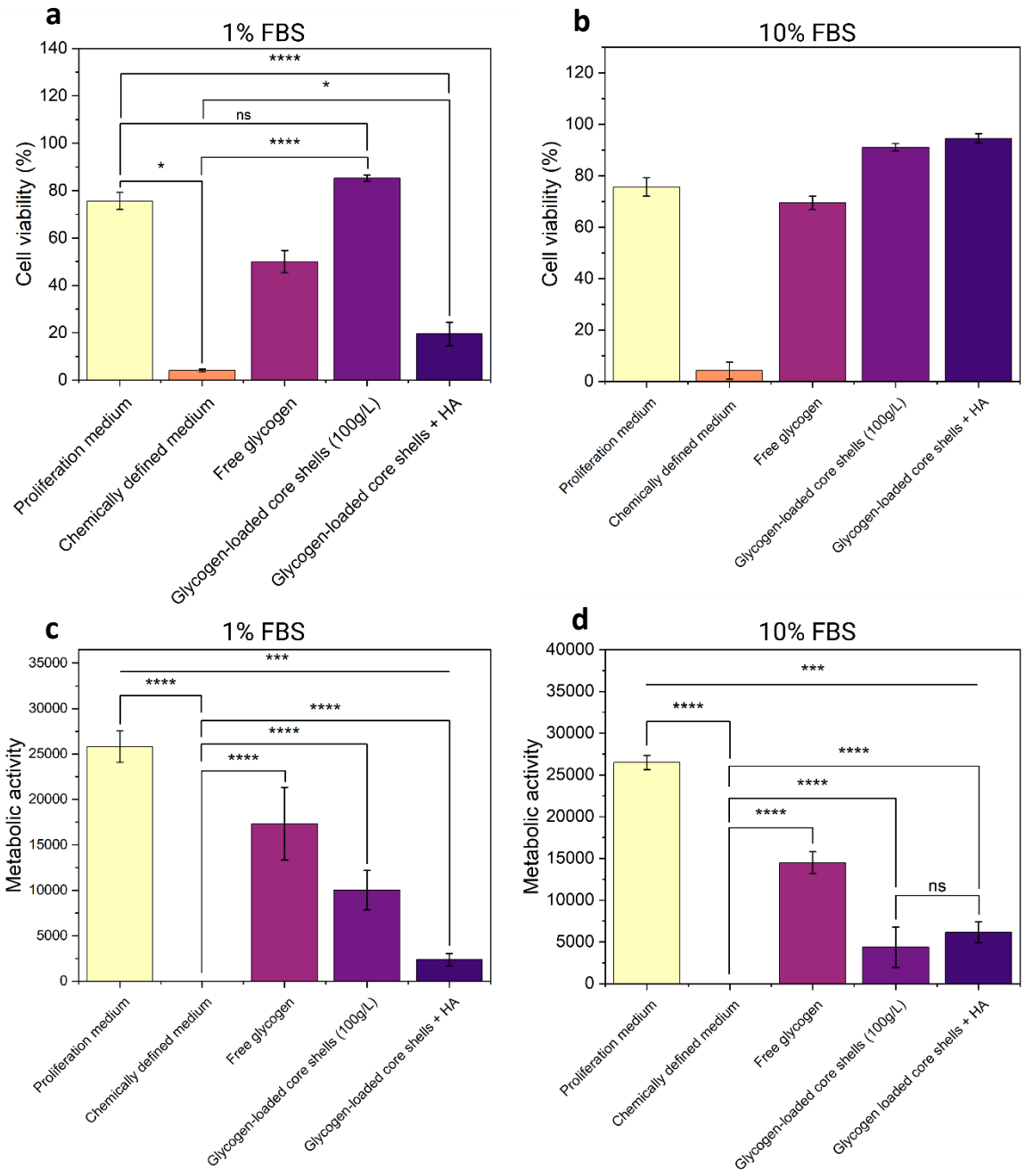

*Figure 60: Complete data set of hMSC-laden collagen gels with glycogen-loaded core shell microgels and hydroxyapatite (HA) block fragments. A) Cell viability on day 7 when chemically defined medium was supplemented with 1% FBS and 9% ITS, Pair-sample t-test. B) Cell viability on day 7 when chemically defined medium was supplemented with 10% FBS, Mann-Whitney test. C) Cell metabolic activity when chemically defined medium was supplemented with 1% FSB and 9% ITS, Mann-Whitney test. D) Cell metabolic activity when chemically defined medium was supplemented with 10% FBS, Mann-Whitney test. *: p≤0.05, **: p≤0.01, ***: p≤0.001, ****: p≤0.0001, n=3. Values presented are given as means ± SD. When not indicated, conditions are non-significant.*

S24. Bottom up tissue engineering – Core shell microgel-hMSC microtissues

To further investigate the potential application of glycogen-loaded core shell microgels in tissue engineering, the formation of aggregates, known as microtissues, with hMSCs was explored. The formation of these aggregates involved the seeding of both hMSCs and core shell microgels into PDMS microwells, allowing them to aggregate overnight before being transferred to an anoxic environment. For aggregate formation, core shell microgels were prepared with dextran-tyramine-biotin (DexTAB) was utilized instead of DexTA. The presence of biotin facilitated the attachment of biotinylated cyclic RGD peptide (biotin-(PEG)2-c(RGDfK)) through supramolecular complexation with neutravidin. These RGD peptides promote the self assembly of hMSCs and functionalized core shell microgels into microtissues.

Initially, different aggregation conditions were examined. It was observed that aggregates formed in proliferation medium remained viable over a two week period, in contrast to aggregates formed in chemically defined medium (Figure 61). Notably, the aggregation process was allowed to proceed overnight, after which the medium in both conditions was replaced with fresh chemically defined medium. This suggests that hMSC survival within the aggregates could be maintained through the release of glucose form the core shell microgels. It is hypothesized the observed low cell viability on day 14 for aggregates formed in chemically defined medium is attributed to excessive stress imposed upon the hMSCs during the aggregation process in a nutrient deprived environment.

Furthermore, it was observed that a core shell to hMSC ratio of 1 to 1,000 yielded better aggregates, which effectively incorporated the core shell microgels within the aggregate structure.

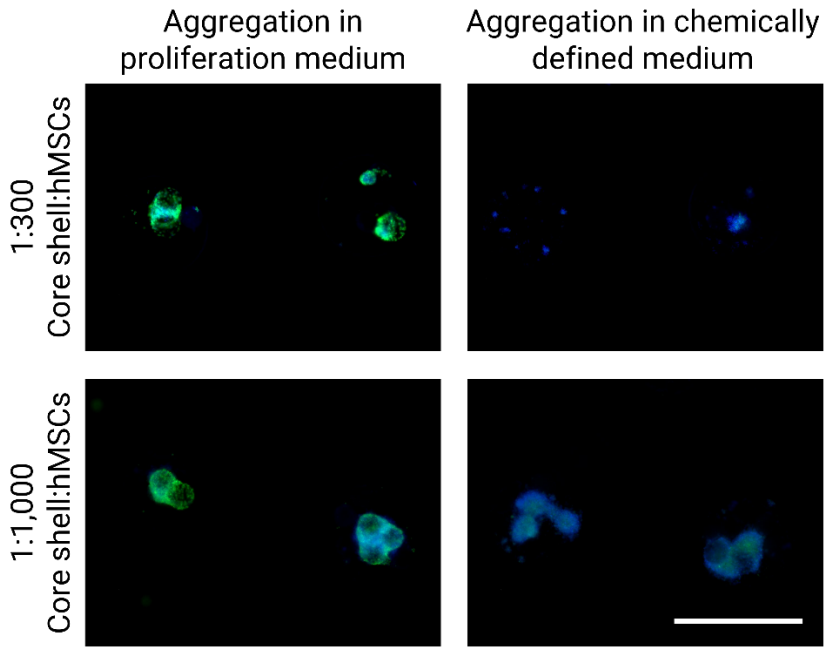

Figure 61: Human mesenchymal stem cell (hMSC) - glycogen-loaded core shell aggerates. Aggregates were formed using two different core shell to hMSC ratios and aggregation was achieved in either proliferation or chemically defined medium. The live staining was done on day 14. Green: live cells (calcein AM), blue: cell nuclei (Hoechst). Scale bar: 1000 µm.

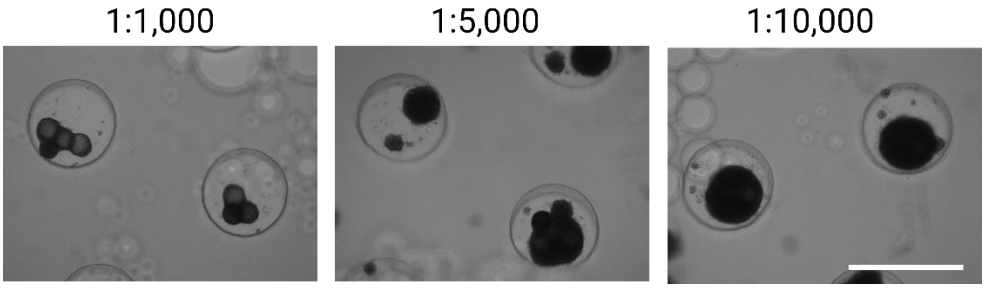

Figure 62: Glycogen-loaded core shell - human mesenchymal stem cell (hMSC) aggregates formed after 1 day. Three different core shell to hMSC ratios were used: 1:1,000, 1:5,000, and 1:10,000. Scale bar: 1000 µm.

The utilization of a a core shell microgel to cell ratio of 1 to 300 was found to be insufficient for the formation of stable aggregates over time. As a results, additional core shell microgel to hMSC ratios were examined. The formation of aggregates on day 1 using three different ratios (1:1,000, 1:5,000, and 1:10,000) is illustrated in Figure 62. It is evident that an increased number of hMSCs leads to improved circularity of the aggregates formed, effectively encompassing nearly all of the core shell microgels present within the microwells.

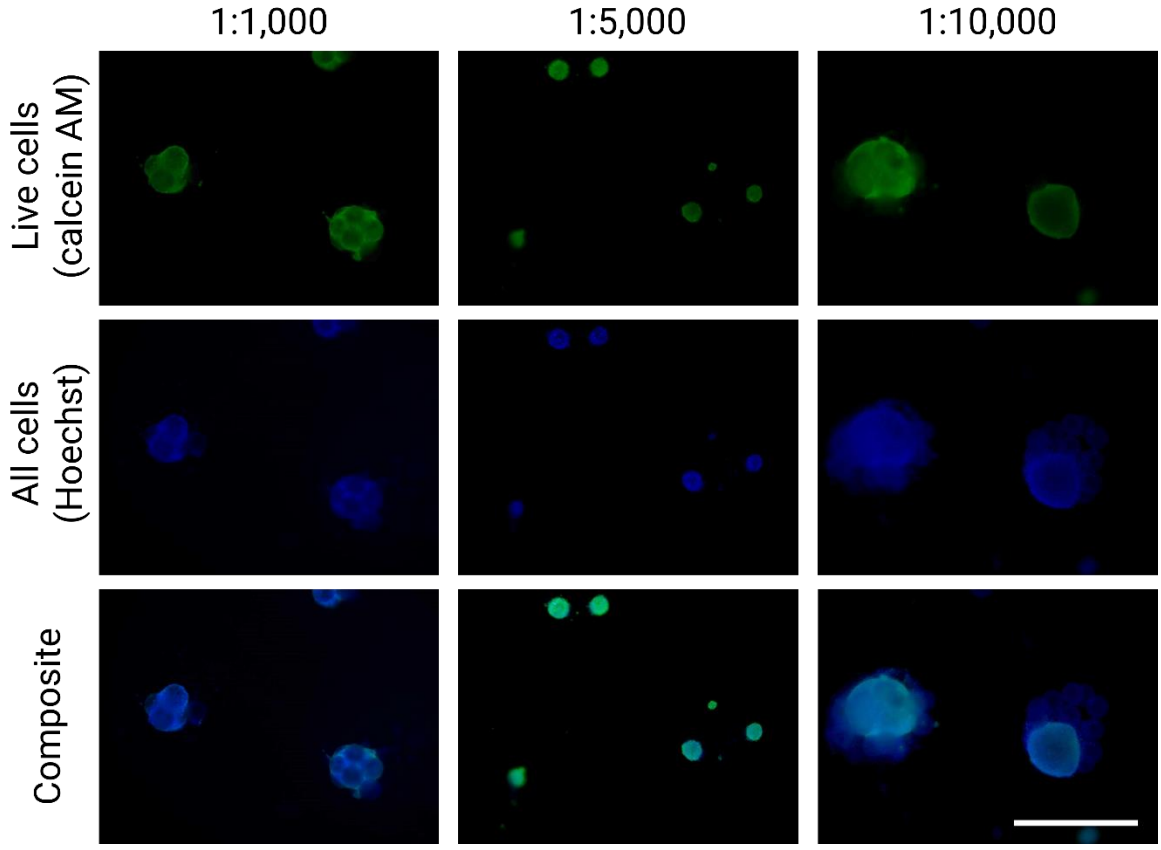

Figure 63: Glycogen-loaded core shell - human mesenchymal stem cell (hMSC) aggregates using different ratios were stained on day 7. Green: live cells (calcein AM), blue: cell nuclei (Hoechst). Scale bar: 1000 µm.

The prepared aggregates, formed using three different ratios of core shell microgels to hMSCs, were cultured for 7 days under anoxic conditions, after which the viability was assessed. Ethidium homodimer-1 staining, typically used to indicated dead cells, could not be employed in this study as it also stains the core shell microgels. therefore, live cells were stained with calcein AM (green), while the nuclei of the all the cells were staining with Hoechst. Quantitative analysis of viability proved

challenging die to the difficulty to distinguish signals from individual cells. However the images of stained hMSCs presented in Figure 63 provide valuable insights into the cell viability. Interestingly, the composite image suggests that aggregates formed with a core shell microgel to hMSC ratio of 1:5,000 exhibit the highest viability. It is noteworthy that, when considering only the first image in which calcein AM stained cells are visualized, hMSCs in all conditions appear to be viable. Concluding, these preliminary results have demonstrated to be promising in the application of glycogen-loaded core shell microgels in the development of viable tissue engineered microtissues.